

LATTICE SIMULATION OF A CENTER  
SYMMETRIC THREE DIMENSIONAL  
EFFECTIVE THEORY FOR  
SU(2) YANG-MILLS

Dissertation  
zur Erlangung des Doktorgrades  
der Naturwissenschaften

vorgelegt beim Fachbereich Physik  
der Johann Wolfgang Goethe-Universität  
in Frankfurt am Main

von  
Dominik Smith  
aus Tennessee, USA

Frankfurt am Main 2010  
(D30)

vom Fachbereich Physik (13) der Johann Wolfgang Goethe-Universität  
als Dissertation angenommen.

Dekan: Prof. Dr. D. H. Rischke

Gutachter: Assoc. Prof. Dr. A. Dumitru, Prof. Dr. S. Schramm

Datum der Disputation:

# Zusammenfassung

## Übersicht

In dieser Arbeit präsentieren wir die Ergebnisse der Gittersimulation einer dreidimensionalen effektiven Theorie für eine  $SU(2)$  Eichtheorie bei endlichen Temperaturen. Unsere Theorie verwendet thermische WILSON Linien und den dreidimensionalen magnetischen Sektor als elementare Freiheitsgrade. Die Wirkung der effektiven Theorie respektiert alle Symmetrien der Eichtheorie in vier Dimensionen. Sie ist invariant unter lokalen  $SU(2)$  Eichtransformationen und zusätzlich invariant unter globalen  $Z(2)$  Transformationen, welche dem ABEL'schem Zentrum der  $SU(2)$  Gruppe entsprechen. Sie enthält das Quadrat des dreidimensionalen Feldstärketensors, einen effektiven kinetischen Term der die Eichfelder an die WILSON Linien koppelt und das störungstheoretische Potential der WILSON Linien bis zur ersten Ordnung. Zusätzlich wird ein "fuzzy bag" Term addiert, welcher einen Phasenübergang erzeugt und nicht-störungstheoretische Fluktuationen zwischen  $Z(2)$  symmetrischen Grundzuständen generiert. Wir untersuchen die Theorie sowohl im Grenzfall verschwindender Magnetfelder, als auch die volle Theorie in welcher dynamische Magnetfelder auftreten. Wir zeigen, dass die Theorie eine Phase mit spontan gebrochener  $Z(2)$  Symmetrie besitzt in welcher der POLYAKOV Loop einen nicht-verschwindenden Wert hat. In Analogie zur Quantenchromodynamik entspricht dies einer Aufhebung des Quark-Confinement. Wir bestimmen das Phasendiagramm der Theorie und ermitteln die Ordnung des Phasenübergangs an verschiedenen Stellen der Phasengrenze mittels Korrelationsfunktionen und des Skalenverhaltens der Suszeptibilität. Wir zeigen dass im Bereich mittel schwacher Kopplung nahe der Phasengrenze in der Symmetrie-gebrochenen Phase der "fuzzy bag" Term Eigenwert Repulsion erzeugt, welche im Grenzfall extrem schwacher Kopplung verschwindet. Wir zeigen dass ein nicht-triviales  $Z(2)$  symmetrisches Vakuum existiert. Für die volle Theorie mit Eichfeldern untersuchen wir die räumliche String Spannung und zeigen dass magnetische Observablen vom elektrischen Sektor nur schwach beeinflusst werden. Desweiteren bestimmen wir das effektive Potential des POLYAKOV Loop, sowohl für den Fall dass alle FOURIER Moden betrachtet werden, als auch für "gekühlte" Konfigurationen ("Block Spins") in welchen das POLYAKOV Loop Feld über kleine Volumina gemittelt wird, wodurch kurzreichweitige Fluktuationen unterdrückt werden. Für den ersten Fall finden wir, dass eine Parametrisierung des Potentials nicht-analytische Terme enthält. Der zweite Fall lässt sich in Analogie zur mittleren Feld Näherung ("mean field") durch quadratische und quartische Terme parametrisieren, plus einen Beitrag des VANDERMONDE Potentials, dessen Stärke für verschiedene Regionen im Phasendiagramm variiert. Qualitative Vergleiche mit der vierdimensionalen Eichtheorie zeigen dass das Verhalten des Block Spin Potentials in der dreidimensionalen Theorie mit der vierdimensionalen Theorie übereinstimmt.

## Einleitung

Schwerionen Kollisions Experimente die am Relativistic Heavy Ion Collider (RHIC) im Brookhaven National Lab in New York durchgeführt wurden haben einen Zustand der Materie erzeugt, in welchem Quarks und Gluonen aus ihrem hadronischen Bindungszustand gelöst werden. Ein solches Verhalten wurde sowohl von Gittersimulationen der Quantenchromodynamik, als auch von analytischen Berechnungen im Hochtemperatur Limes der Theorie vorhergesagt. Vieles deutet jedoch darauf hin dass bei den erzeugten Temperaturen, die zwischen ein und dreimal der vorhergesagten kritischen Temperatur liegen, der erzeugte Materiezustand eher einer stark gebundenen Flüssigkeit als einem schwach gebundenem Plasma entspricht. Der störungstheoretische Harte-Thermische-Schleifen (“Hard-Thermal-Loops”) Formalismus kann thermodynamische Observablen wie den Druck oder die Entropiedichte nur für Temperaturen oberhalb der doppelten Phasenübergangstemperatur beschreiben. Dies impliziert dass der Temperaturbereich knapp oberhalb des Phasenuübergangs von nicht perturbativen Effekten dominiert ist. Ebenso versagt in dieser Region die wohl bekannte dreidimensionale effektive Theorie EQCD

$$\mathcal{L}^{\text{eff}} = \frac{1}{2} \text{tr} F_{ij}^2 + \text{tr} |D_i A_0|^2 + m_D^2 \text{tr} A_0^2 + \dots, \quad (0.1)$$

welche den Hochtemperaturbereich der Quantenchromodynamik beschreibt und die statischen Feldmoden des gluonischen Vektorpotentials als Freiheitsgrade verwendet.

Obige Ansätze gehen von der Annahme aus dass Fluktuationen in der Zeitkomponente des Vektorpotentials als klein angesehen werden können. Dadurch verletzen sie die  $Z(3)$  Zentrumssymmetrie der  $SU(3)$  Eichgruppe. Numerische Berechnungen renormierter POLYAKOV Loops haben gezeigt, dass diese Annahme bei Temperaturen  $\geq 2T_c$  in guter Näherung erfüllt ist. Das Hochtemperatur System ist in einem der (in der reinen Eichtheorie entarteten)  $Z(3)$  Vakuumzustände fixiert. Knapp oberhalb des Phasenüberganges müssen jedoch Fluktuationen zwischen Vakuumzuständen berücksichtigt werden. Eine effektive Theorie die dies leistet, verwendet anstatt der  $A_i$  Felder die Matrix wertige thermische WILSON Linie

$$\mathbf{L}(\mathbf{x}) = \mathcal{Z}_R^{-1} \mathcal{P} \exp \left( ig \int_0^{1/T} d\tau A_0(\mathbf{x}, \tau) \right), \quad (0.2)$$

als effektiven Freiheitsgrad (Die Renormierungskonstante  $\mathcal{Z}$  ist darstellungsabhängig. Wir gehen wir von der Fundamentaldarstellung aus.). Im Rahmen eines solchen Ansatzes ist die deconfined-Phase nicht als Gas freier Quasi-Teilchen beschrieben, sondern als Kondensat Spin-artiger Matrix Variablen. Im Kontrast zu Modellen des Ferromagnetismus kondensieren diese jedoch bei hohen Temperaturen anstatt bei niedrigen. Die normierte Spur der WILSON Linie

$$\ell(\mathbf{x}) = \frac{1}{N} \text{Tr} \mathbf{L}(\mathbf{x}), \quad (0.3)$$

wird als POLYAKOV Loop bezeichnet und ist ein Ordnungsparameter für die spontane Brechung der  $Z(3)$  Symmetrie, welche lokalen Eichtransformationen in der vierdimensionalen Theorie die periodisch in Zeitrichtung bis auf einen globalen  $Z(3)$  Phasenfaktor sind entspricht.

Aufgrund der  $Z(3)$  Zentrumssymmetrie in der vollen Theorie kann der effektive elektrische Beitrag zur dreidimensionalen effektiven Theorie nicht durch  $E_i(\mathbf{x}) \sim D_i A_0$  gegeben sein. PISARSKI zeigte dass für eine effektive Theorie mit beliebig fluktuierendem  $A_0$ , das effektive elektrische Feld durch

$$E_i(\mathbf{x}) = \frac{T}{ig} \mathbf{L}^\dagger(\mathbf{x}) D_i(\mathbf{x}) \mathbf{L}(\mathbf{x}) , \quad (0.4)$$

gegeben ist. Im klassischen Limes ist die LAGRANGE Dichte einer  $Z(3)$  symmetrischen effektiven Theorie daher durch

$$\mathcal{L}_{\text{cl}}^{\text{eff}} = \frac{1}{2} \text{tr} F_{ij}^2 + \frac{T^2}{g^2} \text{tr} |\mathbf{L}^\dagger D_i \mathbf{L}|^2 . \quad (0.5)$$

gegeben wobei  $F_{ij}$  der dreidimensionale magnetische Feldstärketensor ist. Durch Schleifenkorrekturen muss jedoch auch das perturbative Potential der WILSON Linie berücksichtigt werden. Dieses wurde von GROSS, PISARSKI und YAFFE bis zur ersten Schleifenordnung berechnet und lautet

$$\mathcal{L}_{1\text{-loop}}^{\text{eff}} = -\frac{2}{\pi^2} T^4 \sum_{n \geq 1} \frac{1}{n^4} |\text{tr} \mathbf{L}^n|^2 . \quad (0.6)$$

Betrachtet man die Wirkung die durch die Summe der Terme (0.5) und (0.6) gegeben ist, so sieht man dass diese durch das perturbative Vakuum, in welchem  $\mathbf{L} \sim \mathbf{1}$  gilt, minimiert wird. Um einen Phasenübergang herbeizuführen und nicht-perturbative Fluktuationen zu erzeugen müssen zusätzliche Terme addiert werden. Eine Untersuchung der Temperaturabhängigkeit des Wechselwirkungsmaßes (“interaction measure”) suggeriert, dass der naheliegendste Ansatz ein Term der Form

$$\mathcal{L}_{\text{non-pert.}}^{\text{eff}} = B_f T^2 |\text{tr} \mathbf{L}|^2 , \quad (0.7)$$

ist, wobei der Vorfaktor  $B_f$  als “fuzzy bag” Konstante bezeichnet wird in Anlehnung an das MIT Bag Modell. Im Kontrast zu diesem hat der “fuzzy bag” keinen scharf begrenzten Rand.

In dieser Arbeit simulieren wir die effektive Theorie die durch die Summe der Terme (0.5), (0.6) und (0.7) gegeben ist. Die vollständige LAGRANGE Dichte ist also

$$\mathcal{L}^{\text{eff}} = \frac{1}{2} \text{tr} F_{ij}^2 + \frac{T^2}{g^2} \text{tr} |\mathbf{L}^\dagger D_i \mathbf{L}|^2 - \frac{2}{\pi^2} T^4 \sum_{n \geq 1} \frac{1}{n^4} |\text{tr} \mathbf{L}^n|^2 + B_f T^2 |\text{tr} \mathbf{L}|^2 . \quad (0.8)$$

Die Theorie ist nicht renormierbar und auf Längenskalen größer als  $1/T$  gültig. Wir untersuchen die  $SU(2)$  Theorie anstelle von  $SU(3)$  aufgrund der weniger komplexen Struktur der Gruppenmannigfaltigkeit. Durch den nicht-ABEL’schen Charakter der  $SU(2)$  Theorie reproduziert diese das qualitative Verhalten vieler Observablen der  $SU(3)$  Theorie in guter Approximation.

## Grundlagen der Gittersimulation

Wir simulieren die Theorie, welche durch (0.8) gegeben ist auf dreidimensionalen kubischen Gittern mit periodischen Randbedingungen in allen Raumrichtungen. Wir machen zwei

vereinfachende Annahmen: Zuerst vernachlässigen wir alle Terme des perturbativen Potentials von höherer Ordnung als  $n = 1$ . Dadurch kann das perturbative Potential mit dem “fuzzy bag” Term zu einem einzigen Term  $\sim |\text{tr } \mathbf{L}|^2$  zusammengefasst werden, welcher sich wie ein Massenterm verhält. Wir weisen diesem Term eine Gitterkopplungskonstante  $m^2$  zu, deren Betrag und Vorzeichen entscheiden ob perturbative oder nicht-perturbative Effekte dominieren. Zweitens weisen wir dem magnetischen und elektrischen kinetischen Termen eine gemeinsame Gitterkopplungskonstante  $\beta$  zu. Dies ist zulässig, da diese Arbeit die qualitativen Eigenschaften des Gittermodells untersucht und keine vollständige Anpassung der Kopplungskonstanten an die  $4D$  Theorie beabsichtigt.

Für den magnetischen Sektor wird die Standard WILSON Wirkung verwendet in welcher die Eichfelder als Linkvariablen auftreten. Die zu (0.8) korrespondierende Gitterwirkung lautet dann

$$S = \beta \sum_{\square} (1 - \frac{1}{2} \text{Re Tr } \mathbf{U}_{\square}) - \frac{1}{2} \beta \sum_{\langle ij \rangle} \text{tr} (\mathbf{L}_i \mathbf{U}_{ij} \mathbf{L}_j^{\dagger} \mathbf{U}_{ij}^{\dagger} + \text{h.c.}) - m^2 \sum_i |\text{tr } \mathbf{L}_i|^2. \quad (0.9)$$

Wir verwenden den METROPOLIS Algorithmus zur Erzeugung von Gitterkonfigurationen. Es werden stochastische “Overrelaxation” Sweeps beigemischt um die Dekorrelation zu beschleunigen. Der CREUTZ Heat Bath Algorithmus wird zur Konsistenzprüfung implementiert, kann aber aufgrund der quadratischen Terme nur im Fall  $m^2 = 0$  für das  $\mathbf{L}$  Feld eingesetzt werden. Es wird die Binning Methode verwendet um die integrierten Autokorrelationszeiten elektrischer und magnetischer Operatoren abzuschätzen. Diese wird ausgenutzt um die optimale Anzahl der Sweeps zwischen einzelnen Messungen zu ermitteln.

Das Matrix wertige Feld  $\mathbf{L}$  wurde über Kompaktifizierung der EUKLIDischen Zeitdimension erhalten. Im Falle nichtverschwindender Magnetfelder ist in der diskretisierten Gitterformulierung der kinetische Teil der Wirkung (0.9) äquivalent zu einer  $4D$  Gittereichtheorie mit  $N_{\tau} = 1$ . Dies ermöglicht zwei verschiedene Update Verfahren für die Linkvariablen, je nach Umgang mit den Randbedingungen in der kompaktifizierten Zeitrichtung, welche als Zeit-Plaquetten Einfachzählung (“time-plaquette single counting”) und Doppelzählung (“double counting”) bezeichnet werden. Wir stellen beide Vorgehensweisen gegenüber und zeigen dass sie vergleichbare Ergebnisse liefern.

## Ergebnisse

### Effektive Theorie in drei Dimensionen ohne Magnetfelder

Erste Ergebnisse werden im Limes  $A_i = 0$  erhalten (wodurch die Linkvariablen  $\mathbf{U}_{ij}$  auf die Einheitsmatrix fixiert sind). Das resultierende Modell hat im Grenzfall  $m^2 = 0$  eine globale  $SU(2)_L \times SU(2)_R$  Symmetrie und keine lokalen Symmetriegruppen. Hinzufügen des Massenterms bricht die globale Symmetrie explizit zu  $SU(2)$ . Als Ordnungsparameter werden sowohl der Erwartungswert des volumengemittelten POLYAKOV Loops  $\langle \bar{\ell} \rangle$  betrachtet, als auch den Absolutbetrag  $u_0$  der “Länge” des gemittelten  $\mathbf{L}$  Feldes im Raum der Quaternionen, welche durch

$$u = \sqrt{\text{Tr } \bar{\mathbf{L}}^{\dagger} \bar{\mathbf{L}} / 2}, \quad u_0 = \langle u \rangle, \quad (0.10)$$

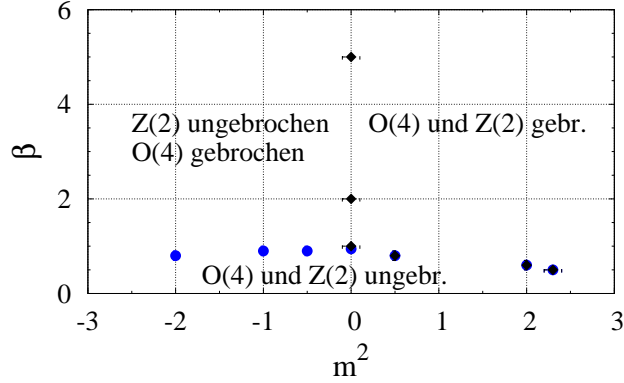


Figure 0.1: Phasendiagramm der effektiven Theorie ohne Eichfelder.

gegeben ist und von welcher ein endlicher Erwartungswert die spontane Brechung der  $SU(2)_L \times SU(2)_R$  Symmetrie zu  $SU(2)_V$  signalisiert. Wir bezeichnen  $u_0$  aufgrund der Isomorphie  $SU(2)_L \times SU(2)_R \approx O(4)$  als  $O(4)$  Ordnungsparameter. Das ermittelte Phasendiagramm ist in Fig. 0.1 zusammengefasst. Es gibt zwei Phasengrenzen welche die Regionen in denen  $SU(2)_L \times SU(2)_R$  gebrochen und ungebrochen ist und die Regionen gebrochener und erhaltener  $Z(2)$  Symmetrie voneinander trennen. Messungen der inversen Korrelationslänge welche mit der Matrix-Matrix Zweipunkt Funktion

$$C_{\mathbf{L}}(r) = \frac{1}{3} \frac{1}{N_s^3} \sum_{\mathbf{r}, \mathbf{r}_0} \frac{1}{2} \left\langle \text{tr} \mathbf{L}^\dagger(\mathbf{r}_0) \mathbf{L}(\mathbf{r}_0 + \mathbf{r}) \right\rangle, \quad (0.11)$$

assoziiert ist bestätigen dass im linken oberen Bereich des Phasendiagramms GOLDSTONE Moden existieren welche den globalen  $SU(2)_V$  Rotationen entsprechen. Extrapolationen der Suszeptibilität zum Limes unendlichen Volumens, wie auch die im Folgenden Diskutierten Eigenwertverteilungen, bestätigen dass der Phasenübergang in allen Bereichen zweiter Ordnung ist. Es werden Skalierungs-Exponenten der Korrelationslängen an der Phasengrenze bestimmt.

Wir verallgemeinern die mittlere Feld Näherung welche von KOGUT, STONE und SNOW für den Fall  $m^2 = 0$  diskutiert wurde auf den Fall  $m^2 \neq 0$  und finden dass diese das Modell in der  $Z(2)$  gebrochenen Phase nur in hinreichender Distanz von der Phasengrenze beschreibt. Nahe der Phasengrenze wird die Gültigkeit der mittleren Feld Näherung durch Fluktuationen zerstört.

Zuletzt bestimmen wir mit Histogrammen die Verteilungsfunktionen der Absolutbeträge der Summe und Differenz der Eigenwerte  $\lambda_{1,2}$  der WILSON Linien  $\mathbf{L}$

$$\rho_1(\mathbf{x}) = \frac{1}{2} |\lambda_1(\mathbf{x}) - \lambda_2(\mathbf{x})|, \quad \rho_2(\mathbf{x}) = \frac{1}{2} |\lambda_1(\mathbf{x}) + \lambda_2(\mathbf{x})|, \quad (0.12)$$

in verschiedenen Regionen des Phasendiagramms. Wir finden dass für  $m^2 = 0$  und  $\beta < \beta_C$  die Verteilungen vollständig durch das  $SU(2)$  Gruppen Integrationsmaß dominiert sind.

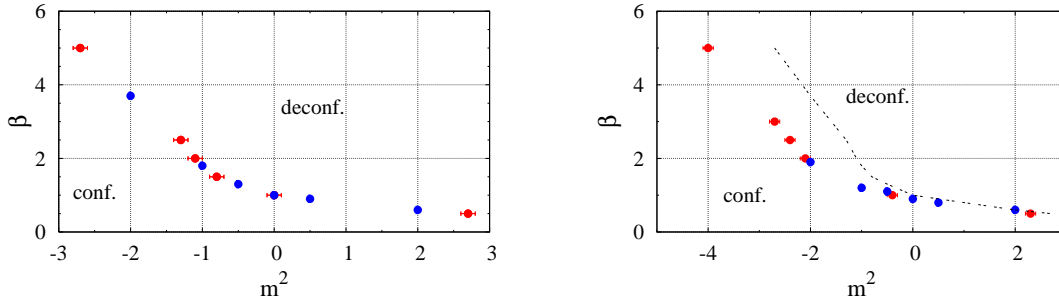


Figure 0.2: Links: Phasendiagramm der effektiven Theorie mit Zeit-Plaquetten Doppelzählung. Rechts: Vergleich zur Zeit-Plaquetten Einfachzählung.

Der linke obere Bereich des Phasendiagramms entspricht einem nichttrivialen  $Z(2)$  symmetrischen Vakuum in welchem Confinement durch Eigenwertrepulsion erzeugt wird und in welchem das mittlere Feld  $\bar{\mathbf{L}}$  im Unterraum der  $SU(2)$  Gruppe, welcher durch die Generatoren aufgespannt wird rotiert. Wir finden dass schwache Eigenwertrepulsion auch in der deconfined Phase (rechts oben) nahe der Phasengrenze existiert und in Bereichen fern der Phasengrenze unterdrückt ist.

### Effektive Theorie in drei Dimensionen mit Magnetfeldern

Nach dem Hinzufügen des magnetischen Sektors hat das Modell die gewünschte lokale  $SU(2)$  Symmetrie. Sowohl im Falle der Zeit-Plaquetten Einfachzählung als auch mit Doppelzählung existiert nur eine einzige Phasengrenze welche der spontanen Brechung der globalen  $Z(2)$  Zentrumssymmetrie entspricht. Die Phasendiagramme beider Updating Verfahren sind in Fig. 0.2 dargestellt. Die Phasengrenzen weichen nur im Bereich  $m^2 < 0$  geringfügig voneinander ab. Wir finden wiederum über das Skalenverhalten der Suszeptibilität und der inversen Korrelationslänge der Matrix-Matrix Zweipunkt Funktion (welche um eichinvariante Resultate zu liefern nun einen Paralleltransport der  $\mathbf{L}$  Felder beinhaltet) an der Phasengrenze dass der Phasenübergang in weiten Bereichen zweiter Ordnung ist. Allerdings liefern die im Folgenden diskutierten POLYAKOV Loop Potentiale den Nachweis dass für sehr große Werte des Parameters  $\beta$  der Phasenübergang zu einem erster Ordnung wird. In keinem Bereich des Phasendiagramms sind masselose GOLDSTONE Moden zu finden.

Nach Hinzufügen der Eichfelder sind eine Reihe von magnetischen Observablen zugänglich. Wir untersuchen wie die Symmetriebrechung im elektrischen Sektor diese beeinflusst. Wir bestimmen zuerst die, durch einen Faktor  $\beta$  geteilte, WILSON Wirkung

$$\frac{1}{\beta} \langle S_{\square} \rangle = \left\langle \sum_{\square} \left( 1 - \frac{1}{2} \text{Re Tr } \mathbf{U}_{\square} \right) \right\rangle \quad (0.13)$$

im Limes  $m^2 = 0$  und finden dass diese mit steigendem  $\beta$  in guter Näherung exponentiell abfällt. Desweiteren wird die räumliche Stringspannung

$$\sigma_S = a^2 K, \quad (0.14)$$



bestimmt, indem Erwartungswerte rechteckiger geschlossener Raum-artiger WILSON Schleifen

$$W(C) = \left\langle \text{Tr} \prod_{i,j \in C} U_{ij} \right\rangle . \quad (0.15)$$

mit verschiedenem Flächeninhalt gemessen werden, und der Exponent des Potenzgesetzes

$$W(X, Y) \sim \exp(-K XY) , \quad (0.16)$$

bestimmt wird, wobei  $X$  und  $Y$  die Seitenlängen der WILSON Schleife sind. Wir finden dass auch  $\sigma_S$  mit steigendem  $\beta$  exponentiell abfällt. Sowohl  $\sigma_S$  als auch  $\langle S_{\square} \rangle / \beta$  weisen für  $m^2 = 0$  keinerlei auffälliges Verhalten am Phasenübergangspunkt  $\beta_C$  auf. Anschliessend berechnen wir Zweipunkt Funktionen gleichsinnig orientierter, einander gegenüberliegender Plaquetten um die effektive Masse magnetischer Anregungen abzuschätzen. Es zeigt sich dass das Signal der Plaquetten Zweipunkt Funktion für  $\beta < \beta_C$  sehr schwach wird und für unsere numerische Genauigkeit im statistischen Rauschen verschwindet. Für  $\beta > \beta_C$  können wir eine Masse extrahieren welche im Rahmen der Meßgenauigkeit  $\beta$  unabhängig ist.

In der  $m^2$  Abhängigkeit von  $\sigma_S$  und  $\langle S_{\square} \rangle / \beta$  äussert sich der einzige beobachtete qualitative Unterschied zwischen Zeit-Plaquetten Doppelzählung und Einfachzählung. In beiden Fällen ist eine Diskontinuität von  $\sigma_S$  und  $\langle S_{\square} \rangle / \beta$  auf  $< 1\%$  Niveau am Phasenübergang zu beobachten. Die Größe des Sprungs nimmt mit steigendem  $\beta$  leicht zu. Ausserhalb der Phasengrenze sind im Falle der Einzelzählung die magnetischen Observablen komplett  $m^2$  unabhängig. Für die Doppelzählung beobachten wir eine schwache Abhängigkeit, wiederum im  $< 1\%$  Bereich. Die magnetische Masse scheint in beiden Fällen nicht von  $\beta$  abzuhängen.

Wir bestimmen als nächstes das effektive Potential des POLYAKOV Loops, welches dem Potential für die in Gleichung (0.12) definiterte Eigenwertfunktion  $\rho_2$  entspricht, da

$$\rho_2(\mathbf{x}) = \frac{1}{2} |\lambda_1(\mathbf{x}) + \lambda_2(\mathbf{x})| = \sqrt{\ell^2} . \quad (0.17)$$

Das Potential wird aus der Verteilungsfunktion über

$$V(|\ell|) = -\log P(|\ell|) \quad (0.18)$$

erhalten. Wir finden, dass das so gewonnene effektive Potential sich in weiten Teilen des Phasendiagramms durch den Ansatz

$$V_{\text{fit}}(\rho) = -\frac{1}{2} \log(1 - \rho^2) + a - b\rho + c\rho^2 \quad (0.19)$$

parametrisieren lässt. Dabei ist der Beitrag  $V_{Vdm} = -\frac{1}{2} \log(1 - \rho^2)$  das VANDERMONDE Potential welches durch das Gruppenmaß erzeugt wird. Der nicht-analytische Term  $\sim \rho$  taucht nicht in der Gitterwirkung auf, wird also durch die Dynamik generiert. Wir finden einfache heuristische Formeln um die  $\beta$  und  $m^2$  Abhängigkeiten der Konstanten  $a, b, c$  zu beschreiben. Der quadratische Koeffizient  $c$  hängt in guter Näherung linear von  $m^2$  ab. Der lineare Koeffizient  $b$  verschwindet in der confined Phase und steigt in der deconfined Phase stetig an. Für  $\beta \gtrsim 5$  beobachten wir am Phasenübergang zwei verschiedene

Potentialminima, was auf einen Übergang erster Ordnung hindeutet. Dort versagt auch der Ansatz (0.19).

Als letztes bestimmen wir das effektive Potential für die langwelligen Feldmoden des  $\ell(\mathbf{x})$  Feldes. Dies wird erreicht, indem vor der Erstellung des Histogramms das Feld  $\ell(\mathbf{x})$  über kleine Würfel der Seitenlänge  $k$  gemittelt wird, also “Block Spins” der Form

$$\bar{\ell}_i^{(k)} = \frac{1}{k^3} \sum_{\mathbf{n}} \frac{1}{2} \text{Tr} \mathbf{L}(\mathbf{i} + \mathbf{n}) , \quad \mathbf{n} = (0, 0, 0) \dots (k, k, k) ,$$

gebildet werden. Dies führt dazu, dass das effektive Potential steiler und symmetrischer um das Minimum wird. Wir betrachten die Differenz zwischen Position des Potentialminimums und numerischem POLYAKOV Loop Erwartungswert und nehmen diese, in Analogie zu einem “mean field” Selbstkonsistenz Kriterium als Maß für die Vollständigkeit der Unterdrückung kurzwelliger Fluktuationen. Wir finden dass mit unserer numerischen Präzision von  $k = 3$  zu  $k = 4$  keine signifikante Verbesserung zu sehen ist und nehmen  $k = 3$  als hinreichend an.

Wir finden, dass eine Parametrisierung des effektiven Block Spin Potentials in weiten Teilen des Phasenübergangs mit dem Ansatz

$$V(\rho) = -d_0 \frac{1}{2} \log(1 - \rho^2) + d_1 + d_2 \rho^2 + d_4 \rho^4 , \quad (0.20)$$

möglich ist. Die polynomischen Terme sind durch die Analogie zu einer LANDAU-GINZBURG “mean field” Theorie motiviert. Es treten keine nicht-analytischen Terme auf. Wir finden, dass ein variabler multiplikativer Parameter  $d_0$  für den VANDERMONDE Beitrag nötig ist. Wir bestimmen die  $\beta$  und  $m^2$  Abhängigkeiten der Fitparameter. Auffällig ist, dass knapp oberhalb des Phasenübergangs der VANDERMONDE Term stark unterdrückt ist und beim entfernen von der Phasengrenze in Richtung steigender  $\beta$  und  $m^2$  ansteigt. Weit in der deconfined Phase saturiert  $d_0$ . Ein analoges Verhalten wird für  $k = 4$  beobachtet. Wir zeigen dass es möglich ist, die Unterdrückung des VANDERMONDE Terms in einen weiteren linearen Term, der zum Potential addiert werden muss, absorbiert werden kann. Ein solcher Ansatz führt aber in Bereichen des Phasendiagramms die nicht unmittelbar über der Phasengrenze liegen zu einem unphysikalischen Potential welches nicht nach unten beschränkt ist.

## Vergleich zur vierdimensionalen Yang-Mills Theorie

Wir führen Simulationen auch in der vollen vierdimensionalen  $SU(2)$  Eichtheorie durch, mit der Standart Gitterwirkung

$$S = \beta \sum_{\square} \left(1 - \frac{1}{2} \text{Re Tr} \mathbf{U}_{\square}\right) . \quad (0.21)$$

Das letztendliche Ziel einer solchen Untersuchung ist die genaue Anpassung der Kopplungsparameter der dreidimensionalen effektiven Theorie an die  $4D$  Eichtheorie (Dies wird erschwert durch die Nicht-Renormierbarkeit der effektiven Theorie.). Dieses Ziel geht jedoch über den Rahmen dieser Arbeit hinaus. Wir präsentieren lediglich einige qualitative Vergleiche.

Wir verwenden zur Simulation der  $4D$  Theorie den Gittereichtheorie Code der MILC Kollaboration<sup>1</sup>. Wir reproduzieren zunächst einige hinreichend bekannte Ergebnisse zur

<sup>1</sup><http://physics.utah.edu/~detar/milc.html>

---

Konsistenzprüfung. Zu diesen gehört der Phasenübergangspunkt  $\beta_C$  für verschiedene  $N_\tau$  und das Verhalten der Stringspannung als Funktion von  $\beta$ . Messungen der inversen Korrelationslängen bestätigen die Abwesenheit von GOLDSTONE Moden. Anschliessend bestimmen wir für ein festes  $N_\tau$  das effektive Potential des POLYAKOV Loops und der oben definierten Block Spins. Wir zeigen, dass das POLYAKOV Loop Potential analog zu (0.19) parametrisieren lässt, dass allerdings der quadratische Term sehr klein ist. Für das Block Spin Potential finden wir ein Verhalten welches mit der 3D Theorie übereinstimmt: Eine Parametrisierung durch (0.20) ist möglich und der VANDERMONDE Term ist knapp oberhalb des Phasenübergangs unterdrückt.



# Abstract

We present lattice simulations of a center symmetric dimensionally reduced effective field theory for  $SU(2)$  Yang Mills which employ thermal WILSON lines and three-dimensional magnetic fields as fundamental degrees of freedom. The action is composed of a gauge invariant kinetic term, spatial gauge fields and a potential for the WILSON line which includes a "fuzzy" bag term to generate non-perturbative fluctuations between  $Z(2)$  degenerate ground states. The model is studied in the limit where the gauge fields are set to zero as well as the full model with gauge fields. We confirm that, at moderately weak coupling, the "fuzzy" bag term leads to eigenvalue repulsion in a finite region above the deconfining phase transition which shrinks in the extreme weak-coupling limit. A non-trivial  $Z(N)$  symmetric vacuum arises in the confined phase. The effective potential for the POLYAKOV loop in the theory with gauge fields is extracted from the simulations including all modes of the loop as well as for cooled configurations where the hard modes have been averaged out. The former is found to exhibit a non-analytic contribution while the latter can be described by a mean-field like *ansatz* with quadratic and quartic terms, plus a VANDERMONDE potential which depends upon the location within the phase diagram. Other results include the exact location of the phase boundary in the plane spanned by the coupling parameters, correlation lengths of several operators in the magnetic and electric sectors and the spatial string tension. We also present results from simulations of the full  $4D$  Yang-Mills theory and attempt to make a qualitative comparison to the  $3D$  effective theory.



# Contents

<b>1</b>	<b>Notations and conventions</b>	<b>1</b>
<b>2</b>	<b>Introduction</b>	<b>3</b>
2.1	Quantum Chromodynamics . . . . .	3
2.2	The pure gauge limit and the Wilson criterium . . . . .	4
2.3	The strongly coupled quark gluon plasma . . . . .	6
2.4	Effective theories . . . . .	8
2.5	Outline of this work . . . . .	9
<b>3</b>	<b>Center symmetric effective field theory</b>	<b>11</b>
3.1	Dimensional reduction . . . . .	11
3.2	Symmetries of SU(N) Yang-Mills theory . . . . .	12
3.3	Center symmetric effective theory of Wilson lines . . . . .	13
<b>4</b>	<b>Lattice simulation</b>	<b>17</b>
4.1	Markov Chain Monte Carlo . . . . .	17
4.2	Autocorrelations . . . . .	19
4.3	Metropolis algorithm . . . . .	22
4.4	Over-relaxation . . . . .	23
4.5	Heat bath . . . . .	24
<b>5</b>	<b>Derivation of lattice action</b>	<b>31</b>
5.1	Wilson line action . . . . .	32
5.2	Action of pure gauge sector . . . . .	36
5.3	Time-like plaquette <i>single counting</i> vs. <i>double counting</i> . . . . .	38
<b>6</b>	<b>Results without magnetic fields</b>	<b>39</b>
6.1	Chiral model of Kogut, Stone and Snow . . . . .	40
6.1.1	$O(4)$ -like order parameter . . . . .	40
6.1.2	Susceptibility . . . . .	43
6.1.3	Internal energy . . . . .	43
6.1.4	Two-point correlation function . . . . .	44
6.2	Model with Polyakov loop potential term . . . . .	45
6.2.1	Mean field approximation . . . . .	46
6.2.2	Phase diagram . . . . .	48
6.2.3	Correlation functions . . . . .	51
6.2.4	Eigenvalue distribution . . . . .	52
6.3	Autocorrelations . . . . .	54

---

<b>7</b>	<b>Results with magnetic fields</b>	<b>57</b>
7.1	Massless limit . . . . .	58
7.1.1	Spontaneous breaking of $Z(2)$ . . . . .	58
7.1.2	Two-point functions . . . . .	59
7.1.3	Magnetic sector . . . . .	60
7.2	Full theory . . . . .	64
7.2.1	Phase diagram . . . . .	64
7.2.2	Effective Polyakov loop potential . . . . .	67
7.2.3	Effective potential for block spins . . . . .	72
7.2.4	Large $\beta$ limit . . . . .	76
7.3	Autocorrelations . . . . .	77
7.4	Single counting scheme . . . . .	79
<b>8</b>	<b>Results in four dimensions</b>	<b>83</b>
8.1	Phase transition . . . . .	83
8.2	Wilson action . . . . .	84
8.3	Creutz ratios . . . . .	85
8.4	Two-point functions . . . . .	85
8.5	Single site loop potential . . . . .	85
8.6	Block spin potential . . . . .	87
<b>9</b>	<b>Summary and conclusions</b>	<b>89</b>
	<b>Appendices</b>	<b>93</b>
<b>A</b>	<b>Group theory</b>	<b>95</b>
<b>B</b>	<b>Summary of consistency checks</b>	<b>103</b>
	<b>Bibliography</b>	<b>105</b>
	<b>Index</b>	<b>121</b>



# 1 Notations and conventions

Here we summarize notations and conventions used throughout this work. We mostly follow the conventions of PESKIN and SCHROEDER [1] for continuum physics and of CREUTZ [2] for lattice physics with a few additions and slight modifications.

## Units

We work in natural units, where

$$\hbar = c = 1 . \quad (1.1)$$

In this system,

$$[\text{length}] = [\text{time}] = [\text{energy}]^{-1} = [\text{mass}]^{-1} . \quad (1.2)$$

Also, we define

$$k_B = 1 , \quad (1.3)$$

which implies

$$[\text{temperature}] = [\text{energy}] . \quad (1.4)$$

## Tensors

We work exclusively in Euclidean space. The four-dimensional metric tensor is

$$g_{\mu\nu} = g^{\mu\nu} = \text{diag}(1, 1, 1, 1) , \quad (1.5)$$

with greek indices running over 0, 1, 2, 3 or ( $\tau \equiv it$ ),  $x, y, z$ . Roman indices  $i, j$ , etc. denote spatial components. Pairs of repeated indices are summed in all cases.

We use roman indices  $i, j, k$  also to label lattice sites and index pairs to label links. Where the difference from vector and matrix elements does not follow directly from the context, we will mention it explicitly in the text.

Four-vectors and numbers are denoted by light italic type. Three-vectors are written in boldface type. We will distinguish between covariant and contravariant four-vectors, even though their components are the same in this metric. For example:

$$x^\mu = (x_0, \mathbf{x}), \quad x_\mu = g_{\mu\nu} x^\nu = (x_0, \mathbf{x}) ; \quad (1.6)$$

$$p \cdot x = g_{\mu\nu} p^\mu x^\nu = p_0 x_0 + p_i p_i = p_0 x_0 + \mathbf{p} \cdot \mathbf{x} \quad (1.7)$$

## Group theory

For all matrices which are elements of the special unitary group  $SU(N)$ , we define the *normalized trace*  $\text{tr } U$  (written in lower-case) as

$$\text{tr } U = \frac{1}{N} \text{Tr } U, \quad U \in SU(N), \quad (1.8)$$

where  $\text{Tr } U$  is the *actual trace* without any normalization factors. The summation convention applies for repeated group indices. These are written as roman letters a, b, c. We use a definition of unitary groups with Hermitian generators throughout most of this work. The single exception is section 5.1 where anti-Hermitian generators are used for better readability.

We have chosen to introduce group theoretical concepts relevant to this work in detail in appendix A, separate from the main text to not interrupt the reader who is thoroughly familiar with them. All  $SU(2)$  matrices considered in this work are parameterized by the *quaternionic parameterization* (see eq. A.22 and following).

## Lattice particulars

This work aims at investigating a lattice model in its own right. Thus throughout most parts of this work, the lattice spacing will be set to one.

For a function  $f$  of a field  $L(\mathbf{x})$ , defined on a three dimensional lattice, we denote the *ensemble average* with angular brackets:

$$\langle f(L) \rangle = \int \prod_n [dL_n] f(L) e^{-S(L)}. \quad (1.9)$$

Here the product runs over all lattice sites. *Volume averages* are marked with a bar

$$\bar{L} = \frac{1}{N_S^3} \sum_i L_i. \quad (1.10)$$

Here the sum runs over all sites and  $N_S$  is the spatial extent of the cubic lattice.

## 2 Introduction

### 2.1 Quantum Chromodynamics

It is a well established fact today, that strongly interacting particles (*hadrons*) such as the proton and the neutron, which are the building blocks of atomic nuclei, are not elementary particles, but possess a sub-structure on length scales smaller than approximately  $10^{-15}$  meters and are in fact bound states of smaller constituents. These constituents are spin-1/2 fermions called *quarks* and spin-1 gauge bosons, called *gluons*, which mediate the force that quarks exert on each other. The quantum field theory which describes the interactions of quarks and gluons is called *Quantum Chromodynamics*<sup>1</sup> (QCD) [3, 4, 5]. It is similar to the theory of electromagnetism, or the respective quantum field theory *Quantum electrodynamics* (QED), in the sense that the fundamental matter fields are described by *Dirac spinors*, which carry a charge and which interact by minimal coupling to quantized vector fields.

What distinguishes QCD from QED are essentially two things: Firstly, instead of having only one charge that can have a positive or a negative sign, in QCD there are three charges together with their negative counterparts. These are called *color charges* and often labeled as red, green and blue in a loose analogy to the *additive color model* which describes how humans perceive overlapping projected light<sup>2</sup>. Secondly, the gauge bosons of QCD themselves carry color charge and thus also interact with each other. This is in stark contrast to electromagnetism, where the gauge bosons, in this case the photons, are blind to each other if quantum loops are neglected and thus can be described by linear equations in the classical limit.

Free color charges are not observed in our everyday low energy world. The color charges in the bound mesonic and baryonic states, which are found in nature or produced in collider experiments, cancel each other yielding a color neutral state. This is known as *confinement* and is a feature of QCD, which to this day cannot be derived from first principles, but is believed to be generated by the gluon-gluon interaction. A number of QCD inspired models, such as the string model or the MIT bag model, as well as numerical results from simulations in discretized space-time (lattice QCD) have generated much confidence in the confinement hypothesis.

The LAGRANGE density of QCD (with a EUCLIDEAN metric) is

$$\mathcal{L} = \sum_{i=1}^{N_f} [\bar{\psi}_i(x)(\gamma^\mu \partial_\mu - ig\gamma^\mu A_\mu^a(x)G^a + M_i)\psi_i(x)] - \frac{1}{4}F_a^{\mu\nu}F_{\mu\nu}^a, \quad (2.1)$$

where  $N_f$  labels the number of quark flavors. The field strength tensor  $F_a^{\mu\nu}$  is related to the vector potential through

$$F_a^{\mu\nu} = \partial_\mu A_\nu^a - \partial_\nu A_\mu^a + g f_{abc}A_\mu^b A_\nu^c, \quad (2.2)$$

<sup>1</sup>*Chromos* is greek for *color*.

<sup>2</sup>Aside from this analogy, the color charge is completely unrelated to the familiar phenomenon of color.

where  $f_{abc}$  are the structure constants of the special unitary group  $SU(3)$ . The indices  $a, b, c$  label the generators of the group, for which the commutation relation

$$[G^a, G^b] = if^{abc}G^c, \quad (2.3)$$

holds. The gluon self interaction is generated by the non-abelian contribution to the field strength tensor  $\sim A_\mu^b A_\nu^c$ . In the 1970s DAVID POLITZER [5], FRANK WILCZEK and DAVID GROSS [4] calculated the *beta function* of QCD, which encodes the renormalization scale dependence of the coupling constant. To one loop order in perturbation theory, it is given by

$$\beta(g) = \mu \frac{\partial g}{\partial \mu} = -\frac{g^3}{16\pi^2} \left[ \frac{11}{3}N_c - \frac{2}{3}N_f \right], \quad (2.4)$$

where  $N_c$  is the number of colors. This corresponds to a running coupling constant, which in terms of the momentum scale  $Q^2$  is given by

$$\frac{g^2(Q^2)}{4\pi} = \frac{4\pi}{(11N_c/3 - 2N_f/3) \log(Q^2/\Lambda_{QCD}^2)}. \quad (2.5)$$

For large momentum transfer the coupling constant becomes small. This feature, which is known as *asymptotic freedom*, implies that processes involving only high momentum or short distance are well described by the perturbative expansion. Furthermore, it implies that the thermodynamics of a quark-gluon system at very high temperatures is well described by the equation of state of an ideal gas of non-interacting quarks and gluons. It has therefore been speculated that for certain values of the temperature or pressure, a *deconfining phase transition* occurs where quarks and gluons are liberated. A deconfined state of matter could have existed in the early universe, could be produced in heavy-ion collisions and could exist in the core of neutron stars.

Today the evidence, from heavy-ion experiments as well as lattice simulations, model calculations, empirical nuclear physics and perturbative calculations in asymptotic regimes, overwhelmingly supports the scenario that quarks and gluons are deconfined for energy densities larger than  $1 - 10 \text{ GeV}/fm^3$ , which is of the order of that of matter inside a proton [6, 7, 8, 9]. A contemporary view of the phase diagram of QCD in the plane spanned by the temperature  $T$  and the baryo-chemical potential  $\mu_B$  (which is related to the baryon density) is shown in Fig. 2.1. The deconfining phase transition for finite  $\mu_B$  and zero  $T$  is believed to be of first order. In contrast, the  $\mu_B = 0$ , finite  $T$  phase transition is not a *real* phase transition, in the sense that it exhibits discontinuities of an order parameter, but rather a cross-over where the thermodynamic quantities change rapidly over a small parameter range. The line across which the first order phase transition occurs is speculated to end in a critical point, the exact location of which has yet to be determined.

## 2.2 The pure gauge limit and the Wilson criterium

Confinement in QCD is a strictly non-perturbative phenomenon. At an intuitive level this can be understood by considering how a weak-coupling perturbative expansion works: At the lowest order approximation in perturbation theory, particles are treated as if they can

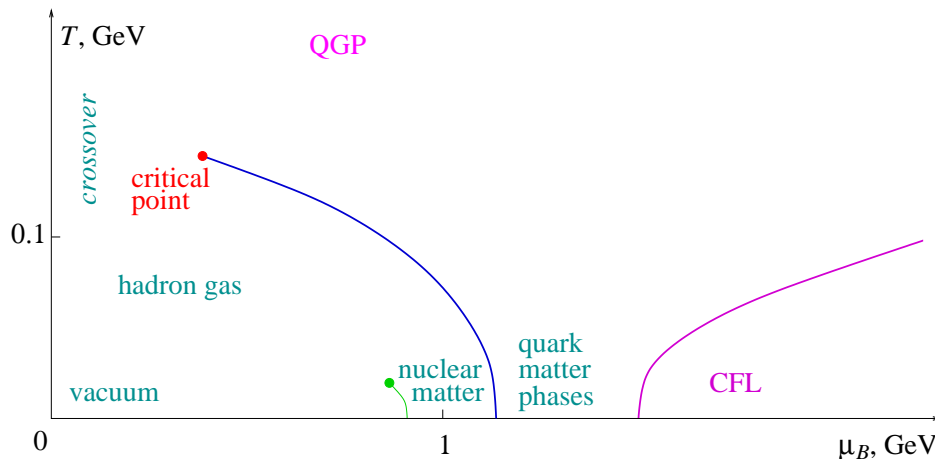


Figure 2.1: A semi-quantitative sketch of the QCD phase diagram. Figure taken from Ref. [7].

propagate completely undisturbed through space-time. Interactions are introduced as a disturbance, which successively becomes stronger when higher orders of the approximation are included. The idea is that most of the dynamics of the system can be understood in terms of the free propagation, while interactions are small corrections. For confined QCD however, the observed state bears no resemblance whatsoever to the free solution. Furthermore, the running coupling constant suggests that at low energies the coupling constant becomes very large, so that rather than being a roughly non-interacting system with some corrections, the system is completely dominated by the interactions.

A non-perturbative way to describe the confined phase of QCD in the limit of infinitely massive quarks was formulated by WILSON [10]. In this limit quarks are “frozen”, in the sense that they act only as static sources of color flux and there is no production of quark anti-quark pairs. The dynamics is then completely determined by the gluonic sector. Wilson calculated the quantum mechanical vacuum expectation value of the propagation of a heavy pair of external test quarks and anti-quarks by computing closed loop integrals in the pure gauge theory. He found that a static potential between a quark and an anti-quark, which rises linearly at large distances, exists at low energies. Although a complete solution to the physical problem of confinement must necessarily also include dynamical quarks and pair production, the existence of a confinement potential in the pure gauge theory is generally taken as evidence that a similar type of potential should be present also with dynamical quarks. Indeed, lattice results for dependence of the quark susceptibilities [11] and the pressure [12, 13] on the number of dynamical flavors suggest that the gluonic sector is a crucial driving force for the confining phase transition. In the pure gauge theory, the order parameter for the deconfining phase transition can be characterized exactly [14, 15, 16] as the normalized trace of an operator  $\mathbf{L}(\mathbf{x})$

$$\ell(\mathbf{x}) = \text{tr } \mathbf{L}(\mathbf{x}) = \text{tr } \mathcal{P} \exp \left( ig \int_0^{1/T} d\tau A_0(\mathbf{x}, \tau) \right), \quad (2.6)$$

where  $\mathbf{L}(\mathbf{x})$  is called the *thermal WILSON line*. It is the exponential of a path ordered integral that wraps around the periodic boundary of the Euclidean time direction of finite temperature field theory and integrates the time-like component of the gluonic vector potential.  $\ell(\mathbf{x})$  is called the *POLYAKOV loop* and measures the free energy of a static quark [17, 18, 19]

$$\langle |\text{tr } \mathbf{L}(\mathbf{x})| \rangle \sim e^{-\frac{F_q}{T}} . \quad (2.7)$$

In the deconfined phase the POLYAKOV loop acquires a non-zero expectation value but vanishes in the confined phase<sup>3</sup> [20]. The transition is of second order for two colors [21, 22, 23], of first order for  $N_c = 3$  [24, 25] and becomes more strongly first order with rising  $N_c$ . It becomes a cross over only when light quarks are included, however an approximate  $T_c$  can then still be defined. The POLYAKOV loop is a bare quantity and must be renormalized in order to obtain a non-zero continuum limit [26, 27, 28, 29, 30, 31].

### 2.3 The strongly coupled quark gluon plasma

At the Relativistic Heavy Ion Collider (RHIC) at Brookhaven National Labs in ultra-relativistic heavy-ion collision experiments temperatures on the order of two times the QCD critical temperature,  $T_c \sim 190 \text{ MeV}$ , were created. Early data from RHIC indicated that the created state of matter behaved more like a strongly coupled fluid, than a plasma of weakly interacting partons [32, 6, 33]. This suggests that non-perturbative effects dominate near  $T_c$ , even in the deconfined phase (see also Ref. [34]). Formal evidence for this scenario can be obtained in a number of ways. It is convenient to plot what is known as the “interaction measure”

$$\Theta(T) = \frac{\varepsilon(T) - 3p(T)}{T^4} , \quad (2.8)$$

where  $\varepsilon$  is the energy,  $p$  is the pressure and  $T$  is the temperature. This is sometimes also referred to as the “trace anomaly” since it is equal to the trace of the energy momentum tensor, divided by  $T^4$ .  $\Theta(T)$  is a dimensionless number that quantifies the deviation from an ideal gas equation of state. Lattice results for  $N_c = 2$  [22] and  $N_c = 3$  [24] in the pure gauge theory indicate that  $\Theta(T)$  is rather large up to  $T \approx 3T_c$  in both cases. In Fig. 2.2 we show the  $SU(3)$  pure glue results. It can be seen that  $\Theta(T)$  is very small below  $T_c$  then rises steeply around  $T_c$  and trails off slowly at larger temperatures.

The naive weak-coupling perturbative expansion for the QCD pressure is known to fail at temperatures on the order of  $10^5 \text{ GeV}$ , which corresponds to roughly  $5 \cdot 10^5 T_c$  and is orders of magnitude higher than the temperatures generated at RHIC or LHC [35]. However, various programs to reorganize the weak-coupling perturbative series to increase its radius of convergence and extend its validity to lower temperatures exist [35, 36]. One successful approach has been the addition of a variational mass parameter to the bare Lagrangian. This is known as Hard-Thermal-Loop (HTL) perturbation theory [37, 38, 39, 40, 41]. In Fig. 2.3 the HTL results for the pressure of a gluon gas, divided by the pressure of an ideal

<sup>3</sup>As we will discuss in detail in the following chapters of this work, this phase transition is related to the spontaneous breaking of a global  $Z(N)$  symmetry.

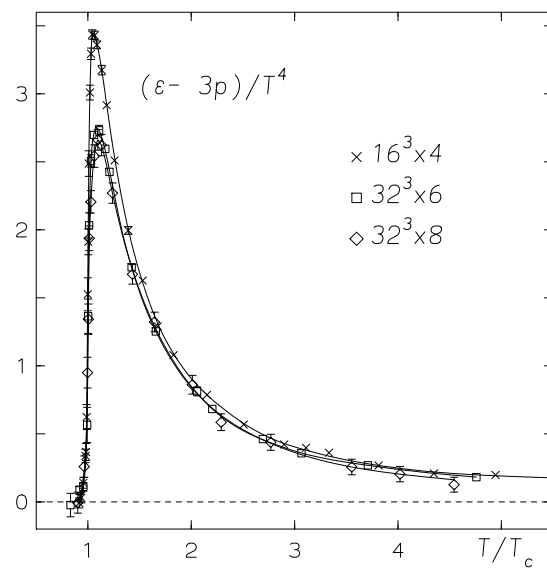


Figure 2.2: Interaction measure in  $SU(3)$  pure gauge theory. Figure taken from Ref. [24].

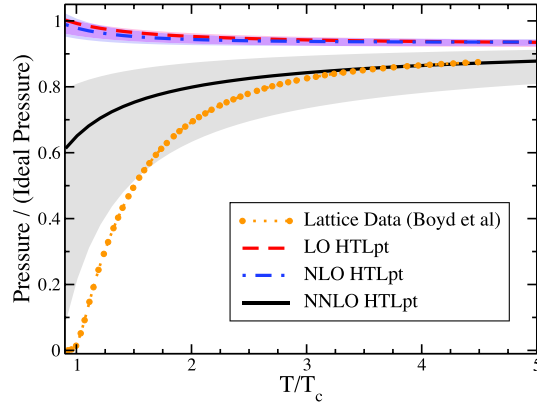


Figure 2.3: Hard thermal loop and lattice results for pressure of  $N_c = 3$  gluon gas, scaled by the pressure of an ideal bose gas. Figure taken from Ref. [37].

bose-gas, at leading order (LO), next to leading order (NLO), and next to next to leading order (NNLO) are shown, in comparison to the lattice results of  $4D$   $SU(3)$  pure gauge theory. The error band indicates variations of the renormalization scale. The NNLO results seem to describe the pressure extremely well, down to temperatures of  $T \approx 2T_c$ . Below  $2T_c$ , in the same region where the interaction measure peaks, however, the deviations from the lattice results are huge. The HTL results for the entropy density [37] exhibit a similar behavior. The magnitude of the deviation at NNLO suggests that the problem may not be solved by simply going to higher order loop calculations. Moreover, as we will discuss in the following chapters, the perturbative method is based on assumptions that violate a symmetry of the  $SU(N)$  pure gauge theory, so a breakdown of perturbation theory at some point is expected.

More evidence for the shortcomings of perturbation theory close above  $T_c$  comes from numerical and analytical computations of the ratio of screening masses defined from two-point correlation functions of the real and the imaginary part of the POLYAKOV loop [42, 43]. The ratio  $m_i/m_r$  changes from  $3/2$  at high temperatures (which is the leading order result from perturbation theory) to  $m_i/m_r \approx 3$  near  $T_c$ .

## 2.4 Effective theories

Aside from numerical simulations and perturbative calculations in full QCD or YANG-MILLS theory, there are also effective theory approaches. The underlying principle of these is that in different limits of the full theory (extremely high or low temperatures, close to the phase boundary or far from it) the dynamics is dominated by very different aspects of the full theory, such that it is sensible to use an effective description in terms of the specific degrees of freedom that are relevant in this particular regime, which is stripped of all features that play no dominant role for this case. Such theories also often have a different number of space-time dimensions than the full theory. Once such a theory has been constructed, it can then again be studied analytically by perturbative expansion in an appropriate small parameter, or numerically by lattice simulations. For QCD, a common approach is to exploit universality [15] to construct a theory in terms of POLYAKOV loop spin variables



[44, 45, 46, 47, 48, 49]. In this work we perform lattice simulations of a matrix model of the thermal WILSON line  $\mathbf{L}(\mathbf{x})$ , which was proposed by PISARSKI [50, 51, 52]. The theory is defined in three dimensional space and is constructed to respect all symmetries of the underlying pure gauge theory. It is valid from the high temperature limit all the way down to  $T_c$ , even in the range between  $T_c$  and  $T \approx 2T_c$  where perturbation theory fails. We currently focus on the gauge group  $SU(2)$  instead of  $SU(3)$ , since the group manifold has a simpler structure, which reduces the complexity of the simulation algorithm greatly and allows for results to be obtained with high numerical precision. Aside from these practical considerations however, there are also physical reasons to be interested in  $SU(2)$  specifically: It appears that a deconfining phase transition is a universal feature of  $SU(N)$  gauge theories and thus much effort has gone into the study of the dependence of various thermodynamic observables on the number of colors [53, 44, 50]. Furthermore, the first order phase transition in  $N = 3$  gauge theory is of very weak first order [24, 25], such that it is close to the second order transition known to occur for two colors.

## 2.5 Outline of this work

This work is structured as follows:

In chapter 3 we start by discussing in general terms the method of dimensional reduction. Then we introduce the three dimensional effective theory of the WILSON line  $\mathbf{L}(\mathbf{x})$  which is studied in this work, motivate the different terms that enter into the Lagrangian and discuss how the theory is related to the usual three dimensional effective theory EQCD. We discuss how non-perturbative effects are introduced into the effective theory.

In chapter 4 we explain the basics of the lattice simulation techniques which are used throughout this work. We start by introducing the underlying principles of Monte Carlo simulations using MARKOV chains. We then discuss the METROPOLIS algorithm, the heat bath methods of CREUTZ and those of KENNEDY and PENDLETON, as well as over-relaxation techniques. We then proceed to derive a lattice action for the effective theory from the continuous LAGRANGE density in chapter 5.

In chapter 6 we present results, which were obtained in a limiting case of the theory where the spatial magnetic sector is neglected. We introduce different order parameters of the model and study the phase diagram of the theory in detail. We present mean field results for the deconfined phase of the model and compare them to simulation. We compute two point functions and respective correlation lengths to confirm the second order phase transition and the presence of GOLDSTONE modes in the confined phase. We then proceed to study the distribution of eigenvalues and show that in certain parts of the phase diagram confinement is driven by eigenvalue repulsion. We also confirm that weak repulsion of eigenvalues exists in the deconfined phase close to the phase boundary. The material found in this chapter is published in part in Ref. [54].

In chapter 7 we present results obtained in the full theory with gauge fields. We first present a study of the phase diagram of the theory, by measuring POLYAKOV loops, susceptibilities and two-point correlation functions. We study also magnetic observables such as the average WILSON action and the spatial string tension. We then extract an effective potential for the POLYAKOV loop at a single site, as well as of for “block spins” where the loops were averaged over small volumes in different regions of the phase diagram. We

discuss in detail how these potentials may be parameterized. The material is published in part in Refs. [55, 56].

Chapter 8 summarizes our attempts to compare the  $3D$  effective theory to full YANG-MILLS theory in four dimensions. We then conclude and offer a short outlook in chapter 9. The appendices contain a summary of cross checks with existing literature and a collection of the group theoretical concepts which are used throughout this work.

## 3 Center symmetric effective field theory

### 3.1 Dimensional reduction

The use of three dimensional effective theories to calculate static quantities such as the pressure or screening lengths of a quantum field theory at finite temperatures has a long history [57, 58, 59, 60, 61, 62]. The underlying principle is the expansion of a field in terms of MATSUBARA *frequencies*. Consider a generic field  $\Phi$  with a LAGRANGE density  $\mathcal{L}(\Phi, \partial_\mu \Phi)$ . Its thermodynamic properties are given by the partition function  $Z$ , which is computed in the imaginary time formalism as a functional integral

$$Z = N \int_{\text{periodic}} [d\Phi] \exp \left( \int_0^\beta d\tau \int d^3x \mathcal{L} \right), \quad (3.1)$$

where  $N$  is a normalization constant. For a bosonic field  $\Phi$  the integral runs over all field configurations which are periodic in the EUCLIDEAN imaginary time direction<sup>1</sup>

$$\Phi(\mathbf{x}, \beta) = \Phi(\mathbf{x}, 0) \quad \forall \mathbf{x}. \quad (3.2)$$

The field can be FOURIER expanded as

$$\Phi(\mathbf{x}, \tau) = \sqrt{\beta} \sum_n \int dp \Phi_n(p) e^{i\mathbf{p}\mathbf{x} + i\omega_n \tau}, \quad (3.3)$$

where due to the constraint of periodicity in  $\tau$  the expansion in the time-like direction is a discrete sum rather than an integral. The  $\omega_n$  are called MATSUBARA frequencies and are given by

$$\omega_n = 2\pi nT. \quad (3.4)$$

This suggests that a thermal field theory of a single field  $\Phi$  in  $d+1$  dimensions is equivalent to a EUCLIDEAN field theory in  $d$  dimensions with infinitely many fields, namely the individual time-like FOURIER modes of  $\Phi$ . One can calculate the free propagator in momentum space for each individual mode [63, 64]. For the  $n$ -th component of the field  $\Phi$  it is given by

$$\Delta(\omega_n, \mathbf{p}) = \frac{1}{p^2 + \omega_n^2}. \quad (3.5)$$

Thus the MATSUBARA frequencies act like masses, by shifting the pole of the propagator. From (3.4) it follows that the static  $n = 0$  mode is massless, while all non-static modes have a mass  $\sim T$ .

---

<sup>1</sup>Fermions are anti-periodic. We do not consider them here however.

One can now construct an effective theory for the three-dimensional static  $n = 0$  mode by integrating out all non-static modes (as well as any present Fermionic fields). By the theorem of APPELQUIST and CARAZZONE [65] the non-static modes decouple from the dynamics on length scales  $\gg 1/T$  (see also Refs. [66, 67, 68, 69, 70]) and contribute only to the parameters of the three-dimensional theory. Such theories generally contain many interaction terms, the parameters of which must be determined by a matching procedure to the full theory.

The reduction procedure can also be applied to (ABELian and non-ABELian) gauge theories. For  $SU(3)$  YANG-MILLS theory, one can construct an effective theory in terms of the electrostatic field  $A_0^a(\mathbf{x})$ , which behaves like a scalar field in the adjoint representation of the gauge group and of the magneto-static fields  $A_i(\mathbf{x})$ . This effective theory is known as *electrostatic QCD* (EQCD) and is defined by the LAGRANGE density

$$\mathcal{L}^{\text{eff}} = \frac{1}{2} \text{tr} F_{ij}^2 + \text{tr} |D_i A_0|^2 + m_D^2 \text{tr} A_0^2 + \dots \quad (3.6)$$

It has been successfully applied to calculations of the free energy and the pressure in the high temperature limit. However, as we will discuss in the following sections, the assumption of static  $A_0^a(\mathbf{x})$  violates a symmetry of the underlying YANG-MILLS theory, which leads to the breakdown of (3.6) close to  $T_c$ . We will then proceed to discuss an alternative to the explicit reduction procedure for the construction of an effective theory in three dimensions that respects all of the symmetries.

## 3.2 Symmetries of $SU(N)$ Yang-Mills theory

The action of  $SU(N)$  YANG-MILLS theory, which is given by

$$S = -\frac{1}{4} \int_0^\beta d\tau \int d^3x F_a^{\mu\nu} F_{\mu\nu}^a, \quad F_a^{\mu\nu} = \partial_\mu A_\nu^a - \partial_\nu A_\mu^a + g f_{abc} A_\mu^b A_\nu^c, \quad (3.7)$$

is invariant under certain types of local gauge transformations

$$A_\mu(x) \mapsto s(x)(A_\mu(x) + i\partial_\mu)s(x)^\dagger, \quad s(x) \in SU(N). \quad (3.8)$$

Firstly, it is invariant under transformations which are strictly periodic in the EUCLIDEAN time direction:

$$s(\mathbf{x}, \beta) = s(\mathbf{x}, 0) \quad \forall \mathbf{x}. \quad (3.9)$$

However, in addition there is also an invariance under transformations which are periodic only up to a global “twist” factor  $z$ , which is an element of the  $Z(N)$  center of the  $SU(N)$  gauge group, i.e. transformations of the form

$$s(\mathbf{x}, \beta) = z s(\mathbf{x}, 0) \quad z \in Z(N). \quad (3.10)$$

The POLYAKOV loop

$$\ell(\mathbf{x}) = \frac{1}{N} \text{Tr} \mathbf{L}(\mathbf{x}), \quad \text{with} \quad \mathbf{L}(\mathbf{x}) = \mathcal{Z}_R^{-1} \mathcal{P} \exp \left( ig \int_0^{1/T} d\tau A_0(\mathbf{x}, \tau) \right), \quad (3.11)$$

which we introduced in the previous chapter is an order parameter for the spontaneous breaking of the global  $Z(N)$  center symmetry. This can be seen, by considering that the thermal WILSON line  $\mathbf{L}(\mathbf{x})$  is a parallel transporter<sup>2</sup> in the time direction, which transforms under  $s(x)$  as

$$\mathbf{L}(\mathbf{x}) \mapsto s(\mathbf{x}, \beta) \mathbf{L}(\mathbf{x}) s(\mathbf{x}, 0) . \quad (3.12)$$

Thus, due to the cyclic property of the trace, under “twisted” transformations the POLYAKOV loop  $\ell(\mathbf{x})$  transforms as

$$\ell(\mathbf{x}) \mapsto z \ell(\mathbf{x}) . \quad (3.13)$$

If the expectation value of  $\ell(\mathbf{x})$  is non-zero, then the transformation (3.13) changes the vacuum state. Since

$$\langle |\text{tr } \mathbf{L}(\mathbf{x})| \rangle \sim e^{-\frac{F_q}{T}} , \quad (3.14)$$

the theory possesses  $N$  degenerate ground states with the same free energy  $F_q$ , which are obtained from each other by such  $Z(N)$  center transformations.

### 3.3 Center symmetric effective theory of Wilson lines

The discussion of the previous section suggests that the full dynamics of  $SU(N)$  YANG-MILLS theory is influenced by the presence of the  $Z(N)$  ground states. However, if for a certain range of temperatures the  $Z(N)$  symmetry is strongly broken, such that tunneling between the different states can be neglected, then it is reasonable in this regime to expand around one specific ground-state. Perturbative methods such as the Hard-Thermal-Loop formalism discussed in chapter 2 exploit this: In HTL one expands around a state where  $A_0/T \ll 1$ , which corresponds to the  $Z(N)$  ground-state where  $\mathbf{L} \sim \mathbf{1}$ . The effective theory EQCD (3.6) is based on the assumption of static  $A_0$  fields, which again corresponds to a system that is “frozen” in a specific  $Z(N)$  state. Such theories should fail however, when fluctuations between  $Z(N)$  ground states become relevant.

Consider Fig. 3.1. It shows numerical results for renormalized  $SU(3)$  POLYAKOV loops (obtained by GUPTA et al, see Ref. [31]). The figure shows a broad range of temperatures, starting from  $T_c$  upward. The expectation value of POLYAKOV loop  $\langle \ell \rangle$  is close to one at high temperatures<sup>3</sup>, which indicates a suppression of  $Z(N)$  tunneling. For temperatures below  $\approx 3T_c$  it is non-zero but drops far below one, down to  $\langle \ell \rangle \approx 0.5$  right above  $T_c$ . Therefore, in the region close above  $T_c$  the dynamics should be heavily influenced by non-perturbative fluctuations. This is in agreement with discussions in section 2.3, where we presented evidence for the failure of perturbative methods for  $T_c < T \lesssim 3T_c$ . Correspondingly, in this region the interaction measure is large.

As an alternative to the explicit integration of non-static field modes, several authors have discussed the construction of effective field theories by identifying appropriate degrees of

<sup>2</sup>A detailed introduction into the concept of parallel transport is found in Chapter 5. There we will also discuss the transformation law of  $\mathbf{L}(\mathbf{x})$  in detail.

<sup>3</sup>Actually one can see that  $\langle \ell \rangle$  is slightly larger than one for large temperatures, which is a well understood systematic error that stems from the fact that Ref. [31] calculates the renormalization to one loop order. The full result should yield an expectation value which is bounded by one from above.

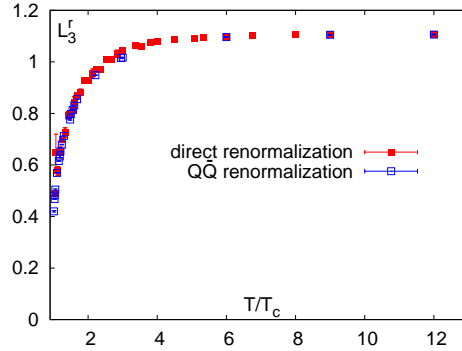


Figure 3.1: Renormalized  $SU(3)$  POLYAKOV loop for  $T > T_c$ . Figure taken from Ref. [31]

freedom of the underlying theory, from which terms that respect all of the symmetries of the full theory can be constructed, writing down Lagrangians containing such terms only and imposing the condition that correlation functions of the underlying theory should be reproduced at large distances [35, 71, 72, 73, 74]. In the case of QCD, this has led to investigations of effective theories of POLYAKOV loops, considered as  $Z(N)$  spin variables, as well as theories for the thermal WILSON line as a  $SU(N)$  matrix model [75, 50, 51, 52].

We study an effective theory of the thermal WILSON line, coupled to the static gauge sector which was first proposed in Ref. [51]. The kinetic energy contribution to the Lagrangian from the three dimensional magnetic fields is simply

$$\mathcal{L}_{\text{mag}}^{\text{eff}} = \frac{1}{2} \text{tr} F_{ij}^2, \quad (3.15)$$

which is of the same form as in (3.6). However, due to the  $Z(N)$  center symmetry the effective electric field cannot simply be  $E_i(\mathbf{x}) \sim D_i A_0(\mathbf{x})$  [51, 76, 77, 78]. As shown in Ref. [51] the effective electric field for arbitrary  $A_0$  is given by

$$E_i(\mathbf{x}) = \frac{T}{ig} \mathbf{L}^\dagger(\mathbf{x}) D_i(\mathbf{x}) \mathbf{L}(\mathbf{x}). \quad (3.16)$$

This leads to a three dimensional theory, which in the classical limit is given by

$$\mathcal{L}_{\text{cl}}^{\text{eff}} = \frac{1}{2} \text{tr} F_{ij}^2 + \frac{T^2}{g^2} \text{tr} |\mathbf{L}^\dagger D_i \mathbf{L}|^2. \quad (3.17)$$

However, quantum corrections also introduce a potential term for the WILSON line. It was obtained to one-loop order, by computing the fluctuation determinant in a constant background  $A_0$  (or  $\mathbf{L}$ ) field in Ref. [79], and is of the form

$$\mathcal{L}_{1\text{-loop}}^{\text{eff}} = -\frac{2}{\pi^2} T^4 \sum_{n \geq 1} \frac{1}{n^4} |\text{tr} \mathbf{L}^n|^2. \quad (3.18)$$

This potential is evidently minimized by the perturbative vacuum, where the WILSON line is  $\mathbf{L} \sim \mathbf{1}$ .

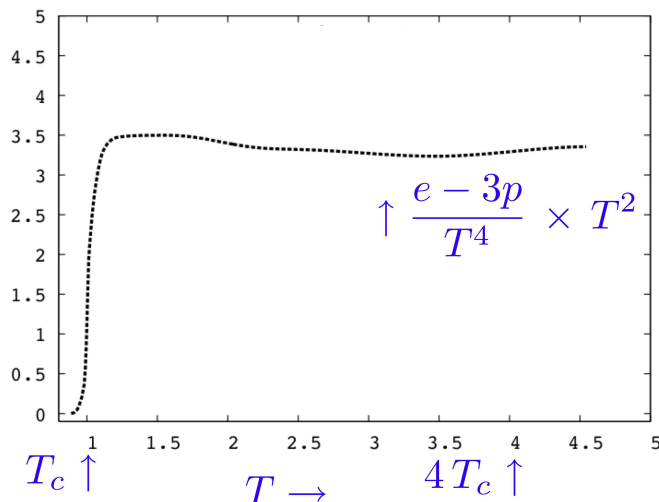


Figure 3.2: Figure taken from Ref. [80]

To generate non-perturbative fluctuations and induce a phase transition, additional terms must be added. While a large variety of terms are conceivable, a simple ansatz for the non-perturbative effects is motivated by the form of the interaction measure  $\Theta(T)$  in the deconfined phase [22, 24]. Consider Fig. 3.2. There we show

$$T^2\Theta(T) = \frac{\varepsilon(T) - 3p(T)}{T^4} T^2. \quad (3.19)$$

One can see that  $T^2\Theta(T)$  is essentially constant above  $T_c$ . This observation has led to the conclusion that the pressure of QCD in the deconfined phase can be expanded in a power series in  $1/T^2$  times the ideal  $T^4$  term

$$p(T) \approx f_{\text{pert}} T^4 - B_{\text{fuzzy}} T^2 - B_{\text{MIT}} + \dots. \quad (3.20)$$

This has been labeled the “fuzzy” bag model [80]. Here  $f_{\text{pert}}$  is dimensionless,  $B_{\text{MIT}}$  is the usual MIT bag constant of mass dimension four, and  $B_{\text{fuzzy}}$  is a “fuzzy” bag constant with mass dimension two (which can be ignored in the high temperature limit). The model (3.20) suggests that the simplest ansatz for the non-perturbative contributions in the effective theory is a term of the form

$$\mathcal{L}_{\text{non-pert.}}^{\text{eff}} = B_f T^2 |\text{tr } \mathbf{L}|^2. \quad (3.21)$$

Effective theories containing contributions such as (3.21) have hence been considered by several authors [81, 51, 82, 83, 84, 85]. There are also attempts to calculate transport properties in a “semi” quark gluon plasma, which assume non-perturbative terms of mass dimension two [86, 87]. At sufficiently low temperature, (3.21) dominates over the perturbative potential and induces a transition to a confined phase with  $\langle \text{tr } \mathbf{L} \rangle = 0$ . It was further suggested in [51] that terms such as (3.21) lead to “repulsion” of eigenvalues of the WILSON line in some temperature range above  $T_c$ . In other words, such terms drive the  $N$  distinct complex eigenvalues of  $\mathbf{L}$ , which lie on the complex unit circle, to maximize their respective distances from one another.

So finally, the complete Lagrangian of the effective theory studied in this work is given by

$$\mathcal{L}^{\text{eff}} = \frac{1}{2} \text{tr} F_{ij}^2 + \frac{T^2}{g^2} \text{tr} |\mathbf{L}^\dagger D_i \mathbf{L}|^2 - \frac{2}{\pi^2} T^4 \sum_{n \geq 1} \frac{1}{n^4} |\text{tr} \mathbf{L}^n|^2 + B_f T^2 |\text{tr} \mathbf{L}|^2 . \quad (3.22)$$

It is defined with a spatial cutoff on the order of the inverse temperature, is non renormalizable in three dimensions<sup>4</sup> and is valid only over distance scales larger than  $1/T$ . We shall focus in particular on measuring the eigenvalue distribution above and at the deconfining phase transition to test the presence of eigenvalue repulsion in the phase transition region, and on obtaining a parameterization for the effective potential of the POLYAKOV loop, which arises from the dynamics.

---

<sup>4</sup>A related renormalizable theory has been formulated in refs. [88, 71]. Ref. [89] derived the relations between lattice and continuum theories to leading order in lattice perturbation theory.



## 4 Lattice simulation

The idea to formulate finite temperature quantum field theory in general, and QCD in particular, on a discretized space-time lattice and to obtain non-perturbative information from such a formulation via Monte-Carlo simulations dates back to the early 1970s and was pioneered by WILSON, WEGNER, POLYAKOV, CREUTZ and several others who we cannot possibly all mention here. The principle idea, which rests upon the solid bedrock of the FEYNMAN path integral formalism, is rather simple: A field, which is a continuous function of space-time, is approximated by a finite set of field variables, which are chosen to lie on the points (*sites*) or links of a space-time grid (*lattice*) with finite spacing. The lattice acts as a regulator and removes all field modes with wavelengths smaller than twice the lattice spacing. For any fixed value of the lattice coupling, which defines a bare coupling constant at the finite spacing, numerical estimates for bare observables are obtained by approximating the functional integral for the partition function by a finite number of representative lattice configurations, which are generated by appropriate algorithms. Physical results for the continuum theory are then obtained via a limiting procedure, where the lattice spacing is taken to zero.

We do not discuss the entire formal derivation of the method here. The subject has been reviewed excessively in literature and several excellent textbook treatments exist (see e.g. Refs. [2, 90, 91] and [92]). We rather take a practical approach: In this chapter we *assume* that a quantum field theory has been formulated on a finite lattice with a fixed spacing in such a way, that the action  $\mathcal{S}$  can be written as a function of the lattice field variables and that the continuum LAGRANGE density is reproduced when the lattice spacing vanishes. We also assume that the number of coupling constants is finite. We proceed to discuss general technical issues regarding the generation of representative lattice configurations for the *thermal ensemble* defined by the action  $\mathcal{S}$  via MARKOV chains. In the following chapter we then present a detailed derivation of the lattice action for the theories studied in this work.

We follow mostly the treatment of Refs. [2] and [92] in this chapter and often restrict ourselves to summarizing definitions and concepts without lengthy derivations. However, we describe in detail the updating algorithms which we use throughout this work to simulate 4D YANG-MILLS theory and the 3D effective theory of WILSON lines introduced in the previous chapters.

### 4.1 Markov Chain Monte Carlo

Let us consider the calculation of an expectation value of an observable  $\mathcal{O}$  in a thermal ensemble defined by a fixed set of external parameters  $g_i$ . For a system with a finite number of micro-states  $K$  (in our case the *lattice configurations*) the expectation value is given by

the sum

$$\langle \mathcal{O} \rangle = Z^{-1} \sum_{k=1}^K \mathcal{O}^{(k)} e^{-\mathcal{S}(g_i)^{(k)}} \quad (4.1)$$

where

$$Z = Z(g_i) = \sum_{k=1}^K e^{-\mathcal{S}(g_i)^{(k)}} \quad (4.2)$$

is the partition function. The index  $k$  labels all configurations. It is in principle conceivable that, given an infinite amount of computing time, an expression such as (4.1) could be evaluated exactly. It becomes immediately clear however, that in practice an exact evaluation is impossible. If we take the simplest possible non-trivial space of field variables, an ISING *model* where each lattice site is assigned a value  $\pm 1$ , then for a modest cubic lattice of side-length  $N_s = 10$  the sum in (4.2) has  $2^{1000}$  terms. Barring a revolutionary breakthrough in quantum computing, no computer that we can ever hope to build could compute a perceptible fraction of these terms during the lifetime of a human being. Moreover, most physically interesting systems possess much more complicated, usually continuous manifolds from which field variables are drawn. The continuity of the field space does not generate any new conceptual problems. In principle the sum in (4.2) should then be replaced by an integral, but a convergent integral can always be arbitrarily well approximated by a finite sum. However, it is clear that the number of terms is then even vastly larger. On a computer, all systems are discrete because of finite word length. Without restricting generality, the discussions in this section will be in terms of sums rather than integrals.

The large number of terms suggests a statistical treatment. More so, since the sum in (4.1) is strongly dominated by a small subset of configurations, which characterize the “thermal” equilibrium of the system with respect to the parameters  $g_i$ . The goal of a *Monte Carlo simulation* is to perform *importance sampling*, i.e. to stochastically generate a small number of representative configurations which are typical for the equilibrium distribution. Given that configurations are produced according to their BOLTZMANN *weights* with probability

$$P_B^{(k)} = c_B w_B^{(k)} = c_B e^{-\mathcal{S}(g_i)^{(k)}}, \quad (4.3)$$

where  $c_B$  is a normalization constant which is determined by the condition  $\sum_k P_B^{(k)} = 1$ , the expectation value (4.1) becomes the arithmetic average

$$\langle \mathcal{O} \rangle = \lim_{N_K \rightarrow \infty} \frac{1}{N_K} \sum_{n=1}^{N_K} \mathcal{O}^{(k_n)}, \quad (4.4)$$

which can be estimated by truncating the sum at some finite  $N_K$ .

It is usually not possible to generate configurations directly with probability (4.3). In practice, one uses a MARKOV *chain*: A stochastic process that generates configuration  $k_{i+1}$  from configuration  $k$  without requiring knowledge of prior configurations in such a way that the *time series* of configurations  $k_{i-2}, k_{i-1}, \dots$  moves through phase space along a path that is consistent with the probability distribution  $P_B^{(k)}$ .

The MARKOV chain is defined by the *transition matrix*

$$W = \left( W^{(l)(k)} \right), \quad (4.5)$$

where the matrix element  $W^{(l)(k)} = W[k \rightarrow l]$  contains the probability to reach configuration  $l$  from configuration  $k$  in one step. It has been shown [92] that in order to generate configurations with the desired probabilities (4.3), the transition matrix  $W$  must fulfill three conditions:

(i) **Ergodicity:**

If  $e^{-S^{(k)}} > 0$  and  $e^{-S^{(l)}} > 0$  then a positive finite integer number  $n$  exists, so that  $(W^n)^{(l)(k)} > 0$ . In words: Each configuration is accessible from any other configuration by a finite number of steps (but not necessarily by a single step).

(ii) **Normalization:**

For a given initial state  $k$ , the transition probabilities to all possible final states  $l$  add to one:  $\sum_l W^{(l)(k)} = 1$ .

(iii) **Balance:**

The BOLTZMANN *ensemble* (4.3) is an *eigenvector* of the transition matrix with eigenvalue 1, in the sense that  $\sum_k W^{(l)(k)} e^{-S^{(k)}} = e^{-S^{(l)}}$ .

There are many ways to construct algorithms that satisfy these conditions. Often in practice, Monte Carlo algorithms fulfill a stronger condition than balance, namely

(iii') **Detailed balance:**

$$W^{(l)(k)} e^{-S^{(k)}} = W^{(k)(l)} e^{-S^{(l)}},$$

which implies balance together with the normalization condition (ii). We define an *equilibrium ensemble* as a probability distribution  $P_{eq}$  which is invariant under the transfer matrix:

$$W P_{eq} = P_{eq} \quad \longrightarrow \quad P_{eq}^{(l)} = \sum_k W^{(l)(k)} P_{eq}^{(k)}. \quad (4.6)$$

It has been shown that under the conditions (i), (ii) and (iii) the BOLTZMANN state is the only equilibrium ensemble of the process and furthermore, that any distribution  $P'$  will converge to the BOLTZMANN state under repeated action of  $W$ . This last statement is of major practical relevance since, given a proper algorithm has been constructed, it allows one to start with nearly arbitrary initial conditions as long as one allows the system enough time to approach equilibrium before taking measurements.

## 4.2 Autocorrelations

A consequence of using a MARKOV chain to generate an ensemble is that subsequent configurations are not statistically independent. Possibly strong *autocorrelations* exist in the time series of measurements obtained from any sequence of configurations.

There are several good reasons why a detailed study of autocorrelations is of major importance: The first is that the statistical error will generally be underestimated if one treats correlated data as independent.

The second (related) reason is that measuring observables can generally be very costly in terms of computer time (for complex operators often much more costly than generating configurations) so in order to improve the efficiency of the code one requires a precise knowledge of the optimal number of Monte Carlo steps between two subsequent measurements.

The third reason is that, as indicated in the previous section, one often starts the lattice simulation with an initial condition that has an extremely small probability in the BOLTZMANN ensemble and one thus should grant the system a proper amount of equilibration steps, after which it can be assumed that the system has “forgotten” about its initial state, before taking data.

Last but not least, there is also a physical reason to be interested in autocorrelations: A system that is close to a phase transition will generally exhibit a major increase in autocorrelation times when approaching the phase boundary. This effect, which is known as *critical slowing down*, aside from the technical difficulties it creates for precise measurements in such a region, may also be exploited as an *indicator* of a phase transition when mapping the phase diagram of some particular model.

We now discuss autocorrelations of a lattice observable  $\mathcal{O}$  obtained from a MARKOV chain of configurations. Consider a *time series* of measurements

$$\mathcal{O}_i = \mathcal{O}_i(x_i), \quad i = 1, \dots, N, \quad (4.7)$$

where  $x_i$  are the generated lattice configurations in the order in which they occur in Monte Carlo time. The *autocorrelation function* is defined as

$$\begin{aligned} \widehat{C}(t) &= \widehat{C}_{ij} = \langle (\mathcal{O}_i - \langle \mathcal{O}_i \rangle)(\mathcal{O}_j - \langle \mathcal{O}_j \rangle) \rangle \\ &= \langle \mathcal{O}_i \mathcal{O}_j \rangle - \langle \mathcal{O}_i \rangle \langle \mathcal{O}_j \rangle \\ &= \langle \mathcal{O}_0 \mathcal{O}_t \rangle - \langle \mathcal{O} \rangle^2 \end{aligned} \quad (4.8)$$

with the notation  $t = |i - j|$ .  $\widehat{C}(t)$  measures the statistical dependence of two measurements, taken a time  $t$  apart, on one another (Note that for  $t = 0$  (4.8) is equal to the variance.). Measurements are statistically independent when  $\widehat{C}(t)$  vanishes.

The asymptotic behavior of (4.8) for  $t \rightarrow \infty$  is

$$\widehat{C}(t) = \text{const} \exp\left(-\frac{t}{\tau_{\text{exp}}}\right). \quad (4.9)$$

The decay constant  $\tau_{\text{exp}}$  is called *exponential autocorrelation time*. For finite  $\tau_{\text{exp}}$ , the function (4.9) can of course never reach exactly zero, but in practice measurements are taken to be independent if the time between them is much larger than  $\tau_{\text{exp}}$ .

Note that generally different autocorrelation times reign for different operators. For a field theoretical simulation which involves several different coupled field variables, one should obtain  $\tau_{\text{exp}}$  for representative observables of each field individually, and use the largest autocorrelation time as a measure for the number of configurations to discard between measurements.

Estimating  $\tau_{\text{exp}}$  is generally very costly in terms of computer time, since the signal for  $\widehat{C}(t)$  quickly becomes very noisy when  $t$  is large. Usually it is more efficient to use a different quantity, the *integrated autocorrelation time* which is defined as

$$\tau_{\text{int}} = \left[ 1 + 2 \sum_{t=1}^{N-1} \left( 1 - \frac{t}{N} \right) \widehat{c}(t) \right] \quad \text{with} \quad \widehat{c}(t) = \frac{\widehat{C}(t)}{\widehat{C}(0)}. \quad (4.10)$$

If the autocorrelation function is dominated by a single exponential autocorrelation time, and  $\tau_{\text{exp}}$  is much larger than one, then  $\tau_{\text{int}} \approx 2\tau_{\text{exp}}$  [92]. Usually the situation is more complicated and there is a factor distinct from two between  $\tau_{\text{exp}}$  and  $\tau_{\text{int}}$ . However, in practice one is on the safe side if one relies on  $\tau_{\text{int}}$  when working to improve the efficiency of an updating algorithm, since it is in general larger than  $\tau_{\text{exp}}$  and the loss of accuracy in determining the optimal number of steps between measurements is outweighed by the fact that  $\tau_{\text{int}}$  is much cheaper to compute than  $\tau_{\text{exp}}$ . The integrated autocorrelation time can be reliably estimated via the *Binning* method.

### Binning

For correlated data, the actual variance of the mean  $\sigma^2(\langle \mathcal{O} \rangle)$  is a factor of  $\tau_{\text{int}}$  larger than the variance of the mean of a corresponding uncorrelated data set. This implies:

$$\tau_{\text{int}} = \frac{\sigma^2(\langle \mathcal{O} \rangle)}{\sigma_u^2(\langle \mathcal{O} \rangle)}. \quad (4.11)$$

Here  $\sigma_u^2(\langle \mathcal{O} \rangle)$  is simply the *naive* variance of the mean, calculated from the given set of measurements  $\mathcal{O}_i$  under the assumption that all measurements were statistically independent, with the usual formula

$$\sigma^2(\langle \mathcal{O} \rangle) = \frac{1}{N} \sigma^2(\mathcal{O}) = \frac{1}{N} (\langle \mathcal{O}^2 \rangle - \langle \mathcal{O} \rangle \langle \mathcal{O} \rangle) = \frac{\widehat{C}(0)}{N}. \quad (4.12)$$

One exploits this fact, to estimate  $\tau_{\text{int}}$ : A sequence of *binned* data points is obtained by grouping  $N_b$  successive data points together and calculating the average of each bin

$$\mathcal{O}_j^{\text{bin}}(N_b) = \frac{1}{N_b} \sum_{i=jN_b}^{(j+1)N_b-1} \mathcal{O}_i. \quad (4.13)$$

If the bin-size  $N_b$  is large enough, then the sequence of bins  $\mathcal{O}_j^{\text{bin}}$  are uncorrelated. One then calculates the variance of the mean for the binned data points

$$\sigma_{N_b}^2 = \frac{1}{N_{bs}} \sum_{j=0}^{N_{bs}-1} \left( \mathcal{O}_j^{\text{bin}}(N_b) - \langle \mathcal{O}^{\text{bin}} \rangle \right)^2. \quad (4.14)$$

Assuming that correlations between subsequent bins vanish, one obtains an estimate for integrated autocorrelation time  $\tau_{\text{int}}$  by comparing the variance of the mean of the binned and the original series:

$$\tau_{\text{int}}(N_b) = \frac{\sigma_{N_b}^2}{\sigma^2}. \quad (4.15)$$

Of course one initially has no way of knowing how  $N_b$  should be chosen. Ideally one wants to choose  $N_b$  just barely large enough, to get the smallest possible statistical error for  $\tau_{\text{int}}$ . In practice, to get the best result one calculates  $\tau_{\text{int}}$  starting at  $N_b = 1$  and then successively increases  $N_b$  until a region is reached where the estimate of  $\tau_{\text{int}}$  is stable under further increases of  $N_b$ . This is then taken as the final estimate. The binning method is used exclusively throughout this work for autocorrelation estimates.

### 4.3 Metropolis algorithm

The METROPOLIS *algorithm* is a simple algorithm that uses a MARKOV chain to generate random variables of a given probability distribution and is widely used in lattice simulations to generate a thermal ensemble of lattice configurations. It was derived by METROPOLIS, ROSENBLUTH, ROSENBLUTH, TELLER and TELLER and was shown to fulfill the requirements of ergodicity, normalization and balance [93]. We use the METROPOLIS algorithm exclusively for the three dimensional effective theory (since non-linear terms in the action rule out using the more efficient *Heat bath algorithms*).

The method is applied as follows: Starting from a given lattice configuration  $S_i$ , one generates from it a new trial configuration  $S_{i+1}$  in a convenient way, e.g. for a theory with matrix valued degrees of freedom by rotating a single matrix by a small angle in a random direction. One then calculates the difference of action between the old and the new configuration  $\Delta S = S_{i+1} - S_i$ . The trial step is accepted with probability

$$p = \min[1, \exp(-\Delta S)] . \quad (4.16)$$

This is known as the METROPOLIS *criterion*. In words: The step is automatically accepted if it leads the system towards the state of minimal action, i.e. if  $\exp(-\Delta S) > 1$ . For the case  $\exp(-\Delta S) < 1$  the step is accepted if  $\exp(-\Delta S)$  is larger than a random number drawn from a uniform distribution in the range  $[0, 1]$ .<sup>1</sup> Otherwise the trial step is rejected and one moves to the next site or link. One defines the *acceptance rate* as the ratio of accepted steps over proposed moves. It generally depends on the distance in phase space between the old and the proposed configurations. Large proposed steps quickly lead to a declining acceptance rate, however choosing the steps too small leads to large autocorrelations. A general rule of thumb in lattice simulations is that tuning the acceptance rate to  $\approx 50\%$  is a good compromise.

For a valid updating algorithm, all lattice sites must be eventually proposed for updating. This is automatically achieved if one moves through the lattice systematically and generates METROPOLIS trial steps for each site. This is known as *sequential updating*. However, one can also propose the sites randomly with a uniform probability. One defines a *sweep* as proposing each site once on average in  $N_S$  trial steps, where  $N_S$  is the number of sites. For sequential updating, each site is proposed exactly once per sweep. The advantage of sequential updating is that it generally leads to shorter autocorrelation times than random updating. We use sequential updating exclusively throughout this work.

---

<sup>1</sup>We use the standard random number generator of the *GNU Compiler Collection (gcc)* for this purpose. We assume that the pseudo random numbers generated in such a way fulfill the standard criteria of randomness.

In our code, random METROPOLIS trial steps are proposed by first generating a  $SU(2)$  matrix

$$U = a_0 \mathbf{1} - i a_j \sigma_j, \quad (4.17)$$

not too far from the identity. We generate  $a_{1,2,3}$  randomly in the interval  $[-0.5, 0.5]$  and fix  $a_0$  to

$$a_0 = \left( 1 - \sum_{j=1}^3 a_j^2 \right)^{1/2}. \quad (4.18)$$

A trial configuration is then generated by multiplying a single site or link by  $U$ .

There is a large amount of freedom in choosing the trial steps. If we denote the normalized probability to propose configuration  $k$  from configuration  $l$  as  $f(k, l)$ , then detailed balance can be fulfilled if

$$f(k, l) = f(l, k). \quad (4.19)$$

However one can still fulfill the weaker condition of balance (which, as we have discussed, is sufficient for simulation of an equilibrium ensemble) with non-symmetric proposal probabilities. One can even choose some of the trial steps deterministically. Ergodicity and balance are preserved as long as one mixes deterministic and stochastic trial steps. We take advantage of this by including *Over-relaxation* into our updating procedure, which is discussed in the following section.

In general one has to take care that a given algorithm generates random matrices with the correct HAAR *measure*<sup>2</sup>. For the METROPOLIS algorithm this is automatic, as long as the matrix  $U$  that multiplies a given field variable to obtain a trial step is a group element [2]. Because of this fact, the METROPOLIS algorithm is applicable even in cases where no exact expression for the group measure is known.

One generally can attempt to update a single matrix several times before moving to the next one. This is useful, when the computing time for calculating the contribution to the action from interactions of a given matrix greatly exceeds the time it takes to generate a trial step. A procedure where each site or link is attempted  $N$  times before moving to the next one is called *N-hit*-METROPOLIS. For  $N \rightarrow \infty$  this becomes equivalent to the heat bath algorithm, which generates sites and links directly according to their BOLTZMANN weights in the thermal ensemble.

## 4.4 Over-relaxation

Several authors<sup>3</sup> have discussed how to accelerate decorrelation of subsequent lattice configurations in theories with  $SU(N)$  degrees of freedom, by performing over-relaxation. The general idea is that one wants to perform some Monte-Carlo steps that take one to a distant region in phase space, but only lead to minor changes in energy so that the METROPOLIS criterium can be applied with a good acceptance rate. Usually this is done by taking steps in

<sup>2</sup>See appendix A, eq. A.37 and following, for a general discussion of group integration.

<sup>3</sup>See for example Refs.[94, 95, 96] and references therein or Ref.[90] for a textbook treatment.

the direction in phase space that minimizes the local action, but going beyond the minimum to the mirror image of the starting point.

Consider a situation where  $U_{old}$  is a single matrix variable which should be updated. If  $U_0$  is the matrix which minimizes the local action, i.e. the contribution to the total action from all interactions containing this matrix variable, then  $(U_0 U_{old}^{-1})$  is a rotation to this minimum:

$$U_0 = (U_0 U_{old}^{-1}) U_{old} . \quad (4.20)$$

Over-relaxation consists of applying this rotation twice [94]:

$$U_{new} = (U_0 U_{old}^{-1})^2 U_{old} = U_0 U_{old}^{-1} U_0 . \quad (4.21)$$

For theories where the local action of each variable is symmetric around its minimum, such an operation can always be applied to arbitrary matrices of a given lattice configuration. Since the change of action is then zero, a METROPOLIS trial step of such kind is always accepted. For this case the over-relaxation procedure is deterministic.

The above assumes the minimum of the action is exactly known. However, in principle any step of the form

$$U_{new} = \hat{X} U_{old}^\dagger \hat{X} , \quad (4.22)$$

where  $\hat{X}$  is a group element, leads to a valid updating algorithm as long as one performs a METROPOLIS check after application of (4.22). We choose to approximate  $U_0$  by

$$\hat{X} = S [\det(S)]^{-1/2} , \quad (4.23)$$

where  $S$  is the *staple matrix* that contains the nearest neighbor matrices of the kinetic term. This choice is reasonable for the thermalized system and appears to give good acceptance rates. Exact non-stochastic over-relaxation is not applied in our case, since due to the non linear terms in the action there is no straight forward way to find an exact expression for the matrix which minimizes the local action.

## 4.5 Heat bath

For some actions, it is possible to construct algorithms that generate individual site or link matrices  $U_{new}$  directly with an equilibrium distribution with respect to the other matrices they interact with, independent of the prior state of  $U_{old}$ . The class of methods that accomplish this are known as heat bath algorithms. The big advantage, compared to the METROPOLIS algorithm, is a much faster decorrelation of lattice configurations.

In practice however, it is extremely difficult to construct such algorithms for different actions and symmetry groups, since a detailed knowledge of the structure of the group manifold, as well as an exact expression for the group measure is required. For a theory with  $SU(N)$  variables, another general requirement is that the local action of a single matrix  $U$  can be rewritten into the form

$$S(U) \propto const. + \text{ReTr}(UM) , \quad (4.24)$$

where the matrix  $M$  is a finite sum over  $SU(N)$  matrices and contains all interactions of  $U$  with other field variables. A necessary criterium for this is that interactions between field



variables are bounded to a finite (spatial and temporal) domain and the action does not contain any non-linear powers of  $U$ .

Exact heat bath algorithms for actions that are relevant to physics are only known for a rather small number of cases. For  $SU(2)$  pure gauge theory, a heat bath algorithm was first constructed by CREUTZ [97]. It generalizes immediately to any theory containing exclusively  $SU(2)$  variables. An improved version of the algorithm was developed by KENNEDY and PENDLETON [98], which has a greater efficiency for a large parameter range in pure gauge theory. These algorithms also provide the basis for the widely used *quasi-heat-bath* method of CABIBBO and MARINARI [99], which updates  $SU(N)$  variables by successively updating  $SU(2)$  subgroups.

The CREUTZ heat-bath algorithm is implemented in our 3D code for cross checking the METROPOLIS results. It is applied to the limiting cases where non-linear terms in the action are zero. For the 4D simulations the improved heat-bath algorithm is used exclusively. In the following sections we describe both procedures.

### Creutz heat-bath

The CREUTZ heat-bath algorithm for updating lattice models with  $SU(2)$  degrees of freedom relies on the concept of the invariant group measure (discussed in appendix A, see eq. (A.37) and following). Consider an action that fulfills (4.24). The partition function of a single matrix variable to be updated at some given step can be written as

$$\mathcal{Z} = \int dU \exp(\beta \operatorname{tr}(UM)) , \quad (4.25)$$

with some coupling constant  $\beta$ .<sup>4</sup>

The trace is always real for  $SU(2)$ . Since  $M$  is a sum of  $SU(2)$  matrices, it is proportional to another  $SU(2)$  matrix:

$$M = c\bar{U} \quad \text{with} \quad c = |\det M|^{\frac{1}{2}} . \quad (4.26)$$

Exploiting the invariance of  $dU$ , the partition function (4.25) can be re-expressed by applying the transformation

$$U \rightarrow U\bar{U}^\dagger . \quad (4.27)$$

This yields the simple form form

$$\mathcal{Z} = \int dU \exp(\beta c \operatorname{tr} U) = \pi^{-2} \int_{-\infty}^{\infty} d^4 a \delta(a^2 - 1) \exp(\beta c a_0) , \quad (4.28)$$

where the explicit form of the HAAR measure (A.40) for the quaternionic parameterization was inserted after the second equality. We separate the ‘‘spatial’’ components  $a_i$  from  $a_0$  and get

$$\mathcal{Z} = \pi^{-2} \int_{-1}^1 da_0 \int_{-\infty}^{\infty} d^3 a \delta(a_0^2 + \mathbf{a}^2 - 1) \exp(\beta c a_0) . \quad (4.29)$$

---

<sup>4</sup>Note that it is generally not straight forward to construct mean field approximations with any predictive power for the bulk system from Eq. (4.25), since  $M$  is usually a complicated function of the fields on other sites.

Note that the boundaries of the integrals can be set to  $\pm 1$  at will, due to the constraint of the delta function. The spatial integral can then be transformed into spherical coordinates with  $\mathbf{a}^2 = r^2$  and  $d^3a = r^2 dr d\Omega$ :

$$\begin{aligned} \mathcal{Z} &= \pi^{-2} \int d\Omega \int_0^1 r^2 dr \int_{-1}^1 da_0 \delta(a_0^2 + r^2 - 1) \exp(\beta c a_0) \\ &= \frac{\pi^{-2}}{2} \int d\Omega \int_{-1}^1 da_0 (1 - a_0^2)^{\frac{1}{2}} \exp(\beta c a_0) . \end{aligned} \quad (4.30)$$

In the second step the well-known theorem for the delta function

$$\delta(g(x)) = \sum_{i=1}^n \frac{\delta(x - x_i)}{|g'(x_i)|} , \quad g(x_i) = 0 , \quad (4.31)$$

was used and the negative solution to  $r^2 = 1 - a_0^2$  dropped. The problem is thus reduced to generating  $a_0$  with the correct weighting

$$p_{a_0}(a_0) da_0 \sim (1 - a_0^2)^{\frac{1}{2}} \exp(\beta c a_0) da_0 , \quad (4.32)$$

in the interval  $[-1, 1]$ , then choosing a random direction for  $\mathbf{a}$  and adjusting its length to fulfill  $a^2 = 1$ .

To generate  $a_0$  with the correct probability distribution one can use a random number generator with a uniform distribution: A series of weighted random numbers can be obtained, by first drawing a uniform random number  $x$  from the allowed interval. One then draws a second random number  $y$  and accepts  $x$  as part of the weighted series, if  $y$  is smaller than  $p_{a_0}(x)$ . Repeating this procedure by taking the second number  $y$  as the new initial number  $x$  at each step eventually produces a series of accepted numbers with the desired weighting. In our case one would terminate the procedure whenever the first accepted number is generated and move to the next lattice site.

However, the weight function (4.32) is strongly peaked, which implies a low acceptance rate for the above procedure. It thus may take very long to produce a single usable number. In practice, one therefore applies another transformation of variables to improve efficiency. In order to smear out the peak of (4.32), one transforms  $a_0$  and  $da_0$  to

$$z = \exp(\beta c a_0) \quad , \quad dz = \beta c z da_0 . \quad (4.33)$$

The distribution of the new variable  $z$  is then

$$p_z(z) dz \sim (1 - \beta^{-2} k^{-2} \log^2 z)^{\frac{1}{2}} dz , \quad (4.34)$$

which is distributed much more evenly over the allowed interval. To obtain the weighted series, trial numbers for  $z$  are drawn from

$$e^{-\beta c} \leq z \leq e^{+\beta c} \quad (4.35)$$

and accepted or rejected as explained above. To obtain a series of  $a_0$  one then applies the inverse of (4.33).

Often one is interested in limiting cases of a given theory, thus the parameter  $\beta$  can be quite large. For very large  $\beta$ , the smearing will not be sufficient to get significant improvements of the acceptance rate. In such a case, one can use the method of KENNEDY and PENDLETON, which provides an efficient way to generate  $a_0$  with the distribution (4.32).

### Kennedy-Pendleton heat bath

Consider another transformation of variables

$$a_0 = 1 - \eta^2 \quad , \quad da_0 = 2\eta d\eta . \quad (4.36)$$

The method of KENNEDY and PENDLETON consists of generating  $\eta$  according to its respective distribution, and then obtaining  $a_0$  by applying (4.36). With (4.32), one finds that  $\eta$  is distributed according to

$$p_\eta(\eta)d\eta \sim \left(1 - \frac{1}{2}\eta^2\right)^{\frac{1}{2}} \exp(-\beta c \eta^2) \eta^2 d\eta , \quad (4.37)$$

in the interval  $[0, \sqrt{2}]$ . For large values of  $\beta c$ , this distribution is strongly peaked near  $\eta = 0$ . We use a two step process to generate (4.37). First we generate random variables according to a different distribution

$$p'_\eta(\eta)d\eta \sim \exp(-\beta c \eta^2) \eta^2 d\eta , \quad (4.38)$$

and then use a accept/reject step to impose a factor of  $(1 - \frac{1}{2}\eta^2)^{\frac{1}{2}}$ .

Note first that, given a random variable  $x$  distributed according to some weight function  $f(x)$ , one can obtain the distribution  $f_g(g)$  of some quantity  $g$  that is a function of  $x$  by solving

$$f_g(g') dg' = \left( \int_a^b dx f(x) \delta(g' - g(x)) \right) dg' , \quad (4.39)$$

where  $[a, b]$  is the total range of  $x$ . The range of the random variable  $g$  is then  $[g(a), g(b)]$ . The transformations discussed previously were just special cases of (4.39), which is the general formula. This can also immediately be generalized to functions of two (or several more) random variables. For  $r(x, y)$  one gets

$$f_r(r') dr' = \left( \int dx \int dy f_x(x) f_y(y) \delta(r' - r(x, y)) \right) dr' . \quad (4.40)$$

Now consider the quantity

$$\xi = \left( \frac{-\ln X}{\beta c} \right)^{\frac{1}{2}} , \quad (4.41)$$

and let  $X$  be a random variable, uniformly distributed in  $[0, 1]$ . By using (4.39) and (4.31) one gets for the distribution of  $\xi$ :

$$\begin{aligned} p_\xi(\xi) d\xi &= \left( \int_0^1 dX \delta \left( \xi - [(-\ln X)/\beta c]^{\frac{1}{2}} \right) \right) d\xi \\ &= \left( \int_0^1 dX \frac{\delta(X - \exp(-\xi^2 \beta c))}{|(2\xi\beta c)^{-1} \exp(\xi^2 \beta c)|} \right) d\xi = 2\xi\beta c \exp(-\beta c \xi^2) d\xi . \end{aligned} \quad (4.42)$$

The random variable  $\xi$  can take values from zero to infinity. Using a random variable distributed by (4.42) one can generate variables with a Gaussian distribution. Consider the variables

$$\rho = \chi \cos(\theta) \quad \text{with} \quad \theta = 2\pi X' , \quad (4.43)$$

where  $X'$  is another uniform random variable in  $[0, 1]$  and  $\chi$  is distributed according to (4.42). Using (4.40) one finds that the distribution of  $\rho$  is given by

$$\begin{aligned} p_\rho(\rho) d\rho &= \left( \int_0^\infty d\chi \int_0^1 dX' p_\xi(\chi) \delta(\rho - \chi \cos(2\pi X')) \right) d\rho \\ &= \left( \int_0^\infty d\chi \int_0^{2\pi} d\theta \frac{\chi \beta c}{\pi} \exp(-\beta c \chi^2) \delta(\rho - \chi \cos \theta) \right) d\rho . \end{aligned} \quad (4.44)$$

To solve this integral one uses a trick: The coordinates  $\chi$  and  $\theta$  are considered to be polar coordinates. They are related to the Cartesian coordinates  $a$  and  $b$  by

$$a = \chi \cos \theta , \quad b = \chi \sin \theta , \quad a^2 + b^2 = \chi^2 , \quad da db = \chi d\chi d\theta . \quad (4.45)$$

In terms of  $a$  and  $b$ , equation (4.44) becomes

$$p_\rho(\rho) d\rho = \left( \int_{-\infty}^\infty da \int_{-\infty}^\infty db \frac{\beta c}{\pi} \exp[-\beta c(a^2 + b^2)] \delta(\rho - a) \right) d\rho . \quad (4.46)$$

where the boundaries of the integrals have been adjusted. The integral over  $da$  can be carried out immediately:

$$p_\rho(\rho) d\rho = \left( \int_{-\infty}^\infty db \frac{\beta c}{\pi} \exp[-\beta c(\rho^2 + b^2)] \right) d\rho . \quad (4.47)$$

The exponential can be factorized. The integral over  $db$  is a simple Gaussian integral of the form

$$\int_{-\infty}^\infty dx e^{-cx^2} = \sqrt{\frac{\pi}{c}} . \quad (4.48)$$

Carrying out the integral then yields

$$p_\rho(\rho) d\rho = \left( \int_{-\infty}^\infty db \frac{\beta c}{\pi} \exp(-\beta c b^2) \exp(-\beta c \rho^2) \right) d\rho = \sqrt{\frac{\beta c}{\pi}} \exp(-\beta c \rho^2) d\rho , \quad (4.49)$$

which is a Gaussian distribution for  $\rho$  (with the range  $[-\infty, \infty]$ ). Moreover, the quantity  $\rho' = \chi \sin \theta$  is also distributed according to (4.49) and is independent of  $\rho$ . Assuming we have applied the above procedure to generate random numbers distributed by (4.49) and (4.42), we can now use them to generate the distribution (4.38). Define

$$\eta = (\xi^2 + \rho^2)^{1/2} . \quad (4.50)$$

One then finds

$$\begin{aligned}
 p''(\eta) d\eta &= \left( \int_0^\infty d\xi \int_{-\infty}^\infty d\rho p_\xi(\xi) p_\rho(\rho) \delta(\eta - (\xi^2 + \rho^2)^{1/2}) \right) d\eta \\
 &= \left( \int_0^\infty d\xi \int_{-\infty}^\infty d\rho \sqrt{\frac{4\beta^3 c^3 \xi^2}{\pi}} \exp[-\beta c(\xi^2 + \rho^2)] \delta(\eta - (\xi^2 + \rho^2)^{1/2}) \right) d\eta .
 \end{aligned} \tag{4.51}$$

This integral can conveniently be solved in the polar coordinate system

$$r = (\xi^2 + \rho^2)^{1/2}, \quad \xi = r \cos \phi, \quad \rho = r \sin \phi, \quad d\xi d\rho = r dr d\phi. \tag{4.52}$$

Because of the boundaries of the  $d\xi$  integral one considers only the upper half-plane, where  $\phi = [-\frac{\pi}{2}, \frac{\pi}{2}]$ . One finds that  $\eta$  is distributed according to

$$\begin{aligned}
 p''_\eta(\eta) d\eta &= \left( \int_0^\infty dr \int_{-\pi/2}^{\pi/2} d\phi 2\beta c r^2 \sqrt{\frac{\beta c}{\pi}} \cos(\phi) \exp(-\beta c r^2) \delta(\eta - r) \right) d\eta \\
 &= \left( 2\beta c \sqrt{\frac{\beta c}{\pi}} \int_{-\pi/2}^{\pi/2} d\phi \cos(\phi) \eta^2 \exp(-\beta c \eta^2) \right) d\eta \\
 &= 4\beta c \eta^2 \sqrt{\frac{\beta c}{\pi}} \exp(-\beta c \eta^2) d\eta .
 \end{aligned} \tag{4.53}$$

which is equal to (4.38) up to a normalization factor and ranges in the interval  $[0, \infty]$ . One can now get to (4.37), by generating a random variable  $\eta$  distributed by  $p''_\eta(\eta)$  and imposing an additional factor  $v(\eta) = (1 - \frac{1}{2}\eta^2)$ : After  $\eta$  was produced according to (4.53), one rejects it if  $\eta^2 \geq 2$ . If  $\eta^2 \leq 2$ , one generates another uniform random number  $X''$  in  $[0, 1]$  and accepts  $\eta$ , if  $X'' \leq v(\eta)$ . From the resulting series of random numbers, one obtains  $a_0$  by applying (4.36).

We summarize the individual steps of the method in the following list:

- (i) Generate two uniform random variables  $X$  and  $X'$  in the interval  $[0, 1]$ .
- (ii) Use them to compute  $\xi = (-\ln X/\beta c)^{1/2}$  and further  $\rho_1 = \xi \cos(2\pi X')$  and  $\rho_2 = \xi \sin(2\pi X')$ .  $\rho_{1,2}$  are independent Gaussian random variables. Each of these can be used for the following steps.
- (iii) Generate another uniform random variable  $X''$  in  $[0, 1]$  and use it to obtain  $\xi' = (-\ln X''/\beta c)^{1/2}$ . Compute  $\eta = (\xi'^2 + \rho^2)^{1/2}$ .
- (iv) For any  $\eta$  generated in such a way perform the following accept/reject step: Reject if  $\eta^2 > 2$ . Otherwise, generate a third uniform variable  $X'''$  in  $[0, 1]$  and accept  $\eta$  only if  $X''' \leq (1 - \frac{1}{2}\eta^2)$ .
- (v) If the  $\eta$  obtained from both  $\rho_{1,2}$  are rejected start again with the first step. If a  $\eta$  is accepted, calculate  $a_0 = 1 - \eta^2$  and use this number.

While the method described in this section initially appears much more complex than the original heat bath algorithm of CREUTZ, it does in fact increase the efficiency of a simulation of (4.25) greatly when  $\beta$  is large and is a widely used standard for lattice gauge theory simulations. A quantitative comparison of the acceptance probabilities of both methods for the WILSON action can be found in the original article [98].

## 5 Derivation of lattice action

In this chapter we derive the lattice action, which is used throughout this work for simulations of the 3D effective theory defined by the Lagrangian

$$\mathcal{L}^{\text{eff}} = \frac{1}{2} \text{tr} F_{ij}^2 + \frac{T^2}{g^2} \text{tr} |\mathbf{L}^\dagger D_i \mathbf{L}|^2 - \frac{2}{\pi^2} T^4 \sum_{n \geq 1} \frac{1}{n^4} |\text{tr} \mathbf{L}^n|^2 + B_f T^2 |\text{tr} \mathbf{L}|^2 . \quad (5.1)$$

We start this discussion with a few general remarks: The most fundamental necessary requirement, which a particular lattice action must meet in order to be useful for field theoretical simulations, is that the correct continuum form is obtained when the lattice spacing is formally taken to zero (this applies even if the continuous theory is defined with a cut-off, as for our case). However, this requirement does not uniquely constrain the lattice action for a particular theory and much effort is put into the search for improved actions for known theories, which approach the continuum limit faster when the lattice spacing shrinks or which reduce the complexity of the updating algorithm. Often lattice actions exhibit unphysical features (e.g. phase transitions which are not present for the continuum theory or the well-known *Fermion doubling* effect), which are discretization artefacts. Such qualitative features must be well understood and a prescription to subtract their effect from physical predictions must be formulated if sensible results are to be obtained. This often involves adding terms to the action, which vanish in the continuum limit and which sometimes explicitly break symmetries of the underlying continuum theory.

In this work we will use a lattice action which is constructed in close analogy to the elegant formulation of lattice gauge theory, introduced by WILSON, which relies on the definition of a gauge theory as a path dependent phase factor. This form is widely used for 4D YANG-MILLS theory simulations. Its most striking feature is that gauge freedom remains as an exact local symmetry at finite spacing. In this formulation, an element of the gauge group is associated with each bond, connecting a pair of nearest neighbor lattice sites  $(i, j)$

$$U_{ij} = e^{-ig_0 A_\mu(x_\mu)^a} \in G . \quad (5.2)$$

The  $U_{ij}$  are called link variables. However, in our case the pure gauge sector is constrained to three dimensions and in addition to the space-like links the Lagrangian (5.1) also contains the thermal WILSON line  $\mathbf{L}(\mathbf{x})$ , which transforms under the static local gauge transformation  $\omega(\mathbf{x}) \in SU(N)$ <sup>1</sup> as

$$\mathbf{L}(\mathbf{x}) \mapsto \omega(\mathbf{x}) \mathbf{L}(\mathbf{x}) \omega(\mathbf{x})^{-1} . \quad (5.3)$$

The origin of this transformation law will become clear in the course of this chapter. We associate the  $\mathbf{L}(\mathbf{x})$  with the lattice sites. Given that the periodic boundary condition of the time dimension is preserved by compactification, the WILSON line  $\mathbf{L}(\mathbf{x})$  can also be viewed

---

<sup>1</sup>Note that  $\omega$  depends on spatial coordinates  $\mathbf{x}$  only.

as the single time-like link variable of a  $N_\tau = 1$  gauge theory. As we will discuss at the end of this chapter, this allows for two different updating schemes for the space-like links, which we both consider in this work.

This chapter proceeds as follows: First we obtain a lattice formulation for the terms in the action containing the WILSON line  $\mathbf{L}(\mathbf{x})$ . These expressions will be derived from first principles. The kinetic term in (5.1) contains the gauge covariant derivative  $D_i\mathbf{L}$ , thus it will be necessary to define covariant differentiation at finite spacing. We therefore introduce the concept of *parallel transport*. For the magnetic sector we will take the opposite approach: We consider the well known WILSON *action*, which is widely used for  $4D$  lattice gauge theory simulations and note that this easily generalizes to three dimensions. We then review the crucial steps that show that it has the correct continuum limit.

We currently employ several approximations. We consider only the  $n = 1$  term of the perturbative potential, which then can be combined with the “fuzzy” bag term into a single quadratic expression which acts like a mass term in the Lagrangian. Also, we define a common lattice coupling constant  $\beta$  for both the kinetic energy term of the WILSON line and the magnetic sector. The motivation behind these simplifications is that this work investigates the properties of the lattice model in its own right, and does not aim at matching the coupling constants to the  $4D$  theory yet. For the same reason we will set the lattice spacing  $a$  equal to one in later chapters.

Note that in the following section we define the generators of the  $SU(N)$  group to be anti-Hermitian rather than Hermitian. This is a matter of convention, since both choices give equally valid definitions of a LIE algebra. We have chosen anti-Hermitian generators here out of convenience, since it makes the derivations in this section easier to read. We have also absorbed the coupling constant  $g$  into the definition of the gauge field  $A_i$ . We use these conventions **only** in section 5.1. In the remainder of the text Hermitian generators are used and coupling constants are written explicitly.

## 5.1 Wilson line action

The effective theory (5.1) is constructed to respect all symmetries of  $4D$  YANG-MILLS theory. Thus, all terms must respect local invariance under static gauge transformations  $\omega(\mathbf{x})$ . We can immediately write down the contribution to the lattice action that arises from the quadratic terms as

$$\mathcal{S}_{\text{pot}} = -m^2 \sum_i |\text{tr } \mathbf{L}_i|^2, \quad (5.4)$$

where the sum runs over all lattice sites and see that it is unchanged under transformations of the form (5.3), due to the cyclic property of the trace. The kinetic term

$$\mathcal{L}_{\text{kin}} = \frac{T^2}{g^2} \text{tr} |\mathbf{L}^\dagger D_i \mathbf{L}|^2 \quad (5.5)$$

contains the covariant derivative  $D_i\mathbf{L}(\mathbf{x})$ , which is generally defined in such a way, that under action of  $\omega(\mathbf{x})$  it has the same transformation law as the un-differentiated field  $\mathbf{L}(\mathbf{x})$ . Thus with (5.3) we demand that

$$D_i\mathbf{L} \mapsto \omega(\mathbf{x})D_i\mathbf{L}(\mathbf{x})\omega(\mathbf{x})^{-1}, \quad (5.6)$$



must hold. Gauge invariance of the kinetic energy then follows simply by permutating the terms under the trace and using

$$\omega(\mathbf{x})\omega(\mathbf{x})^{-1} = \mathbf{1} . \quad (5.7)$$

One can show that (5.6) is fulfilled, if  $D_i\mathbf{L}$  has the form

$$D_i\mathbf{L} = \partial_i\mathbf{L} - [A_i, \mathbf{L}] , \quad (5.8)$$

and if the *gauge field*  $A_i(\mathbf{x})$  is a matrix valued field that obeys the transformation law

$$A_i(\mathbf{x}) \mapsto A_i^\omega(\mathbf{x}) = \omega(\mathbf{x})A_i(\mathbf{x})\omega(\mathbf{x})^{-1} + \partial_i\omega(\mathbf{x})\omega(\mathbf{x})^{-1} . \quad (5.9)$$

By applying the transformation laws (5.3) and (5.9) to (5.8) one gets

$$\begin{aligned} D_i\mathbf{L} \mapsto (D_i\mathbf{L})^\omega &= \partial_i(\omega\mathbf{L}\omega^{-1}) - [\omega A_i\omega^{-1} + (\partial_i\omega)\omega^{-1}, \omega\mathbf{L}\omega^{-1}] \\ &= (\partial_i\omega)\mathbf{L}\omega^{-1} + \omega(\partial_i\mathbf{L})\omega^{-1} + \omega\mathbf{L}(\partial_i\omega^{-1}) \\ &\quad - \omega A_i\omega^{-1}\omega\mathbf{L}\omega^{-1} - (\partial_i\omega)\omega^{-1}\omega\mathbf{L}\omega^{-1} \\ &\quad + \omega\mathbf{L}\omega^{-1}\omega A_i\omega^{-1} + \omega\mathbf{L}\omega^{-1}(\partial_i\omega)\omega^{-1} \\ &= \omega(\partial_i\mathbf{L})\omega^{-1} + \omega\mathbf{L}(\partial_i\omega^{-1}) - \omega A_i\mathbf{L}\omega^{-1} \\ &\quad + \omega\mathbf{L}A_i\omega^{-1} + \omega\mathbf{L}\omega^{-1}(\partial_i\omega)\omega^{-1} . \end{aligned} \quad (5.10)$$

Here we have suppressed the  $\mathbf{x}$  dependence. With

$$\partial_i(\mathbf{1}) = \partial_i(\omega\omega^{-1}) = (\partial_i\omega)\omega^{-1} + \omega(\partial_i\omega^{-1}) = 0 \quad (5.11)$$

one sees that the second and the last term of (5.10) cancel, which then leaves the desired transformation law

$$\begin{aligned} (D_i\mathbf{L})^\omega &= \omega(\partial_i\mathbf{L})\omega^{-1} - \omega A_i\mathbf{L}\omega^{-1} + \omega\mathbf{L}A_i\omega^{-1} \\ &= \omega\{\partial_i\mathbf{L} - [A_i, \mathbf{L}]\}\omega^{-1} = \omega(D_i\mathbf{L})\omega^{-1} . \end{aligned} \quad (5.12)$$

Thus the expression (5.8) apparently works in the continuum. However, as it stands, this particular form is not applicable on the lattice. The expression contains the continuous derivative  $\partial_i\mathbf{L}$ , which is not well-defined on the lattice since there one always has a finite spacing i.e. a smallest possible separation between two points. To obtain a usable expression the continuous derivative must therefore be replaced by a finite differential of some sort. The naive replacement

$$\partial_i\mathbf{L} \longrightarrow \frac{\mathbf{L}(\mathbf{x} + \Delta\mathbf{x}) - \mathbf{L}(\mathbf{x})}{\Delta\mathbf{x}} \quad (5.13)$$

does not work, since it does not transform covariantly. Moreover, the forms (5.8) and (5.9), even though they generate the desired transformation law, appear somewhat arbitrary. We have simply postulated them here without really motivating them from basic principles. We will show in the following, that both of these issues can be solved simultaneously. By introducing the *parallel transporter* one can obtain a general covariant differential with the correct transformation law, which converges to (5.8) in the limit of vanishing distances.

### Parallel transport and lattice covariant derivative

The concept of parallel transport provides an elegant way to define a local  $SU(N)$  symmetry. Consider a  $N$  component complex vector field  $\Phi(\mathbf{x})$  and demand that expressions containing scalar products of  $\Phi$  at different arbitrary points  $\mathbf{x}_1$  and  $\mathbf{x}_2$ , e.g.

$$\Phi^\dagger(\mathbf{x}_1)\Phi(\mathbf{x}_2) \quad (5.14)$$

should be unchanged under a local change of basis

$$\Phi(\mathbf{x}) \mapsto \omega(\mathbf{x})\Phi(\mathbf{x}) \quad \omega(\mathbf{x}) \in SU(N) . \quad (5.15)$$

Since every point  $\mathbf{x}$  is assigned a different set of unit vectors,  $\Phi(\mathbf{x}_1)$  and  $\Phi(\mathbf{x}_2)$  belong to different vector spaces  $V_1$  and  $V_2$  and expressions such as (5.14) are not well-defined. To obtain an invariant product one must define some operator  $U$ , which provides a mapping between vector spaces at different points in a continuously differentiable way. As we will see, this mapping generally depends on the unique path between  $\mathbf{x}_1$  and  $\mathbf{x}_2$ .

Now let  $C_{xy}$  be some curve in space from a point  $\mathbf{x}$  to a point  $\mathbf{y}$  that is parameterized in some convenient way. With every curve  $C_{yx}$ , one associates an operator  $U(C_{yx}) \in SU(N)$  which fulfills the conditions:

- (i)  $U(0) = \mathbf{1}$ , i.e. the unit operator is associated with a curve of length zero.
- (ii)  $U(C_2 \circ C_1) = U(C_2)U(C_1)$  where  $C_2 \circ C_1$  is the path that is obtained by connecting the curves  $C_{1,2}$ .
- (iii)  $U(-C) = U^{-1}(C)$ , where  $-C$  is the curve  $C$ , traversed in the opposite direction.

One further demands that under local gauge transformations,  $U(C_{yx})$  transforms as

$$U(C_{yx}) \mapsto U(C_{yx})^\omega = \omega(\mathbf{y})U(C_{yx})\omega(\mathbf{x})^{-1} . \quad (5.16)$$

The vector

$$U(C_{yx})\Phi(\mathbf{x}) \in V_y \quad (5.17)$$

is the vector  $\Phi(\mathbf{x})$ , parallel transported to the point  $\mathbf{y}$  along the curve  $C_{yx}$ . With the above definitions, the product

$$\Phi(\mathbf{y})^\dagger U(C_{yx})\Phi(\mathbf{x}) \quad (5.18)$$

is invariant under local gauge transformations.

The operators  $U(C_{yx})$  are elements of the Lie group  $SU(N)$ , so

$$U^{-1} = U^\dagger . \quad (5.19)$$

Due to  $U(0) = \mathbf{1}$ , for infinitesimal displacements one thus can write

$$U_{\mathbf{x}+d\mathbf{x},\mathbf{x}} = \mathbf{1} + A_i(\mathbf{x})d\mathbf{x}_i \quad (5.20)$$

where the field  $A_i(\mathbf{x})$  associates an element of the Lie algebra of  $SU(N)$ , i.e. a traceless anti-Hermitian  $N \times N$  matrix, with every spatial coordinate  $\mathbf{x}$ . One sees immediately, that

if one identifies the  $A_i(\mathbf{x})$  with the gauge fields introduced above, the transformation law (5.9) follows from (5.16). By choosing  $\mathbf{y} = \mathbf{x} + d\mathbf{x}$  and TAYLOR expanding  $U(C_{yx})^\omega$  and  $U(C_{yx})$  one gets

$$\mathbf{1} + A_i^\omega(\mathbf{x})d\mathbf{x}_i = \omega(\mathbf{x} + d\mathbf{x})\omega^{-1}(\mathbf{x}) + \omega(\mathbf{x} + d\mathbf{x}) A_i(\mathbf{x})\omega^{-1}(\mathbf{x}) d\mathbf{x}_i . \quad (5.21)$$

Some slight rearrangements and making the replacement  $\mathbf{1} = \omega(\mathbf{x})\omega^{-1}(\mathbf{x})$  yields

$$A_i^\omega(\mathbf{x})d\mathbf{x}_i = [\omega(\mathbf{x} + d\mathbf{x}) - \omega(\mathbf{x})]\omega^{-1}(\mathbf{x}) + \omega(\mathbf{x} + d\mathbf{x}) A_i(\mathbf{x})\omega^{-1}(\mathbf{x}) d\mathbf{x}_i . \quad (5.22)$$

The desired transformation law (5.9) follows after dividing by  $d\mathbf{x}_i$  and taking the limit  $d\mathbf{x} \rightarrow 0$ . Note that the parallel transporter  $U$  along a curve  $C_s$  can be obtained from the  $A_i(\mathbf{x})$  by using DYSON's formula

$$U(C_s) = P \exp \left( - \int_{C_s} A_i d\mathbf{x}_i \right) . \quad (5.23)$$

Here the operator  $P$  denotes path ordering of the integral, with respect to the parameter  $s$ . From this formula, the expression (5.2) for the link variable  $U_{ij}$  follows, with  $|d\mathbf{x}_i| \equiv a$  and  $A_i(\mathbf{x}) = \text{const.}$  over the length of one lattice spacing. Also, we see that the definition of the WILSON line (2.6) is of the form (5.23), so the transformation law of  $\mathbf{L}(\mathbf{x})$  follows from (5.16).

We now look for an expression analogous to (5.13) but with the correct transformation law. Derivatives on the lattice are generally written as finite difference quotients, but in order to compare  $\mathbf{L}(\mathbf{x} + d\mathbf{x})$  with the field at a different point  $\mathbf{L}(\mathbf{x})$ , it must be parallel transported to  $\mathbf{x}$ . We have seen above in eq. (5.17) how a vector  $\Phi(\mathbf{x})$  is parallel transported. The field  $\mathbf{L}(\mathbf{x})$  however is a rank two tensor. The analogous expression to (5.17) is

$$U(C_{yx})\mathbf{L}(\mathbf{x})U(C_{yx})^{-1} \in V_y . \quad (5.24)$$

In analogy to (5.13) now one can define the lattice covariant derivative as

$$D\mathbf{L}(\mathbf{x}) d\mathbf{x} = U_{\mathbf{x}+d\mathbf{x},\mathbf{x}}^{-1} \mathbf{L}(\mathbf{x} + d\mathbf{x}) U_{\mathbf{x}+d\mathbf{x},\mathbf{x}} - \mathbf{L}(\mathbf{x}) \quad (5.25)$$

It transforms covariantly and converges to (5.8) when taking  $d\mathbf{x} \rightarrow 0$ . This is shown by two short calculations. We expand the  $U$  in terms of the  $A_i$

$$\begin{aligned} D\mathbf{L}(\mathbf{x})d\mathbf{x} &\approx (\mathbf{1} - A_i(\mathbf{x})d\mathbf{x}_i)\mathbf{L}(\mathbf{x} + d\mathbf{x})(\mathbf{1} + A_i(\mathbf{x})d\mathbf{x}_i) - \mathbf{L}(\mathbf{x}) \\ &= \mathbf{L}(\mathbf{x} + d\mathbf{x}) - \mathbf{L}(\mathbf{x}) - [A_i(\mathbf{x}), \mathbf{L}(\mathbf{x} + d\mathbf{x})]d\mathbf{x}_i + \mathcal{O}(d\mathbf{x}_i^2) , \end{aligned} \quad (5.26)$$

and find that (5.8) is reproduced. Applying a local gauge transformation  $\omega(\mathbf{x})$  to (5.25) yields

$$\begin{aligned} (D\mathbf{L}(\mathbf{x}))^\omega d\mathbf{x} &= \omega(\mathbf{x})U_{\mathbf{x}+d\mathbf{x},\mathbf{x}}^{-1}\omega^{-1}(\mathbf{x} + d\mathbf{x})\omega(\mathbf{x} + d\mathbf{x})\mathbf{L}(\mathbf{x} + d\mathbf{x}) \\ &\quad \times \omega^{-1}(\mathbf{x} + d\mathbf{x})\omega(\mathbf{x} + d\mathbf{x})U_{\mathbf{x}+d\mathbf{x},\mathbf{x}}\omega^{-1}(\mathbf{x}) - \omega(\mathbf{x})\mathbf{L}(\mathbf{x})\omega^{-1}(\mathbf{x}) \\ &= \omega(\mathbf{x})U_{\mathbf{x}+d\mathbf{x},\mathbf{x}}^{-1}\mathbf{L}(\mathbf{x} + d\mathbf{x})U_{\mathbf{x}+d\mathbf{x},\mathbf{x}}\omega^{-1}(\mathbf{x}) - \omega(\mathbf{x})\mathbf{L}(\mathbf{x})\omega^{-1}(\mathbf{x}) \\ &= \omega(\mathbf{x}) \left( U_{\mathbf{x}+d\mathbf{x},\mathbf{x}}^{-1} \mathbf{L}(\mathbf{x} + d\mathbf{x}) U_{\mathbf{x}+d\mathbf{x},\mathbf{x}} - \mathbf{L}(\mathbf{x}) \right) \omega^{-1}(\mathbf{x}) \\ &= \omega(\mathbf{x}) D\mathbf{L}(\mathbf{x}) d\mathbf{x} \omega^{-1}(\mathbf{x}) \end{aligned} \quad (5.27)$$

which has the desired form.

### Kinetic term for the Wilson lines

The kinetic energy on the lattice is obtained by inserting (5.25) into (5.5). With

$$\mathcal{L}_{\text{kin}} = \frac{T^2}{g^2} \text{tr} |\mathbf{L}^\dagger D_i \mathbf{L}|^2 = \frac{T^2}{g^2} \text{tr} \left[ \mathbf{L}^\dagger (D_i \mathbf{L}) (D_i \mathbf{L})^\dagger \mathbf{L} \right] = \frac{T^2}{g^2} \text{tr} \left[ (D_i \mathbf{L}) (D_i \mathbf{L})^\dagger \right] \quad (5.28)$$

one gets

$$\begin{aligned} \mathcal{L}_{\text{kin}} \sim & \text{tr} \left\{ \mathbf{L}^\dagger(\mathbf{x}) \left[ U_{\mathbf{x}+d\mathbf{x},\mathbf{x}}^\dagger \mathbf{L}(\mathbf{x}+d\mathbf{x}) U_{\mathbf{x}+d\mathbf{x},\mathbf{x}} - \mathbf{L}(\mathbf{x}) \right] \right. \\ & \left. \times \left[ U_{\mathbf{x}+d\mathbf{x},\mathbf{x}}^\dagger \mathbf{L}^\dagger(\mathbf{x}+d\mathbf{x}) U_{\mathbf{x}+d\mathbf{x},\mathbf{x}} - \mathbf{L}^\dagger(\mathbf{x}) \right] \mathbf{L}(\mathbf{x}) \right\} \end{aligned} \quad (5.29)$$

And after some rearrangements

$$\begin{aligned} \mathcal{L}_{\text{kin}} \sim & \text{tr} \left\{ \left[ \mathbf{L}^\dagger(\mathbf{x}) U_{\mathbf{x}+d\mathbf{x},\mathbf{x}}^\dagger \mathbf{L}(\mathbf{x}+d\mathbf{x}) U_{\mathbf{x}+d\mathbf{x},\mathbf{x}} - \mathbf{1} \right] \right. \\ & \left. \times \left[ U_{\mathbf{x}+d\mathbf{x},\mathbf{x}}^\dagger \mathbf{L}^\dagger(\mathbf{x}+d\mathbf{x}) U_{\mathbf{x}+d\mathbf{x},\mathbf{x}} - \mathbf{1} \right] \right\} \\ = & -\text{tr} \left\{ \mathbf{L}^\dagger(\mathbf{x}) U_{\mathbf{x}+d\mathbf{x},\mathbf{x}}^\dagger \mathbf{L}(\mathbf{x}+d\mathbf{x}) U_{\mathbf{x}+d\mathbf{x},\mathbf{x}} + \text{h.c.} \right\} + \text{tr} (2\mathbf{1}) \end{aligned} \quad (5.30)$$

To get the action, the Lagrangian is integrated over the entire volume

$$S = \int \mathcal{L}^{\text{eff}}(\mathbf{x}) d^3x . \quad (5.31)$$

The constant  $\text{tr} (2 * \mathbf{1})$  can be neglected. With finite lattice spacing  $a \equiv 1$  the integral becomes a simple sum over all sites or links. The contribution from the kinetic energy can therefore be written as

$$S_{\text{kin}} = -\frac{\beta}{2} \sum_{\langle ij \rangle} \text{tr} (\mathbf{L}_i^\dagger U_{ji}^\dagger \mathbf{L}_j U_{ji} + \text{h.c.}) \quad (5.32)$$

where the sum runs over all pairs of nearest neighbors. The relationship between  $\beta$  and the coupling constant in the continuum must later be determined. The factor 1/2 accounts for double counting.

## 5.2 Action of pure gauge sector

The elegant lattice formulation of the action of the four-dimensional YANG-MILLS field, which uses the *elementary plaquette* was first introduced by WILSON [10] and has since been discussed excessively (e.g. see Refs. [100, 90, 2, 101]). It is considered a standard today. The concept is easily generalized to the three dimensional theory. We review the crucial steps in this section, following the treatment of Ref. [2]. We will take the opposite approach compared to our previous discussion of the kinetic term. Instead of deriving the lattice action from first principles we just postulate the WILSON action and show that it gives the correct result in the continuum limit. Consider a group element

$$U_{ij} = e^{-ig_0 A_\mu(x_\mu)^a} , \quad (5.33)$$

to be associated with each link  $(i,j)$ . Traversing the link in the opposite direction should give the inverse element. Here the Lorentz index  $\mu$  is the direction of the link. The coordinate  $x_\mu$  associated with a particular link is assumed to lie in the middle of the link

$$x_\mu = \frac{a}{2}(i_\mu + j_\mu) . \quad (5.34)$$

The action is simply a sum over all plaquettes, which are elementary squares on the lattice

$$\mathcal{S} = \sum_{\square} \mathcal{S}_{\square} , \quad (5.35)$$

with the contribution of each individual plaquette being

$$\mathcal{S}_{\square} = \beta \left\{ 1 - \frac{1}{N} \text{ReTr} (U_{ij} U_{jk} U_{kl} U_{li}) \right\} . \quad (5.36)$$

The sites  $i, j, k, l$  lie at the corner points of the square. With (5.33) the contribution of a plaquette, centered at  $x_\mu$  and oriented in the  $(1, 2)$  plane is written as

$$\begin{aligned} \mathcal{S}_{\square} = \beta \left\{ 1 - \frac{1}{N} \text{ReTr} \left[ \exp \left( -ig_0 a A_1 \left( x_\mu - \frac{a}{2} \delta_{\mu 2} \right) \right) \exp \left( -ig_0 a A_2 \left( x_\mu + \frac{a}{2} \delta_{\mu 1} \right) \right) \right. \right. \\ \left. \left. \times \exp \left( ig_0 a A_1 \left( x_\mu + \frac{a}{2} \delta_{\mu 2} \right) \right) \exp \left( ig_0 a A_2 \left( x_\mu - \frac{a}{2} \delta_{\mu 1} \right) \right) \right] \right\} \end{aligned} \quad (5.37)$$

Using  $f(x_0 + \Delta x) \approx f(x_0) + \Delta x f'(x_0)$  we expand the vector potential  $A_\mu$  in powers of  $a$ :

$$\begin{aligned} \mathcal{S}_{\square} = \beta \left\{ 1 - \frac{1}{N} \text{ReTr} \left[ \exp \left( -ig_0 a A_1 + ig_0 \frac{a^2}{2} (\partial_2 A_1) \right) \exp \left( -ig_0 a A_2 - ig_0 \frac{a^2}{2} (\partial_1 A_2) \right) \right. \right. \\ \left. \left. \times \exp \left( ig_0 a A_1 + ig_0 \frac{a^2}{2} (\partial_2 A_1) \right) \exp \left( ig_0 a A_2 - ig_0 \frac{a^2}{2} (\partial_1 A_2) \right) \right] \right\} . \end{aligned} \quad (5.38)$$

Terms of order  $\mathcal{O}(a^3)$  are dropped since they are sub-leading in the continuum limit  $a \rightarrow 0$ . We must keep the  $\mathcal{O}(a^2)$  since otherwise the linear terms would simply cancel and the action would be zero for any  $\beta$ .

Since all nested commutators of the form  $[A, [A, B]]$ , of operators appearing in the exponents of (5.38) are of order  $\mathcal{O}(a^3)$  we can drop them and use the simple BAKER-CAMPBELL-HAUSDORFF formulas

$$e^X e^Y = e^Y e^X e^{[X,Y]} \quad , \quad e^{X+Y} = e^X e^Y e^{-[X,Y]/2} , \quad (5.39)$$

to rearrange (5.38)

$$\begin{aligned} \mathcal{S}_{\square} = \beta \left\{ 1 - \frac{1}{N} \text{ReTr} \left[ \exp \left( -ig_0 a^2 (\partial_1 A_2 - \partial_2 A_1) \right) \exp \left( -ig_0 a (A_1 + A_2) \right) \right. \right. \\ \left. \left. \times \exp \left( ig_0 a (A_1 + A_2) \right) \exp \left( ig_0 a ig_0 a [A_1, A_2] \right) \right] \right\} \\ = \beta \left\{ 1 - \frac{1}{N} \text{ReTr} \left[ \exp \left( -ig_0 a^2 (\partial_1 A_2 - \partial_2 A_1 - ig_0 [A_1, A_2]) \right) \right] \right\} . \end{aligned} \quad (5.40)$$

After identifying the element of the field strength tensor  $F_{12} = \partial_1 A_2 - \partial_2 A_1 - ig_0[A_1, A_2]$  we get

$$\mathcal{S}_\square = \beta \left\{ 1 - \frac{1}{N} \text{ReTr} \left[ \exp(-ig_0 a^2 F_{12}) \right] \right\}. \quad (5.41)$$

We now expand the exponential. Since we are dealing with unitary groups, the  $A_\mu$  that appear in  $F_{\mu\nu}$  are hermitian operators. Thus their trace is always real and the  $\mathcal{O}(a^2)$  terms vanish because of the factor  $i$ . We obtain finally

$$\mathcal{S}_\square = \beta \frac{g_0 a^4}{2N} \text{Tr}(F_{12}^2) + \mathcal{O}(a^6). \quad (5.42)$$

### 5.3 Time-like plaquette single counting vs. double counting

Setting  $m^2 = 0$  yields the lattice action

$$S = \beta \sum_{\square} \left( 1 - \frac{1}{2} \text{Re Tr } \mathbf{U}_\square \right) - \frac{1}{2} \beta \sum_{\langle ij \rangle} \text{tr} (\mathbf{L}_i \mathbf{U}_{ij} \mathbf{L}_j^\dagger \mathbf{U}_{ij}^\dagger + \text{h.c.}). \quad (5.43)$$

With our choice<sup>2</sup> of setting the coupling parameter of the gauge sector equal to that of the kinetic energy term of the WILSON line, we have obtained a lattice action that in the  $m^2 = 0$  limit is equivalent to the  $N_\tau = 1$  case of 4D YANG-MILLS theory, if one considers the WILSON line  $\mathbf{L}_i$  to be the single link in the time direction for each site.

The  $N_\tau = 1$  case however, is a special case of 4D YANG-MILLS since it allows for two different formulations, depending how one chooses to deal with the periodic boundary conditions in the  $\tau$ -direction.

Motivated by the sum over plaquettes in the partition function, one may assume that there is one time-like plaquette for each coordinate. In this case, space-like links require a special treatment, because they possess conjugate staples only in the positive time-direction direction (while there are two staples in each space-like direction). Space-like links differ from time-like links, because they are connected to five staples instead of six. Following the discussion in Ref. [102], we refer to this as *time-like plaquette single counting*. A second way is to consider  $N_\tau = 1$  to be the limiting case of arbitrary  $N_\tau$ . In this case, there is no special treatment of space-like links. They possess staples in the positive as well as the negative time direction, which happen to give equal contributions. This case we refer to as *time-like plaquette double counting*.

The WILSON line field in our case is obtained by compactification. This amounts to shrinking the time dimension while preserving the boundary conditions. We generally adopt the double counting scheme in this work. Some observables are also investigated in a single counting scheme and are discussed for comparison.

---

<sup>2</sup>The considerations in this section do not depend strictly on this choice, but the equivalence to  $N_\tau = 1$  gauge theory is exact in this case. Any other choice would require similar considerations.

## 6 Results without magnetic fields

In this chapter we present Monte-Carlo results of a simplified model, where the magnetic sector is neglected:

$$A_i = 0 . \quad (6.1)$$

This approximation fixes the link variables to unity, and yields a lattice action of the form

$$\mathcal{S} = -\frac{1}{2}\beta \sum_{\langle ij \rangle} \text{tr} \left( \mathbf{L}_i \mathbf{L}_j^\dagger + \text{h.c.} \right) - m^2 \sum_i |\text{tr} \mathbf{L}_i|^2 . \quad (6.2)$$

With this constraint, the theory is essentially reduced to a spin system. Such an approximation is useful since, with a suitable choice of parameters  $\beta$  and  $m^2$  it allows one to obtain a qualitative understanding of the eigenvalue structure of the deconfined phase of the  $3D$  effective theory introduced previously, with a drastic reduction in computing time. Note that the model (6.2) lies in a different universality class than the theory with gauge fields, due to the absence of a local symmetry, and thus one cannot expect a full correspondence of the phase structure. However the model (6.2) is also interesting in its own right. Spin models have long been considered as a simple analog of gauge theories, since their degrees of freedom are elements of LIE groups, which makes their properties depend on the geometry of the group. They share with gauge theories the property of asymptotic freedom in an appropriate dimension. Numerical and analytical data for different observables in the limit  $m^2 = 0$  of (6.2) exists in literature, with which a consistency check can be performed. Also, the action (6.2) possesses a simple local mean-field approximation, which can be compared to our numerical results in order to illustrate the importance of fluctuations close to the critical point. We will drop the constraint (6.1) in later chapters.

This chapter is structured as follows: First we discuss the symmetry breaking pattern of the kinetic energy term only. This corresponds to moving along the line of  $m^2 = 0$  in the  $\beta$ - $m^2$  plane. We then generalize to non-zero  $m^2$ , discuss the mean-field approximation, compare it to lattice results in different regions of the  $\beta$ - $m^2$  plane and map the phase diagram of the theory. To deepen our understanding of the different phases, we measure the inverse correlation length in various regions of the phase diagram and look in particular for divergences at the phase boundary. Next, we measure the distribution of sums and differences of eigenvalues in different regions of the phase diagram and search for eigenvalue repulsion in the region close above the phase transition. A detailed study of autocorrelations in the Monte Carlo time series can be found at the end of the chapter. We choose to present these measurements separate from the other material, since the reader who is primarily interested in the physics may want to skip these (very relevant) technical matters.

We employ a standard single hit METROPOLIS algorithm with sequential updating and periodic boundary conditions to generate lattice configurations. We start with an ordered initial condition where all field variables are set equal to the unit matrix. All Monte Carlo

sample sizes quoted in this chapter are statistically independent measurements of the equilibrium distribution, where a number of Monte Carlo steps larger than the integrated auto-correlation time was discarded between data points. The results in the  $m^2 = 0$  limit have been confirmed by replacing the updating algorithm by a CREUTZ heat bath.

## 6.1 Chiral model of Kogut, Stone and Snow

A model consisting only of the kinetic energy term of the action (6.2) was first studied in three dimensions<sup>1</sup> numerically by lattice simulations and analytically by mean-field approximation in Ref. [105] by KOGUT, STONE and SNOW. Later, Refs. [106, 107] and [108] obtained improved results with higher precision. The action of this model

$$S = -\frac{1}{2}\beta \sum_{\langle ij \rangle} \text{tr} (\mathbf{L}_i \mathbf{L}_j^\dagger + \text{h.c.}) , \quad (6.3)$$

has a global  $SU(2)_L \times SU(2)_R$  symmetry, which is an invariance under the transformation

$$\mathbf{L}_i \mapsto \Omega_L \mathbf{L}_i \Omega_R^\dagger \quad \forall i , \quad (6.4)$$

where  $\Omega_{L,R}$  are two distinct  $SU(2)$  matrices which are constant over space<sup>2</sup>. The model is formally equivalent to a *nonlinear sigma model* for the chiral phase transition of QCD [111, 112], however here it is investigated in the context of deconfinement and the degrees of freedom are WILSON lines, rather than mesonic fields.

### 6.1.1 $O(4)$ -like order parameter

The model (6.3) possesses a global order parameter of which a finite expectation value signals the spontaneous breaking of the  $SU(2)_L \times SU(2)_R$  symmetry. This occurs when the coupling constant  $\beta$  is larger than a certain threshold value  $\beta_C$ . To understand the symmetry breaking pattern, note that the symmetry under (6.4) is equivalent to a global symmetry under  $SU(2)_V \times SU(2)_A$ , where  $SU(2)_V$  denotes the *vector transformations*

$$\mathbf{L}_i \mapsto \Omega_V \mathbf{L}_i \Omega_V^\dagger \quad \forall i , \quad (6.5)$$

and  $SU(2)_A$  denotes the *axial transformations*

$$\mathbf{L}_i \mapsto \Omega_A \mathbf{L}_i \quad \forall i . \quad (6.6)$$

Equivalence to (6.4) follows if one identifies

$$\Omega_V \equiv \Omega_R \quad \text{and} \quad \Omega_A \equiv \Omega_L \Omega_R^\dagger . \quad (6.7)$$

For any  $\mathbf{L} = \ell_0 \mathbf{1} + i \ell_j \sigma_j$  the vector transformations  $SU(2)_V$  rotate the  $\sigma_j$  amongst themselves, but leave  $\ell_0$  invariant since

$$\ell_0 = \text{tr} \mathbf{L} \mapsto \text{tr} (\Omega_V \mathbf{L}_i \Omega_V^\dagger) = \text{tr} \mathbf{L} , \quad (6.8)$$

<sup>1</sup>Other authors have studied similar models in two spatial dimensions. See e.g. Refs. [103, 104].

<sup>2</sup>The model therefore differs from others which deal exclusively with the trace of  $\mathbf{L}$ , such as  $\mathcal{S} \sim -\beta \sum (\text{tr} \mathbf{L}_i \text{tr} \mathbf{L}_j^\dagger + \text{c.c.})$  [109, 110]



and

$$[U, \sigma_i] \neq 0 \quad \text{for} \quad U \neq a_0 \mathbf{1} \in SU(2) . \quad (6.9)$$

The axial transformations  $SU(2)_A$  rotate the  $\ell_0$  and the  $\ell_i$  into each other. The “length”  $\ell_0^2 + \ell_i^2$  is preserved for both  $SU(2)_V$  and  $SU(2)_A$  individually, since

$$\ell_0^2 + \ell_i^2 = \det \mathbf{L} = \det(U\mathbf{L}) = \det(U\mathbf{L}U^\dagger) \quad \text{for} \quad U \in SU(2) . \quad (6.10)$$

Thus, since  $SU(2)_V$  does not change  $\ell_0$  it also preserves  $\ell_i^2$  (where the sum convention is implied).

The symmetry broken phase of the action (6.3) is a state where nearest neighbor matrices are forced to align. This corresponds to the breaking of  $SU(2)_L \times SU(2)_R$  down to  $SU(2)_V$  as we will see further down. To obtain an expression for the order parameter in terms of the volume averaged field  $\bar{\mathbf{L}}$ , one uses the fact that the sum over any number of  $SU(2)$  matrices is proportional to another  $SU(2)$  matrix (see appendix A). One can thus calculate

$$\frac{1}{N_s^3} \sum_i \mathbf{L}_i = \bar{\mathbf{L}} = c \Omega , \quad (6.11)$$

where  $N_s$  is the spatial extent of the lattice, and extract the constant  $u_0 = \langle |c| \rangle$  (which is always  $\geq 0$  by construction). Considering

$$\text{Tr}(c \Omega^\dagger)(c \Omega) = |c|^2 \text{Tr}(\Omega^\dagger \Omega) = 2 |c|^2 , \quad (6.12)$$

allows us to isolate  $u_0$ :

$$u = \sqrt{\text{Tr} \bar{\mathbf{L}}^\dagger \bar{\mathbf{L}} / 2} , \quad u_0 = \langle u \rangle . \quad (6.13)$$

This is the “length” of the average of the field  $\mathbf{L}$  in the space of quaternions, or correspondingly the length of the four dimensional vector defined by the parameters  $a_{i=0\dots 4}$  of  $\bar{\mathbf{L}} = a_0 \mathbf{1} + a_j i \sigma_j$ . Thus we refer to it as the  $O(4)$  order parameter.

When  $u_0$  is non-zero the system chooses a ground state at random on the four-dimensional sphere defined by  $a_0^2 + a_i^2 = u_0^2$ . Assuming that the system has chosen  $\bar{\mathbf{L}} = a_0 \mathbf{1}$  one can see the residual  $SU(2)_V$  symmetry by considering that

$$\bar{\mathbf{L}} = a_0 \mathbf{1} \mapsto \Omega_V a_0 \mathbf{1} \Omega_V^\dagger = a_0 \mathbf{1} . \quad (6.14)$$

Note that the expectation value of  $\bar{\mathbf{L}}$

$$\langle \bar{\mathbf{L}} \rangle = \frac{1}{N_s^3} \langle \sum_i \mathbf{L}_i \rangle , \quad (6.15)$$

is not a good order parameter since even though the nearest neighbor matrices become aligned for large  $\beta$ , there is no preferred direction for  $\mathbf{L}$  in group space and therefore Monte-Carlo estimates for (6.15) converge to zero for long run-times.<sup>3</sup>

We perform lattice simulations of (6.3) on lattice sizes  $N_s = 12, 24, 36, 48$ . Fig. 6.1 shows measurements of the order-parameter  $u_0$  in the range  $\beta = 0.0 \dots 3.0$ . The left-hand side

<sup>3</sup>This is an example of ELITZUR’s *theorem* [113].

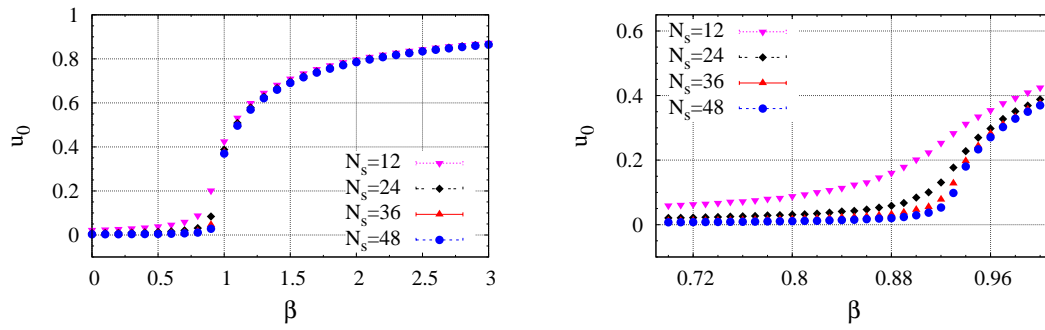


Figure 6.1: The order-parameter (6.13) measured on  $N_s = 12, 24, 36, 48$ . Left: Step-size  $\Delta\beta = 0.1$ , 2500 configurations per  $\beta$ . Right: Step-size  $\Delta\beta = 0.01$ , 1250 configurations per  $\beta$ .

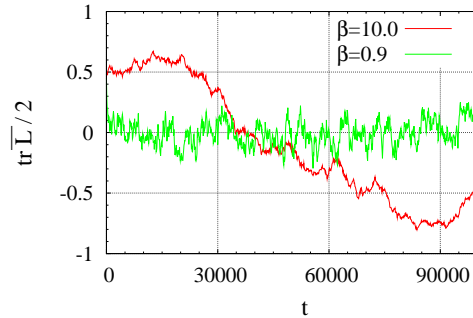


Figure 6.2: Time evolution of the volume averaged POLYAKOV loop below ( $\beta = 0.9$ ) and far above  $\beta_C$  ( $\beta = 10$ ), measured on  $N_s = 12$ .

shows results for a coarse resolution with step-size  $\Delta\beta = 0.1$ , where 2500 configurations were generated for each value of  $\beta$ . The system clearly undergoes a phase transition at  $\beta_C \approx 0.9$ . The right-hand side shows precision measurements in the immediate vicinity of  $\beta_C$ , with the increased resolution of  $\Delta\beta = 0.01$ . Due to critical slowing down, independent configurations are much more costly in simulation time in this region. We generate 1250 configurations for each point in  $\beta = 0.7 \dots 1.0$ .

To demonstrate the slow rotation of  $\bar{\mathbf{L}}$  in the ordered phase, which leads to vanishing expectation values for local order parameters, in Fig. 6.2 we show the evolution in Monte-Carlo time of the volume averaged POLYAKOV loop  $\bar{\ell} = \frac{1}{2}\text{Tr} \bar{\mathbf{L}}$  for two values of  $\beta$  below and far above  $\beta_C$ . One observes that  $\bar{\ell}$  wildly fluctuates around 0 in the disordered phase. Above  $\beta_C$ , where the WILSON lines are aligned,  $|\bar{\ell}|$  is far from 0 for long time intervals.

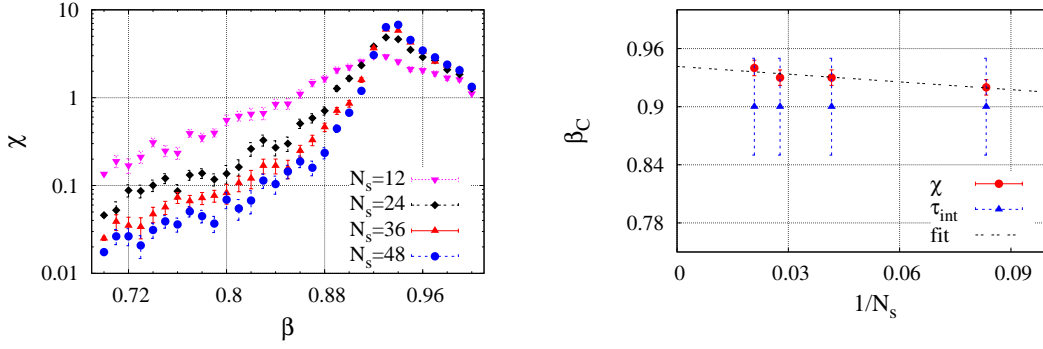


Figure 6.3: Left: The susceptibility  $\chi$  for lattice sizes  $N_s = 12, 24, 36, 48$ . Right: The linear  $1/N_s \rightarrow 0$  extrapolation of  $\beta_C$ . The triangles show the consistency with the peak of the integrated autocorrelation time (see end of chapter for discussion)

### 6.1.2 Susceptibility

To estimate the infinite volume limit of  $\beta_C$  we compute the *temperature susceptibility*

$$\chi(\beta) = \frac{\partial u_0}{\partial \beta}, \quad (6.16)$$

check how the position of the peak shifts as a function of  $1/N_s$  and extrapolate to  $1/N_s \rightarrow 0$ . An estimate for (6.16) is obtained directly from our data for  $u_0$ , by taking

$$\chi(\beta) = \frac{u_0(\beta + \Delta\beta) - u_0(\beta - \Delta\beta)}{2\Delta\beta}, \quad (6.17)$$

and applying standard error propagation formulas. The position of the peak defines  $\beta_C$  for any given lattice size. A linear extrapolation to  $1/N_s = 0$  yields

$$\beta_C = 0.942(5), \quad (6.18)$$

(see Fig. 6.3). This value is slightly larger than the estimate obtained in Ref.[105], where smaller lattices and lower statistics were used.

### 6.1.3 Internal energy

Another observable which is immediately available once the updating algorithm has been implemented is the *internal energy* per link.

$$\overline{E} = \frac{1}{3N_s^3} \sum_{\langle ij \rangle} \text{tr}(\mathbf{L}_i \mathbf{L}_j^\dagger). \quad (6.19)$$

Fig. 6.4 shows results for (6.19) obtained on cubic lattices of  $N_s = 12, 24, 36, 48$  (we used the same data sets as for the measurements of  $u_0$ ) together with the corresponding susceptibility

$$\chi_E(\beta) = \frac{\partial \langle \overline{E} \rangle}{\partial \beta}. \quad (6.20)$$

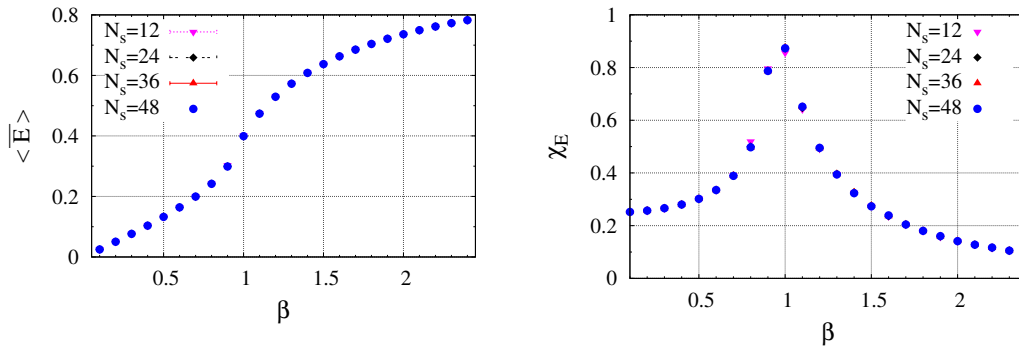


Figure 6.4: Left: The internal energy per link  $\langle \bar{E} \rangle$ , measured on  $N_s = 12, 24, 36, 48$ . Right: The susceptibility  $\chi_E(\beta)$ .

Our measurements of the internal energy reproduce those of Refs. [106, 108] for all values of  $\beta$  considered, but differs slightly from Ref. [105]. Note that the peak of  $\chi_E(\beta)$  is consistent with  $\beta_C = 0.942(5)$  within numerical precision.

#### 6.1.4 Two-point correlation function

We expect that in the region  $\beta < \beta_C$  the *adjoint fields*

$$\tilde{\ell}^a(\mathbf{x}) = \frac{1}{2i} \text{Tr} \mathbf{L}(\mathbf{x}) \boldsymbol{\tau}^a \quad (6.21)$$

as well as the *singlet field*

$$\ell(\mathbf{x}) = \frac{1}{2} \text{Tr} \mathbf{L}(\mathbf{x}) \quad (6.22)$$

are massive, since long range correlations are screened by thermal fluctuations. At  $\beta_C$ , the critical fluctuations that emerge at a second order phase transition should generate correlations over large distances. For  $\beta > \beta_C$ , since there is a spontaneously broken continuous global symmetry we also expect massless modes to be present, which correspond to the slow rotations in group space discussed in section 6.1.1 (Fig. 6.2) and which induce long-range collective behavior<sup>4</sup>. To confirm these expectations, we measure the two-point matrix-matrix correlation function

$$\mathcal{C}_{\mathbf{L}}(r) = \frac{1}{3} \frac{1}{N_s^3} \sum_{\hat{\mathbf{r}}, \mathbf{r}_0} \frac{1}{2} \left\langle \text{tr} \mathbf{L}^\dagger(\mathbf{r}_0) \mathbf{L}(\mathbf{r}_0 + \mathbf{r}) \right\rangle. \quad (6.23)$$

which mixes excitations of (6.21) and (6.22), and extract the inverse spatial correlation length  $m_\xi = \frac{1}{\xi}$ , which is the effective *Debye screening mass*, by performing a  $\chi^2$  fit to the functional form

$$\mathcal{C}_{\mathbf{L}}(r) \sim \frac{1}{rm_\xi} e^{-rm_\xi} + \text{const.}, \quad (6.24)$$

<sup>4</sup>By *Goldstone's theorem*, the number of massless modes is equal to the dimension of the symmetry group  $G$  of the Lagrangian minus the dimension of  $H$ , which is the symmetry group of the vacuum. For our case  $SU(2)_L \times SU(2)_R$  is broken to  $SU(2)_V$ , so since  $SU(N)$  has  $N^2 - 1$  generators, the number of massless modes should be  $2 * (2^2 - 1) - (2^2 - 1) = 3$ . For a proof of the theorem see e.g. Refs. [1] or [114].

at  $r \geq 4$  (see also Ref. [42]).

Fig. 6.5 shows  $m_\xi$  measured on  $N_s = 12, 24, 36, 48$  for  $\beta = 0.7 \dots 1.0$ . Below  $\beta_C$  we measured  $\mathcal{C}_L(r)$  for 2500 independent configurations for each value of  $\beta$  on all lattice sizes. For  $\beta \geq \beta_C$  successively larger number of configurations must be discarded for larger  $N_s$  due to critical slowing down. At  $N_s = 48$  we measured on the order of 250 data points for  $\beta \geq \beta_C$ .

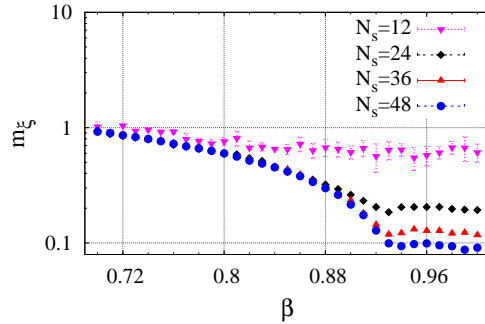


Figure 6.5: The inverse spatial correlation length  $m_\xi$  as a function of  $\beta$  measured on  $N_s = 12, 24, 36, 48$ .

The results shown in fig. 6.5 indicate that  $m_\xi$  is zero up to finite size effects for  $\beta \geq \beta_C$ , which confirms the presence of massless modes. At  $\beta_C$  we extract a scaling exponent  $\nu_\xi$  by performing a fit of the form

$$m_\xi(\beta_C) \sim N_s^{-1/\nu_\xi} . \quad (6.25)$$

Fitting the  $N_s = 24, 36, 48$  lattices only, we find

$$\nu_\xi = 0.938(5) . \quad (6.26)$$

We have measured the correlation lengths also individually for the singlet field  $\ell(\mathbf{x})$  and adjoint field  $\tilde{\ell}^a(\mathbf{x})$  by fitting (6.24) to correlation functions of the form

$$\mathcal{C}_\ell(r) \sim \sum_{\hat{\mathbf{r}}, \mathbf{r}_0} \langle \ell(\mathbf{r}_0) \cdot \ell(\mathbf{r}_0 + \mathbf{r}) \rangle , \quad (6.27)$$

$$\mathcal{C}_{\tilde{\ell}}(r) \sim \sum_{\hat{\mathbf{r}}, \mathbf{r}_0} \langle \tilde{\ell}(\mathbf{r}_0) \cdot \tilde{\ell}(\mathbf{r}_0 + \mathbf{r}) \rangle . \quad (6.28)$$

We refrain from showing explicit results, since they closely resemble Fig. 6.5.

## 6.2 Model with Polyakov loop potential term

We now turn to the action

$$\mathcal{S} = -\frac{1}{2}\beta \sum_{\langle ij \rangle} \text{tr} \left( \mathbf{L}_i \mathbf{L}_j^\dagger + \text{h.c.} \right) - m^2 \sum_i |\text{tr} \mathbf{L}_i|^2 , \quad (6.29)$$

where  $m^2$  is non-zero. The inclusion of the mass term breaks the  $SU(2)_L \times SU(2)_R$  symmetry down to global  $SU(2)$ . The action (6.29) is invariant under

$$\mathbf{L}_i \mapsto \Omega \mathbf{L}_i \Omega^\dagger \quad \forall i. \quad (6.30)$$

We expect that for large values of  $m^2$  there should be a phase where  $\langle |\frac{1}{2} \text{Tr} \bar{\mathbf{L}}| \rangle \approx 1$  since for such a configuration the mass term gives a negative contribution to the action. We therefore investigate the expectation value of the volume averaged POLYAKOV loop

$$\bar{\ell} = \frac{1}{2} \text{Tr} \bar{\mathbf{L}} \quad (6.31)$$

in addition to the  $O(4)$  order-parameter defined in eq. (6.13). In particular, the mean-field approximation in the following paragraph yields analytic predictions for  $\langle |\bar{\ell}| \rangle$  above the phase transition, which are compared to Monte-Carlo results in later sections.

### 6.2.1 Mean field approximation

The mean field approximation of the model (6.3) without a mass term was discussed at length in Ref. [105]. We generalize this discussion to non-zero  $m^2$ . Consider the partition function

$$\mathcal{Z} = \int \prod_k [d\mathbf{L}_k] \exp \left\{ \frac{1}{2} \beta \sum_{\langle ij \rangle} \text{tr} \left( \mathbf{L}_i \mathbf{L}_j^\dagger + \text{h.c.} \right) + m^2 \sum_i |\text{tr} \mathbf{L}_i|^2 \right\}, \quad (6.32)$$

where  $d\mathbf{L}_k$  denotes the invariant group measure at each site, and replace the interaction of each  $\mathbf{L}_i$  with its  $2d$  nearest neighbors, where  $d$  is the number of spatial dimensions, by interactions with a fixed matrix  $\bar{\mathbf{L}}$ :

$$\sum_j \mathbf{L}_j \longrightarrow 2d \bar{\mathbf{L}}. \quad (6.33)$$

The partition function (6.32) then factorizes

$$\mathcal{Z} \longrightarrow \mathcal{Z}_{ss}^N, \quad (6.34)$$

and thus the problem is completely determined by considering a single lattice site. The free energy of a single site  $\mathcal{F}_{ss}$  can then be obtained from the single site partition function

$$e^{-N\mathcal{F}_{ss}(\bar{\mathbf{L}})} = \mathcal{Z}_{ss}^N, \quad (6.35)$$

where  $N$  is the number of lattice sites and

$$\mathcal{Z}_{ss} = \int [d\mathbf{L}] \exp \left[ d\beta \text{tr} \left( \mathbf{L} \bar{\mathbf{L}}^\dagger + \bar{\mathbf{L}} \mathbf{L}^\dagger \right) + m^2 |\text{tr} \mathbf{L}|^2 \right]. \quad (6.36)$$

We now consider the expectation value

$$\begin{aligned} \langle (\mathbf{L})_{lk}^* \rangle &= \frac{1}{\mathcal{Z}_{ss}} \int [d\mathbf{L}] (\mathbf{L})_{lk}^* \exp \left\{ d\beta \sum_i \sum_j [(\mathbf{L})_{ij} (\bar{\mathbf{L}})_{ij}^* + (\bar{\mathbf{L}})_{ij} (\mathbf{L})_{ij}^*] + m^2 |\text{tr} \mathbf{L}|^2 \right\} \\ &= \frac{1}{\mathcal{Z}_{ss}} \int [d\mathbf{L}] \frac{1}{d\beta} \frac{\partial}{\partial (\bar{\mathbf{L}})_{lk}} \exp(-\mathcal{S}_{ss}) = \frac{1}{d\beta} \frac{1}{\mathcal{Z}_{ss}} \frac{\partial \mathcal{Z}_{ss}}{\partial (\bar{\mathbf{L}})_{lk}} \\ &= \frac{1}{d\beta} \frac{\partial}{\partial (\bar{\mathbf{L}})_{lk}} \log \mathcal{Z}_{ss}(\bar{\mathbf{L}}). \end{aligned} \quad (6.37)$$

Note that the indices  $i, j, k, l$  here label matrix elements, not lattice sites. Mean field self consistency requires (6.37) to be equal to

$$(\bar{\mathbf{L}})_{lk}^* = \frac{\partial}{\partial (\bar{\mathbf{L}})_{lk}} (\bar{\mathbf{L}})_{lk}^* (\bar{\mathbf{L}})_{lk} , \quad (6.38)$$

where the sum convention is implied for the second index pairs on the right hand side, so

$$\frac{\partial}{\partial (\bar{\mathbf{L}})_{lk}} \left[ \frac{1}{d\beta} \log \mathcal{Z}_{ss}(\bar{\mathbf{L}}) - (\bar{\mathbf{L}})_{lk}^* (\bar{\mathbf{L}})_{lk} \right] = 0 . \quad (6.39)$$

This is equivalent to demanding that the *mean field free energy*, defined as

$$\mathcal{F}_{\text{mf}}(\bar{\mathbf{L}}) = \mathcal{F}_{ss}(\bar{\mathbf{L}}) + d\beta \text{tr} \bar{\mathbf{L}}^\dagger \bar{\mathbf{L}} , \quad (6.40)$$

must be minimized, with respect to  $\bar{\mathbf{L}}$ :

$$\frac{\partial}{\partial \bar{\mathbf{L}}} \mathcal{F}_{\text{mf}}(\bar{\mathbf{L}}) = 0 . \quad (6.41)$$

To proceed, we note that  $\bar{\mathbf{L}}$  must be proportional to a  $SU(2)$  matrix

$$\bar{\mathbf{L}} = \bar{\ell} \mathbf{U} . \quad (6.42)$$

We exploit the invariance of the group measure  $[d\mathbf{L}]$  to rotate  $U$  in (6.36) to the identity, by transforming

$$\mathbf{L} \rightarrow \mathbf{L} \mathbf{U} \quad (6.43)$$

The partition function (6.36) then becomes

$$e^{-\mathcal{F}_{ss}(\bar{\ell})} = \int [d\mathbf{L}] \exp \left[ 2d\beta\bar{\ell} \text{tr} (\mathbf{L} + \mathbf{L}^\dagger) + m^2 |\text{tr} \mathbf{L}|^2 \right] . \quad (6.44)$$

This group integral can be expressed as an ordinary integral using the parameterization of WEYL and VANDERMONDE [105]. The matrix  $\mathbf{L}$  can be diagonalized by unitary transformation:

$$\mathbf{L} = \mathbf{D} \begin{pmatrix} e^{i\phi_1} & 0 & \dots & \\ 0 & e^{i\phi_2} & \dots & \\ \vdots & \vdots & \ddots & \\ & & & e^{i\phi_N} \end{pmatrix} \mathbf{D}^\dagger . \quad (6.45)$$

Since  $\mathbf{L}$  belongs to  $SU(N)$ , the sum over  $\phi$  must be zero, modulo  $2\pi$ , to fulfill  $\det \mathbf{L} = 1$ . The matrices  $\mathbf{D}$  and  $\mathbf{D}^\dagger$  cancel each other in (6.44) due to the cyclic property of the trace. The group measure factorizes

$$[d\mathbf{L}] = d\mu(\phi) [d\mathbf{D}] , \quad (6.46)$$

with

$$d\mu(\phi) = \prod_{i=1}^N \frac{d\phi_i}{2\pi} |\Delta(\phi)|^2 \cdot \sum_{l=-\infty}^{l=+\infty} 2\pi\delta\left(\sum_{i=1}^N \phi_i - 2\pi l\right), \quad (6.47)$$

$$\Delta(\phi) = \frac{1}{\sqrt{N!}} \sum_{i_1, \dots, i_N} \epsilon_{i_1, i_2, \dots, i_N} e^{i\phi_1(N-i_1)} e^{i\phi_2(N-i_2)} \dots e^{i\phi_N(N-i_N)}. \quad (6.48)$$

The delta functions in (6.47) are needed to ensure special unitarity.  $\Delta(\phi)$  is called the VANDERMONDE *determinant*. We set  $l = 0$  and find for the group  $SU(2)$

$$[d\mathbf{L}] \sim d\phi |\Delta(\phi)|^2 = d\phi \sin^2 \phi. \quad (6.49)$$

With  $\int [d\mathbf{D}] = 1$  we can write

$$e^{-\mathcal{F}_{ss}(\bar{\ell})} = \int_{-1}^1 d\cos\phi \exp\left[4d\beta\bar{\ell}\cos\phi + 4m^2\cos^2\phi + \frac{1}{2}\log(1-\cos^2\phi)\right]. \quad (6.50)$$

The quantity  $\bar{\ell}$  is simply the volume averaged POLYAKOV loop. The VANDERMONDE determinant contributes a potential term. We evaluate the expression (6.50) numerically using a standard Gaussian quadrature algorithm [115]. We write (6.40) in terms of  $\bar{\ell}$

$$\mathcal{F}_{\text{mf}}(\bar{\ell}) = \mathcal{F}_{ss}(\bar{\ell}) + 2d\beta\bar{\ell}^2, \quad (6.51)$$

and extract the value of  $\bar{\ell}$  at the minimum for various combinations of  $\beta$  and  $m^2$ . Lattice results for  $\bar{\ell}$  are obtained in the next paragraph. We will then show comparisons of (6.51) to lattice data.

### 6.2.2 Phase diagram

To map the phase diagram of (6.2) in terms of  $\beta$  and  $m^2$ , we measure the  $O(4)$  order-parameter  $u_0$  defined in Eq. (6.13) as well as the volume averaged POLYAKOV loop

$$\bar{\ell} = \frac{1}{2} \text{Tr} \bar{\mathbf{L}}, \quad (6.52)$$

with their respective susceptibilities. We have already seen that a second order phase transition occurs along the line of  $m^2 = 0$  at  $\beta_C = 0.942(5)$ , where nearest neighbor matrices are forced to align, but the direction of alignment remains arbitrary. We expect that a positive value of  $m^2$  would give preference to an alignment with the (positive or negative) unit matrix, while a negative value of  $m^2$  would prefer an alignment outside of the group center, with  $\mathbf{L} \sim i\sigma_3$  or  $SU(2)$  rotations thereof, where the trace vanishes.

We now consider fixed positive and negative values of  $m^2$  and measure  $u_0$  and  $\bar{\ell}$  for large ranges of  $\beta$ , as well as fixing  $\beta$  to different positive values and measuring  $u_0, \bar{\ell}$  as a function of  $m^2$ . We consider  $N_s = 12, 24, 36, 48$  lattices and generate on the order of a few thousand independent configurations for each combination of parameters far from the phase boundaries and on the order of a few hundreds close to the phase boundary. We refrain from discussing each data set individually here. Our findings are summarized in the diagram



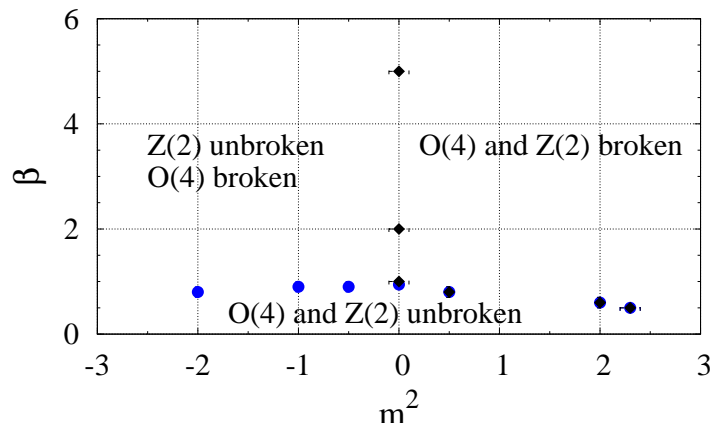


Figure 6.6: Phase diagram of the theory defined by (6.29). The diamonds mark the phase boundary between phases where  $Z(2)$  is broken/unbroken. The dots indicate the phase boundary of spontaneous breaking of  $SU(2)_L \times SU(2)_R \approx O(4)$  down to  $SU(2)_V \approx SO(3)$ , which coincides with breaking of the  $Z(2)$  center symmetry for  $m^2 > 0$ .

in Fig. 6.6. For  $m^2 < 0$ , as expected, the phase transition along the  $\beta$  axis is driven by the alignment of nearest neighbors, forced by the kinetic term in the action, but the sites are aligned outside of the group center. In the upper left region  $u_0$  is non-zero while  $\langle |\bar{\ell}| \rangle$  vanishes.

For  $\beta > \beta_C$  there is a  $Z(2)$  breaking phase transition along the  $m^2$  axis at exactly  $m^2 = 0$ , where the direction of alignment changes to  $\mathbf{L} = \pm \mathbf{1}$ . Fig. 6.7 illustrates this explicitly for  $\beta = 1.0$ . The derivative  $\partial \langle |\bar{\ell}| \rangle / \partial m^2$  peaks at

$$m_c^2 = 0.000(2) , \quad (6.53)$$

within errors on all lattice sizes considered. The transition in terms of  $m^2$  is evidently rather sharp, but the scaling of the inverse correlation length  $m_\xi$  shown in the next section and the integrated autocorrelation time  $\tau_{int}$ , discussed at the end of the chapter, suggests a second order phase transition. For positive  $m^2$  at  $\beta < \beta_C$  the phase transition is driven by the potential, rather than the kinetic term. Crossing the phase boundary here yields non-zero  $u_0$  and  $\langle |\bar{\ell}| \rangle$ .

Fig. 6.8 shows the expectation value of the POLYAKOV loop from a  $N_s = 24$  lattice (which is close to the infinite volume limit except very close to the phase boundary) together with the mean field prediction discussed in section 6.2.1 over a broad range of  $m^2$  for  $\beta = 1.0$  and  $\beta = 0.5$ . The mean field curves have been shifted to the right to match the data far above the transition. Such a shift is expected by analogy to the tadpole contribution in a scalar theory, for example. Not surprisingly, the mean field works well far from the transition to both sides, when fluctuations are suppressed, but fails close to the phase transition due to critical fluctuations. As we will see in the next section, effective masses for  $\ell$  are large far from the transition, which is consistent with these findings.

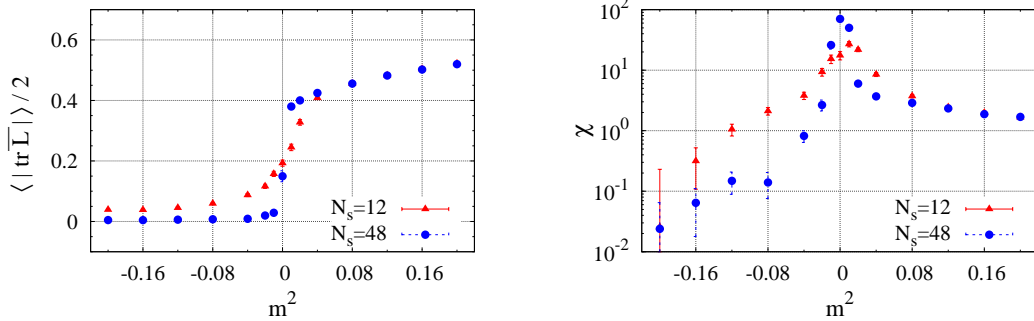


Figure 6.7: Spontaneous breaking of  $Z(2)$  center symmetry occurs at  $m^2 = 0$  for  $\beta = \beta_C$ . Left: Volume averaged POLYAKOV loop  $|\overline{\ell}|$ , on  $N_s = 12, 48$  lattices. Right: Susceptibility  $\partial \langle |\overline{\ell}| \rangle / \partial m^2$ .

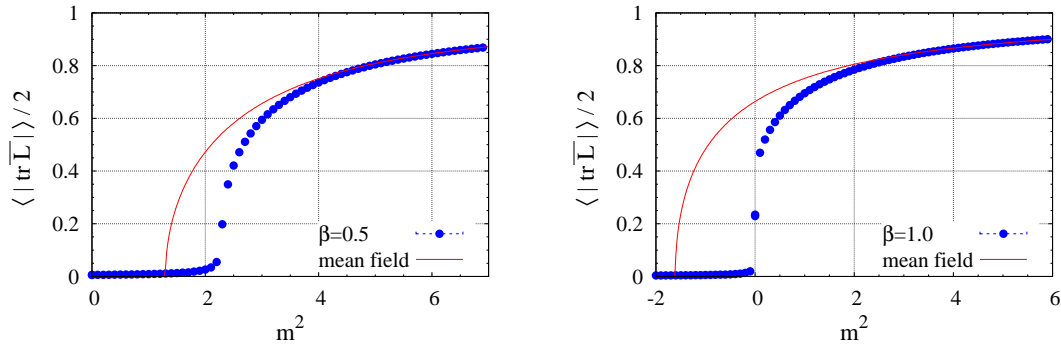


Figure 6.8: Volume averaged POLYAKOV loop  $|\overline{\ell}|$  for  $\beta = 0.5$  (left) and  $\beta = 1.0$  (right) together with the mean field prediction discussed in section 6.2.1. The mean field curves were shifted along the  $m^2$  axis to match  $|\overline{\ell}|$  at large  $m^2$ .

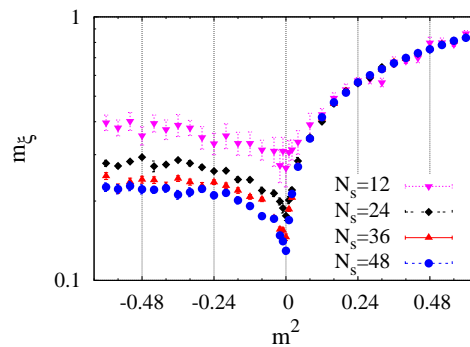


Figure 6.9: The inverse matrix-matrix correlation length defined by the two-point function (6.23), measured on  $N_s = 12, 24, 36, 48$  lattices at  $\beta = 1.0$ .

### 6.2.3 Correlation functions

To deepen our understanding of the symmetry breaking patterns present in the  $\beta - m^2$  plane, we measure matrix-matrix correlation functions (6.23) as well as correlation functions for POLYAKOV loops (6.27) and adjoint fields (6.28) also for non-zero  $m^2$  and extract screening masses by fitting to Eq. (6.24). Fig. 6.9 shows the behavior of the inverse matrix-matrix correlation length, for fixed  $\beta = 1.0$  when crossing the phase boundary at  $m^2 = 0$ . The vanishing screening mass at exactly  $m^2 = 0.0$  is expected from our prior results. Fitting  $m_\xi \sim N_s^{-1/\nu_\xi}$  to the  $N_s = 24, 36, 48$  data at  $\beta = 1.0/m^2 = 0.0$  gives the scaling exponent

$$\nu_\xi = 2.28(8) . \quad (6.54)$$

An interesting observation are the long range correlations that also appear to be present for  $m^2 < 0$ . Here the volume dependence of  $m_\xi$  is weaker than at exactly  $m^2 = 0.0$ , but we have confirmed that  $m_\xi$  vanishes in infinite volume here as well (e.g. with the scaling exponent  $\nu'_\xi = 3.5(3)$  at  $m^2 = -0.2$ ). To understand how these correlations emerge, consider Fig. 6.10, which shows inverse correlation lengths also in the singlet and the adjoint channels on  $N_s = 12, 24$  lattices. The adjoint channel is massless for negative  $m^2$ , but unlike for the KSS model the POLYAKOV loop channel is massive on both sides of the phase boundary. This confirms that the massless excitations in this case, are the global rotations in the sub-manifold spanned by the group generators in contrast to the KSS model, where rotations in the full  $SU(2)$  group were possible. The matrix-matrix correlation function simply mixes both channels, and is dominated at large distances by the lowest excitation, which in this case is the massless mode.

Separate measurements on larger lattices were performed precisely at the transition at  $\beta = 1.0/m^2 = 0.0$  on 3500 configurations. For the singlet channel on  $N_s = 24, 36, 48$  lattices, with  $m_\xi \sim N_s^{-1/\nu_\xi}$  we find

$$\nu_\xi^{\text{singl}} = 1.3(1) . \quad (6.55)$$

For the adjoint channel we find

$$\nu_\xi^{\text{adj}} = 2.1(7) . \quad (6.56)$$

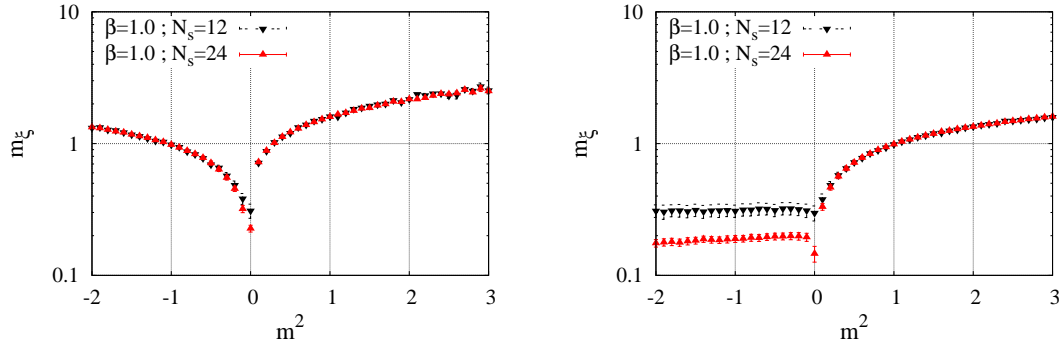


Figure 6.10: The inverse correlation length of POLYAKOV loops (left) and of the adjoint fields (right) at  $\beta = 1.0$ , measured on  $N_s = 12, 24$  lattices on 5000 configurations for  $|m^2| \geq 0.5$  and 2000 configurations for  $|m^2| \leq 0.5$ .

#### 6.2.4 Eigenvalue distribution

Finally, we determine the distribution of eigenvalues of the WILSON line. Measurements were performed on lattice sizes  $N_s = 9, 12, 24, 48$  with sample sizes ranging from 2000 to 5000 configurations. We find that the results discussed here are independent of  $N_s$  for  $N_s \geq 12$ . The figures shown in this section represent the  $N_s = 24$  results.

For any given configuration we compute the eigenvalues  $\lambda_1$  and  $\lambda_2$  of the WILSON line  $\mathbf{L}$  at each site. In terms of the parameters  $a_{0\dots 3}$  of  $\mathbf{L}$ , they are given by

$$\lambda_{1,2} = a_0 \pm \sqrt{a_0^2 - 1} \quad (6.57)$$

(see appendix A for explicit calculation). We define two functions  $\rho_1$  and  $\rho_2$  as

$$\rho_1(\mathbf{x}) = \frac{1}{2} |\lambda_1(\mathbf{x}) - \lambda_2(\mathbf{x})| = \sqrt{a_0^2 - 1} = \sqrt{\ell^2 - 1} . \quad (6.58)$$

and

$$\rho_2(\mathbf{x}) = \frac{1}{2} |\lambda_1(\mathbf{x}) + \lambda_2(\mathbf{x})| = a_0 = \ell , \quad (6.59)$$

and determine their normalized distribution functions  $P(\rho_1)$  and  $P(\rho_2)$  in the thermal ensemble via histogramming. Note that with the definitions (6.58) and (6.59) eigenvalue attraction corresponds to a peak of  $P(\rho_2)$  around  $\rho_2 = 1$ , while a flat distribution or a peak around  $\rho_2 = 0$  indicate the presence of eigenvalue repulsion.

Considering that the partition function of a single site can be written as

$$\mathcal{Z}_{ss} = \int d\ell P(\ell) = \int d\ell e^{-V(\ell)} , \quad (6.60)$$

the probability distributions  $P(\rho_1)$  and  $P(\rho_2)$  can be turned into effective potentials for  $\rho_{1,2}$  by taking the negative logarithm

$$V_{\text{eff}}(\rho_1) = -\log P_1(\rho_1) , \quad V_{\text{eff}}(\rho_2) = -\log P_2(\rho_2) . \quad (6.61)$$

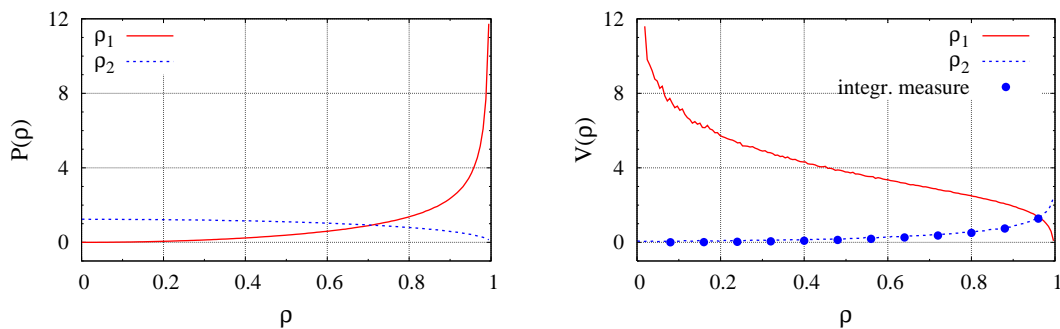


Figure 6.11: Left: Weight function  $P$  for the difference  $\rho_1$  and the average  $\rho_2$  of eigenvalues  $\lambda_{1,2}$  of the WILSON line  $\mathbf{L}$  measured on  $N_s = 24$  at  $\beta = 1.0, m^2 = 0.0$ . Right: Corresponding potentials  $V_{\text{eff}} = -\log P$  together with the contribution to  $V_{\text{eff}}(\rho_2)$  generated by the HAAR measure (dots).

Fig. 6.11 shows the distributions  $P(\rho_1), P(\rho_2)$  and their corresponding potentials for  $\beta = 1$  at  $m^2 = 0$ . The potentials show evidence for a logarithmic divergence for  $\rho_1 \rightarrow 0, \rho_2 \rightarrow 1$  respectively. This is expected, as the  $SU(2)$  integration measure, for which in (4.30) we found the expression in terms of  $a_0 \equiv \ell$

$$dU \sim d\Omega da_0 (1 - a_0^2)^{\frac{1}{2}}, \quad (6.62)$$

contributes to the effective potential as

$$V_{\text{Vdm}} = -\frac{1}{2} \ln(1 - \ell^2), \quad (6.63)$$

and thus generates logarithmic repulsion of eigenvalues. Below the transition, at  $\beta = 0.5$  we obtain similar curves. Note that the potential for  $\rho_2$  is entirely flat aside from the contribution of (6.63) (which is called the VANDERMONDE potential). Fig. 6.11 (right) shows a comparison of the pure VANDERMONDE potential to the measured  $V_{\text{eff}}(\rho_2)$ , which agree exactly within numerical precision. The flat distribution of  $\rho_2$  is consistent with the slow global rotations of  $\bar{\mathbf{L}}$  in  $SU(2)$  space for  $\beta > \beta_C$ .

Fig. 6.12 shows the distributions  $P(\rho_1)$  and  $P(\rho_2)$  in the confined phase at  $\beta = 2.0, m^2 = -1.0$  and  $\beta = 5.0, m^2 = -1.0$ . These plots are exemplary for  $\beta > \beta_C, m^2 < 0$  corresponding to the upper left region in the phase diagram (Fig. 6.6). For this case,  $\rho_2$  peaks around  $\rho \approx 0$  which corresponds to the non-trivial confined vacuum with  $\bar{\mathbf{L}} \sim i\sigma_3$  or  $SU(2)$  rotations thereof. This is in agreement with our prior results for the  $Z(2)$  and  $O(4)$  order-parameters and the inverse correlation lengths. These results illustrate clearly that the negative mass term leads to strong repulsion of eigenvalues<sup>5</sup>. Also they demonstrate how fluctuations are suppressed with increasing  $\beta$ .

In Fig. 6.13 we show  $P(\rho_1)$  and  $P(\rho_2)$  at  $\beta = 1.0, m^2 = 3.9$ , which lies deeply in the deconfined phase, and at  $\beta = 1.0, m^2 = 0.8$ , which exceeds the critical  $m_c^2$  for deconfinement

<sup>5</sup>In other words, the distributions of the eigenvalues  $\lambda_1$  and  $\lambda_2$ , which are gauge invariant, peak about  $\pm 1$ . That distinct confined phases with different eigenvalue structure can also arise in 4d models of Polyakov loops coupled to gauge fields, was shown in refs. [116, 117]

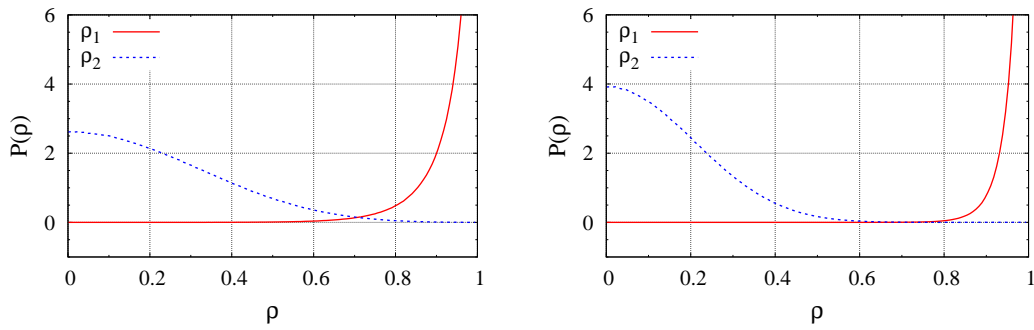


Figure 6.12: Distributions  $P(\rho_1)$  and  $P(\rho_2)$  measured on  $N_s = 24$  in the confined phase at  $\beta > \beta_C$ ,  $m^2 < 0$ . Strong eigenvalue repulsion is observed. Raising  $\beta$  suppresses fluctuations. Left:  $[\beta = 2.0/m^2 = -1.0]$ . Right:  $[\beta = 5.0/m^2 = -1.0]$ .

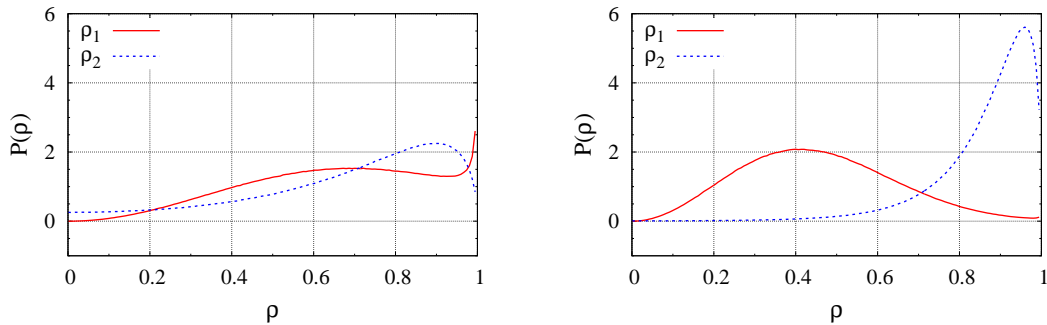


Figure 6.13:  $P(\rho_1)$  and  $P(\rho_2)$  measured on  $N_s = 24$  in the deconfined phase. Left:  $[\beta = 1.0/m^2 = 0.8]$ . Right:  $[\beta = 1.0, m^2 = 3.9]$ .

but lies close to the phase boundary. We observe that close to phase boundary, where the perturbative potential is partly cancelled by the “fuzzy bag” term, the eigenvalue distributions are rather broad. This result demonstrates that the “fuzzy bag” term can generate eigenvalue repulsion in the deconfined phase at  $\beta \approx \beta_C$ , which corresponds to the moderately weak coupling regime in the underlying four-dimensional gauge theory. For larger  $m^2$  the distributions become sharper and their maxima move towards  $\rho_1 = 0$  and  $\rho_2 = 1$ . Far in the deconfined phase, the eigenvalue distributions qualitatively exhibit the behavior appropriate for the perturbative regime.

### 6.3 Autocorrelations

We use the binning method described in section 4.2 to extract the integrated autocorrelation time  $\tau_{\text{int}}$  in different regions of the  $\beta - m^2$  plane. We consider  $\tau_{\text{int}}$  for the  $O(4)$  order-parameter  $u_0$  and the POLYAKOV loop  $\bar{l}$  separately, although for  $m^2 > 0$  they are equal. Note that the results of this section were taken into account for the actual measurements

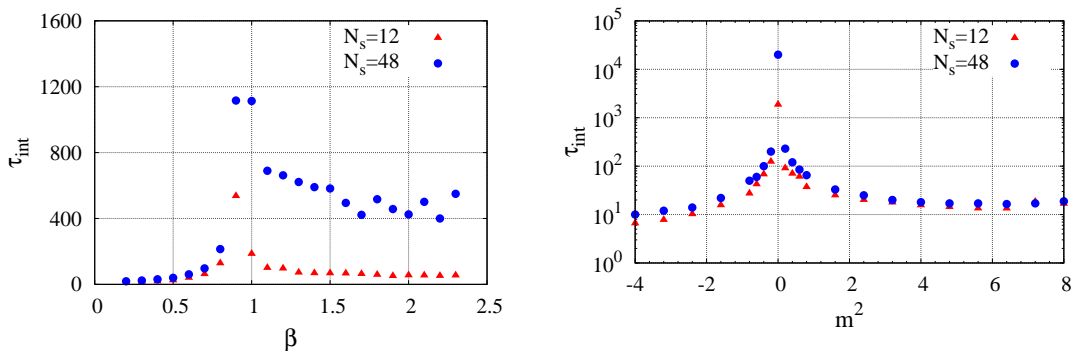


Figure 6.14: Left: Integrated autocorrelation time  $\tau_{\text{int}}$  of  $u_0$  at  $m^2 = 0.0$  for a range of  $\beta$ . Right:  $\tau_{\text{int}}$  of  $\bar{\ell}$  at  $\beta = 1.0$  for a range of  $m^2$ .

presented previously. In practice, short runs with low statistics were used to find the rough location of the phase boundary, followed by a detailed investigation of autocorrelations. Final measurements were then performed in a separate run with high precision. We discuss two exemplary cases explicitly here.

Fig. 6.14 shows  $\tau_{\text{int}}^{u_0}$  for the case  $m^2 = 0.0$  for a large range of  $\beta$  as well as  $\tau_{\text{int}}^{\bar{\ell}}$  at  $\beta = 1.0$  for a large range of  $m^2$ . We show  $N_s = 12, 48$  explicitly although actual measurements were performed on  $N_s = 12, 24, 36, 48$  with a Markov time series of 320000 successive configurations for each combination of  $\beta/m^2$  on each lattice. Exactly at  $[\beta = 1.0/m^2 = 0.0]$  we performed a high precision run with 700000 configurations. The optimal bin-size for each  $\beta/m^2$  is determined by looking at  $\tau_{\text{int}}(N_b)$ . It increases when approaching the phase boundary. For the results presented here, the final bin-size is slightly larger than the estimate for  $\tau_{\text{int}}$  at each  $\beta/m^2$ . We present the results without errorbar estimates.

In the vicinity of the phase transition, critical slowing down is observed.  $\tau_{\text{int}}$  diverges in the infinite volume limit for both  $u_0$  and  $\bar{\ell}$ . Away from the phase transition  $\tau_{\text{int}}^{\bar{\ell}}$  decreases. However,  $\tau_{\text{int}}^{u_0}$  also increases with volume for  $m^2 = 0.0/\beta > \beta_C$ . It exhibits the standard behavior for  $\beta < \beta_C$ .

At  $m^2 = 0.0/\beta = \beta_C$  the  $N_s = 24, 36, 48$  results for  $\tau_{\text{int}}^{u_0}$  can be fitted to the form  $\tau_{\text{int}} \sim N_s^{1/\nu_\tau}$ , with the scaling exponent

$$\nu_\tau^{u_0} = 0.72(4) . \quad (6.64)$$

At  $m^2 = 0.0, \beta = 1.0$  for  $\tau_{\text{int}}^{\bar{\ell}}$  we find

$$\nu_\tau^{\bar{\ell}} = 1.3(4) . \quad (6.65)$$





## 7 Results with magnetic fields

In this chapter we drop the constraint (6.1) and study the full theory with magnetic fields included. The action of this theory is

$$S = \beta \sum_{\square} \left(1 - \frac{1}{2} \text{Re Tr } \mathbf{U}_{\square}\right) - \frac{1}{2} \beta \sum_{\langle ij \rangle} \text{tr} (\mathbf{L}_i \mathbf{U}_{ij} \mathbf{L}_j^{\dagger} \mathbf{U}_{ij}^{\dagger} + \text{h.c.}) - m^2 \sum_i |\text{tr } \mathbf{L}_i|^2, \quad (7.1)$$

which is invariant under local  $SU(2)$  transformations:

$$\mathbf{L}_i \rightarrow \Omega_i \mathbf{L}_i \Omega_i^{\dagger}, \quad \mathbf{U}_{ij} \rightarrow \Omega_i \mathbf{U}_{ij} \Omega_j^{\dagger}, \quad \Omega_i \in SU(2) \quad \forall i. \quad (7.2)$$

Unlike for the action (6.2) without gauge fields, there are no larger symmetry groups in any limit of  $\beta$  or  $m^2$ . The only order parameter of this system is the POLYAKOV loop, which corresponds to the spontaneous breaking of global  $Z(2)$ .

The rough structure of this chapter is similar to the previous one: To map the phase diagram in terms of the parameters  $\beta$  and  $m^2$  we first study the massless limit  $m^2 = 0$  and then generalize to non-zero  $m^2$ . We compute the POLYAKOV loop expectation value and correlation lengths of various operators in broad ranges of the  $\beta - m^2$  plane.

However, an entire new class of magnetic observables is now also available. To assess the impact of deconfinement in the electric sector on the gauge fields, we compute the magnetic screening mass, as well as spatial WILSON loops of different sizes, which we use to extract the spatial string tension. Furthermore, in addition to the POLYAKOV loop potential at a single site, we compute *block spins*, where the POLYAKOV loop is averaged over a small region, and use them to extract an effective potential for the long-range field modes. A detailed discussion of parameterizations for POLYAKOV loop potential follows, with all field modes included as well as for long-range modes only. We also discuss evidence for the breakdown of the theory as an effective model for 4D  $SU(2)$  YANG-MILLS for roughly  $\beta \geq 5.0$ .

All results discussed in this chapter were obtained by employing METROPOLIS updating with over-relaxation for the WILSON lines  $\mathbf{L}$  as well as the gauge fields on cubic lattices with periodic boundary conditions. The lattice was updated sequentially. For the WILSON lines, sweeps were performed by applying 5 random METROPOLIS hits and 2 over-relaxed METROPOLIS hits on each site before moving to the next site. For the gauge links we mixed 8 random METROPOLIS hits with 3 over-relaxed hits per step. Again, a discussion of autocorrelations is found in a separate section. Autocorrelation times are measured in terms of full sweeps.

For the  $m^2 = 0$  case we have cross-checked the METROPOLIS results by replacing the updating algorithm for the WILSON lines by a CREUTZ heat bath algorithm. We have implemented the CREUTZ heat-bath also for the 3D gauge sector (corresponding to  $\mathbf{L} \equiv \mathbf{0}$ ) and confirmed that plaquette measurements in the 3D pure gauge theory are consistent

with existing literature<sup>1</sup>. The quadratic powers of  $\mathbf{U}$  in the kinetic term rule out using the heat bath also for updating the gauge fields in the effective theory.

All results presented in the main body of this chapter were obtained via the time-plaquette double counting scheme. The last section of this chapter shows similar results within a single counting scheme and discusses a qualitative comparison. We confirm that both methods are in qualitative agreement for measurements in the electric sector. Quantitative differences arise, since there is a slight change in the exact location of the phase boundary. Measurements of the string tension and WILSON action show that in the magnetic sector, there is also a qualitative difference between the two methods.

## 7.1 Massless limit

In this section we study the limit where the mass term  $m^2$  has been set to zero. This yields the lattice action

$$S = \beta \sum_{\square} \left(1 - \frac{1}{2} \text{Re Tr } \mathbf{U}_{\square}\right) - \frac{1}{2} \beta \sum_{\langle ij \rangle} \text{tr} (\mathbf{L}_i \mathbf{U}_{ij} \mathbf{L}_j^{\dagger} \mathbf{U}_{ij}^{\dagger} + \text{h.c.}) . \quad (7.3)$$

### 7.1.1 Spontaneous breaking of $Z(2)$

We compute the expectation value of the volume averaged POLYAKOV loop

$$\bar{\ell} = \frac{1}{2} \text{Tr } \bar{\mathbf{L}} \quad (7.4)$$

on lattice sizes  $N_s = 9, 12, 16, 24$ . Fig. 7.1 shows results for  $\langle |\bar{\ell}| \rangle$  in the range  $\beta = 0 \dots 4$  with step-size  $\Delta\beta = 0.1$ . The same figure shows measurements of the respective susceptibility

$$\chi = \frac{\partial \langle |\bar{\ell}| \rangle}{\partial \beta} \quad (7.5)$$

in the range  $\beta = 0.95 \dots 1.05$ , which is the immediate phase transition region, with a finer resolution of  $\Delta\beta = 0.01$ . We display only the results  $N_s = 12, 24$ . For the coarse resolution as well as the fine resolution 5000 independent configurations were generated for each value of  $\beta$ . Spontaneous breaking of  $Z(2)$  is evident for large  $\beta$ . Extrapolating the peak of the susceptibility for  $N_s \geq 12$  to infinite volume yields

$$\beta_C = 1.00(1) . \quad (7.6)$$

---

<sup>1</sup>We do not discuss measurements in the 3D pure gauge theory in detail here. For our purpose, it is used mainly as a sub-component of the effective theory. An investigation of the 3D gauge theory in its own right was performed by Ref. [118]. In Appendix B we show that our code reproduces plaquette expectation values presented in this reference.

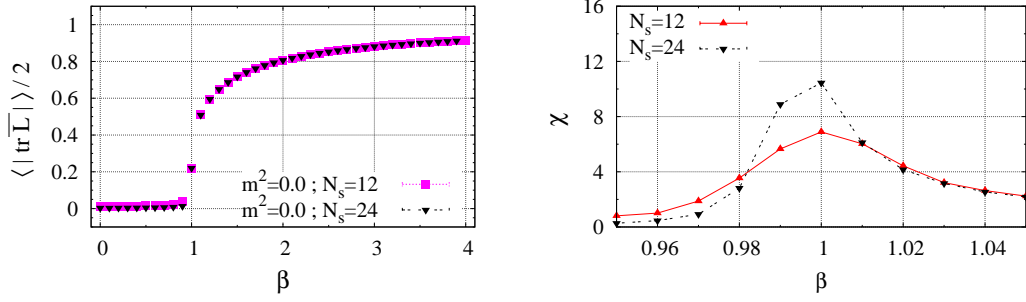


Figure 7.1: Left: Volume averaged POLYAKOV loop  $|\overline{\ell}|$ , measured on  $N_s = 12, 24$  for  $m^2 = 0$ . Right: Susceptibility  $\chi = \frac{\partial \langle |\overline{\ell}| \rangle}{\partial \beta}$  measured on  $N_s = 12, 24$  in vicinity of  $\beta_C = 1.00(1)$ .

### 7.1.2 Two-point functions

The presence of spatial gauge fields invalidates the expression

$$\mathcal{C}_{\mathbf{L}}(r) = \frac{1}{3} \frac{1}{N_s^3} \sum_{\hat{\mathbf{r}}, \mathbf{r}_0} \frac{1}{2} \left\langle \text{tr} \mathbf{L}^\dagger(\mathbf{r}_0) \mathbf{L}(\mathbf{r}_0 + \mathbf{r}) \right\rangle, \quad (7.7)$$

which we used previously in section 6.1.4 and following, for the two-point matrix-matrix correlation function. To obtain sensible results we may consider only forms which are strictly gauge invariant. A gauge invariant expression analogous to (7.7) is obtained by parallel transporting the field  $\mathbf{L}(\mathbf{r}_0 + \mathbf{r})$  to the point  $\mathbf{r}_0$  by using the operator  $\mathbf{U}_{\mathbf{r}_0, \mathbf{r}_0 + \mathbf{r}}$ :

$$\mathbf{L}(\mathbf{r}_0 + \mathbf{r}) \rightarrow \mathbf{U}_{\mathbf{r}_0, \mathbf{r}_0 + \mathbf{r}} \mathbf{L}(\mathbf{r}_0 + \mathbf{r}) \mathbf{U}_{\mathbf{r}_0, \mathbf{r}_0 + \mathbf{r}}^\dagger. \quad (7.8)$$

$\mathbf{U}_{\mathbf{r}_0, \mathbf{r}_0 + \mathbf{r}}$  is the product of link variables  $\mathbf{U}_{ij}$  along the shortest path connecting the points  $\mathbf{r}_0$  and  $\mathbf{r}_0 + \mathbf{r}$  and corresponds to the parallel transporter introduced in section 5.1. It transforms under the local  $SU(2)$  transformation  $\Omega(\mathbf{r}')$  as

$$\begin{aligned} \mathbf{U}_{\mathbf{r}_0, \mathbf{r}_0 + \mathbf{r}} &\rightarrow \Omega(\mathbf{r}_0) \mathbf{U}_{\mathbf{r}_0, \mathbf{r}_0 + \mathbf{r}} \Omega^\dagger(\mathbf{r}_0 + \mathbf{r}), \\ \mathbf{U}_{\mathbf{r}_0, \mathbf{r}_0 + \mathbf{r}}^\dagger &\rightarrow \Omega(\mathbf{r}_0 + \mathbf{r}) \mathbf{U}_{\mathbf{r}_0, \mathbf{r}_0 + \mathbf{r}}^\dagger \Omega^\dagger(\mathbf{r}_0). \end{aligned} \quad (7.9)$$

The gauge invariant matrix-matrix correlation function therefore is

$$\mathcal{C}_{\mathbf{L}}(r) = \frac{1}{3} \frac{1}{N_s^3} \sum_{\hat{\mathbf{r}}, \mathbf{r}_0} \frac{1}{2} \left\langle \text{tr} \mathbf{L}^\dagger(\mathbf{r}_0) \mathbf{U}_{\mathbf{r}_0, \mathbf{r}_0 + \mathbf{r}} \mathbf{L}(\mathbf{r}_0 + \mathbf{r}) \mathbf{U}_{\mathbf{r}_0, \mathbf{r}_0 + \mathbf{r}}^\dagger \right\rangle. \quad (7.10)$$

The correlation function in the singlet sector

$$\mathcal{C}'_{\ell}(r) = \frac{1}{3} \frac{1}{N_s^3} \sum_{\hat{\mathbf{r}}, \mathbf{r}_0} \frac{1}{2} \left\langle \text{tr} \mathbf{L}^\dagger(\mathbf{r}_0) \text{tr} \mathbf{L}(\mathbf{r}_0 + \mathbf{r}) \right\rangle. \quad (7.11)$$

is gauge invariant without further modification, since the local gauge transformation is cancelled under the trace.

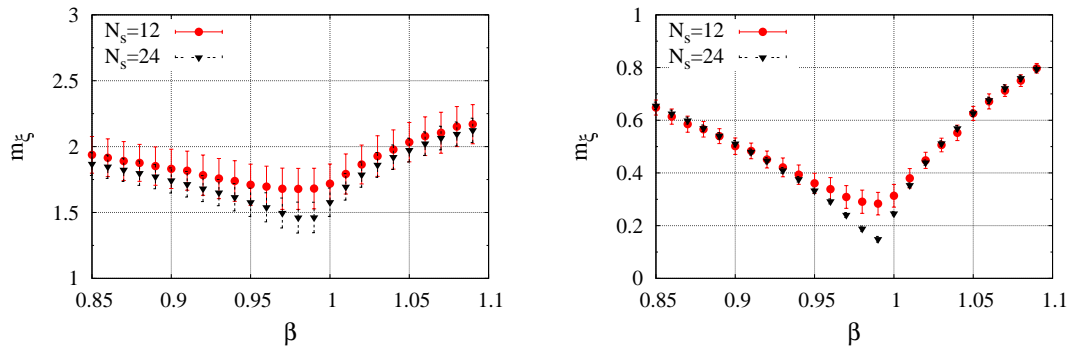


Figure 7.2: Left: Inverse correlation length  $m_\xi$  for matrix-matrix correlation function, measured on  $N_s = 12, 24$  at  $m^2 = 0.0$  for a range of  $\beta$  close to  $\beta_C \approx 1.0$ . Right: Inverse correlation length at  $m^2 = 0.0$  for POLYAKOV loop two-point function.

We measure the matrix-matrix correlation function (7.10) and the singlet correlation function (7.11) on  $N_s = 9, 12, 16, 24$  in the vicinity of the phase transition for  $\beta = 0.95 \dots 1.05$  with  $\Delta\beta = 0.01$  on 5000 independent configurations for each value of  $\beta$ . Fig. 7.2 shows the inverse correlation length  $m_\xi$  obtained from a  $\chi^2$  fit to

$$\mathcal{C}(r) \sim \frac{1}{rm_\xi} e^{-rm_\xi} + \text{const.} , \quad (7.12)$$

for both cases. For visibility, we again only display  $N_s = 12, 24$ . Note, that  $m_\xi$  has a minimum at  $\beta = 0.99$  on  $N_s = 24$  in the singlet channel as well as the matrix-matrix channel, which differs slightly from the value of  $\beta_C$  obtained above, but is consistent within the errorbar. We investigate the finite size scaling of  $m_\xi$  at  $\beta = 0.99$  by fitting  $m_\xi \sim N_s^{-1/\nu_\xi}$  to  $N_s \geq 12$ . We find

$$\nu_\xi = 5.1(6) , \quad (7.13)$$

for the matrix-matrix correlation length and

$$\nu_\xi^{\text{singl}} = 1.10(6) , \quad (7.14)$$

for the singlet channel. The diverging correlation lengths for  $N_s \rightarrow \infty$  at  $\beta \approx \beta_C$  confirm the second order phase transition. A point to note here, is that unlike for the model without gauge fields there are no massless GOLDSTONE modes in the deconfined phase. This is expected, since the global  $Z(2)$  symmetry which is broken here is discrete, rather than continuous as for the  $SU(2)_L \times SU(2)_R$  model.

### 7.1.3 Magnetic sector

The simplest gauge invariant observable in the magnetic sector is the trace of the elementary plaquette, or correspondingly the volume averaged expectation value of the WILSON action (we divide by a factor of  $\beta$ ).

$$\frac{1}{\beta} \langle S_\square \rangle = \frac{1}{V} \left\langle \sum_\square \left( 1 - \frac{1}{2} \text{Re Tr } \mathbf{U}_\square \right) \right\rangle . \quad (7.15)$$

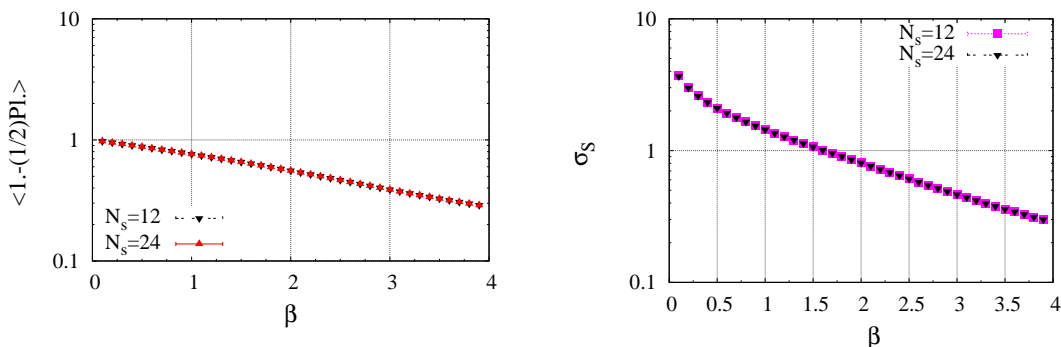


Figure 7.3: Left:  $\beta$  dependence of WILSON action  $\langle S_{\square} \rangle / \beta$ , measured on  $N_s = 12, 24$  at  $m^2 = 0.0$ . The phase transition at  $\beta \approx 1.0$  is not visible. Right: Spatial string tension  $\sigma_s$  measured on  $N_s = 12, 24$ .

Since it is part of the updating routine it is immediately available. Eq. (7.15) is an order-parameter in the  $4D$  gauge theory in the sense that it exhibits singularities of the bulk thermodynamics, although it never vanishes exactly except at zero temperature. We investigate whether the transition in the  $3D$  theory can be seen as a jump or singularity in (7.15) as a function of the coupling  $\beta$ . Note that the  $4D$  version of (7.15) mixes time-like and space-like plaquettes, while here we consider only plaquettes in spatial planes. We extract (7.15) from the same data set as the POLYAKOV loop measurements in section 7.1.1. Fig. 7.3 (left) shows the  $\beta$  dependence of  $\langle S_{\square} \rangle / \beta$  on  $N_s = 12, 24$  lattices for  $m^2 = 0$ . The fall off is nearly exponential with  $\beta$  (note the logarithmic y-axis) and there are no discontinuities seen for any value of  $\beta$ . Also, there is no visible finite size scaling when going from  $N_s = 12$  to  $N_s = 24$ .

Another gauge invariant order parameter in the  $4D$  theory is the trace of the product of links around a closed loop of arbitrary size, which is called the WILSON loop

$$W(C) = \left\langle \text{Tr} \prod_{i,j \in C} U_{ij} \right\rangle. \quad (7.16)$$

The plaquette considered previously is a special case of this. It is simply the smallest non trivial WILSON loop. In the  $4D$  theory, the static quark-antiquark potential in the confined phase can be calculated from rectangular WILSON loops in the space-time planes [2]. If the loop is of size  $T$  by  $R$  (which denote the space and time-like extent of the loop respectively), for large loops of long rectangular shape,  $W(R, T)$  is dominated in the confined phase by an exponential fall off with the area of the loop

$$W(R, T) \sim \exp(-KRT). \quad (7.17)$$

The coefficient of this area law is the coefficient of the linear potential and vanishes in the deconfined phase. Measuring in lattice units, what one actually obtains is the dimensionless combination

$$\sigma = a^2 K, \quad (7.18)$$

which is called the string tension. In general, in addition to the area dependence there is also a contribution from the perimeter of the contour, in both the confined and deconfined phases (in the deconfined phase the perimeter dependence is dominant). In the 4D theory one therefore considers CREUTZ ratios

$$\chi(I, J) = -\ln \left( \frac{W(I, J) W(I-1, J-1)}{W(I, J-1) W(I-1, J)} \right), \quad (7.19)$$

which contain loops of different area but same perimeter. The perimeter dependence cancels out and  $\chi(I, J)$  directly measures the string tension when  $W(I, J)$  is dominated by an area law.

In the 3D theory we extract the *spatial string tension*  $\sigma_S$ , by considering loops in the three spatial planes and looking for an area law dependence

$$W(X, Y) \sim \exp(-KXY). \quad (7.20)$$

in analogy to (7.17). While not directly related to any physical potential, this quantity has been considered as a useful observable for comparisons between 4D YANG-MILLS theory and 3D effective theories (see e.g. [119], [120] and [121]). We find, that obtaining  $\sigma_S$  by a fit to (7.20) or by using the CREUTZ ratio  $\chi(I, J)$  yield similar results within numerical precision, although with (7.20) the errors are smaller.

Fig. 7.3 (right) shows the  $\beta$  dependence of  $\sigma_S$ , obtained from  $N_s = 12, 24$  lattices at  $m^2 = 0$  with 5000 configurations for each value of  $\beta$ . Again, there is no sign of any discontinuities at  $\beta_C$ .  $\sigma_S$  falls off smoothly with rising  $\beta$  and appears to be independent of volume for  $N_s \geq 12$ . These results indicate that spatial string tension and WILSON action are not affected by symmetry breaking in the electric sector at  $m^2 = 0$ .

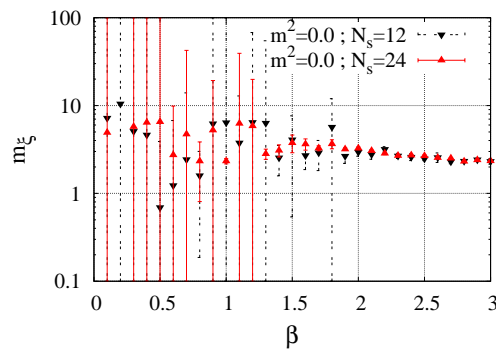


Figure 7.4: Inverse plaquette-plaquette correlation length measured on  $N_s = 12, 24$  for  $m^2 = 0$ . Below  $\beta \approx 1$  the signal for the two point function diminishes.

Last, we attempt to extract the screening mass of excitations of the spatial gauge fields. We compute the two-point correlation function of plaquettes  $P_{\square}$

$$\mathcal{C}^{\text{mag}}(r) = \frac{1}{3} \frac{1}{N_s^3} \sum_{\hat{\mathbf{r}}, \mathbf{r}_0} \frac{1}{2} \langle \text{tr} P_{\square}(\mathbf{r}_0) \text{tr} P_{\square}(\mathbf{r}_0 + \mathbf{r}) \rangle, \quad (7.21)$$

---

where the plaquettes at the points  $\mathbf{r}_0$  and  $\mathbf{r}_0 + \mathbf{r}$  have the same orientation and face each other. We find that in the confined phase correlations are screened over distances on the order of a single lattice site, which leads to a diminishing signal for the inverse correlation length when approaching  $\beta_C$  from above. For  $\beta > \beta_C$  using (7.12) one can extract a mass which is constant within numerical precision for the range  $\beta = 1 \dots 3$  considered. Fig. 7.4 shows the numerical results for  $m_\xi^{\text{mag}}$  on  $N_s = 12, 24$  lattices.

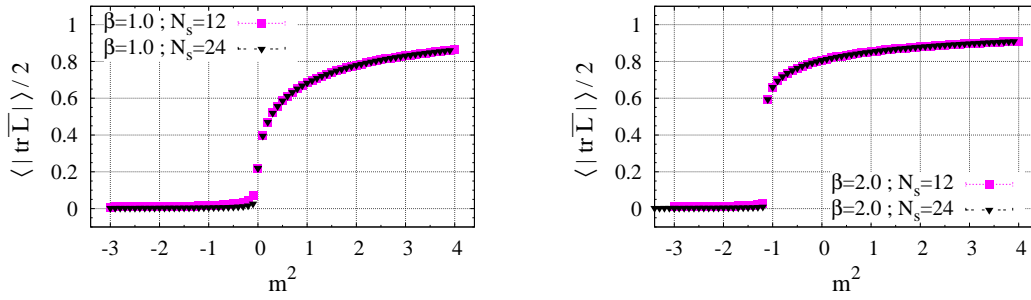


Figure 7.5: Expectation value of volume averaged POLYAKOV loop  $\langle |\bar{\ell}| \rangle$  at  $\beta = 1.0$  (left) and  $\beta = 2.0$  (right) measured on  $N_s = 12, 24$ .

## 7.2 Full theory

We now consider non-zero values for  $\beta$  and  $m^2$  and study the full theory defined by the action

$$S = \beta \sum_{\square} \left(1 - \frac{1}{2} \text{Re Tr } \mathbf{U}_{\square}\right) - \frac{1}{2} \beta \sum_{\langle ij \rangle} \text{tr} (\mathbf{L}_i \mathbf{U}_{ij} \mathbf{L}_j^{\dagger} \mathbf{U}_{ij}^{\dagger} + \text{h.c.}) - m^2 \sum_i |\text{tr } \mathbf{L}_i|^2. \quad (7.22)$$

### 7.2.1 Phase diagram

To map the phase diagram we measure the expectation value of the volume averaged POLYAKOV loop  $\langle |\bar{\ell}| \rangle$  for several fixed values of  $\beta$  for broad ranges of  $m^2$ , as well as for fixed positive and negative values of  $m^2$  as a function of  $\beta$ . Fig. 7.5 shows exemplary results, from  $N_s = 12, 24$  lattices for  $\beta = 1.0/2.0$ . The phase boundary is obtained by finding the peak of the susceptibility for each data set. Fig. 7.6 summarizes our findings. Note that, unlike for the spin model with  $A_i = 0$ , there is a single phase boundary and  $\langle |\bar{\ell}| \rangle$  is non-zero for  $m^2 < 0$  at large  $\beta$ . The phase transition along the  $m^2$ -axis becomes sharper with rising  $\beta$ . With the resolution used in Fig. 7.5 for  $\beta = 2.0$  there appears to be a gap, which would indicate a first order phase transition. However, the effective potential which we discuss in the following sections confirm that this is a very sharp phase transition of second order, but that the transition becomes first order at  $\beta \approx 5.0$

Fig. 7.7 shows the inverse correlation lengths, obtained from the matrix-matrix and the singlet correlation functions defined by (7.10) and (7.11) for  $\beta = 2.0$ . The phase transition is visible as non-analytic behavior at  $m^2 \approx -1.1$ , however with the given resolution finite size scaling is only barely visible (and only in the singlet channel). What these results clearly show, however, is the absence of any GOLDSTONE modes on both sides of the phase boundary.

In Figs. 7.8, 7.9 and 7.10 we show the WILSON action  $\langle S_{\square} \rangle / \beta$  together with the spatial string tension  $\sigma_S$  for fixed  $\beta = 0.5/1.0/2.0$  for wide ranges of  $m^2$ , obtained from  $N_S = 12, 24$  lattices. These values of  $\beta$  correspond to  $\beta < \beta_C$ ,  $\beta = \beta_C$  and  $\beta > \beta_C$  at  $m^2 = 0$ . Both observables exhibit a similar behavior. The most immediate observation is that the  $m^2$  dependence of  $\langle S_{\square} \rangle / \beta$  and  $\sigma_S$  is very weak for all of these cases. The observed  $m^2$



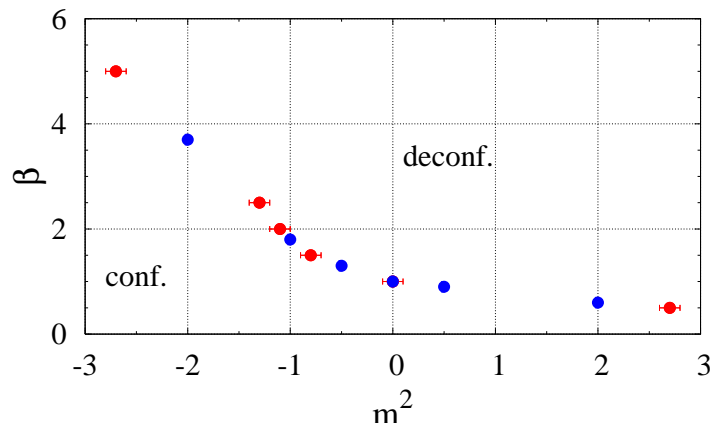


Figure 7.6: Phase diagram of the theory defined by (7.1).  $Z(2)$  symmetry is broken in the upper right region. In the  $Z(2)$  symmetric phase, the WILSON loop  $\mathbf{L}$  moves randomly over the group manifold  $\beta$  yielding  $\langle |\bar{\ell}| \rangle = 0$  when  $m^2 \approx 0$ . For large negative  $m^2$  preference is given to configurations where the POLYAKOV loop  $\ell$  vanishes locally for each configuration. Unlike for the case  $A_i = 0$  in chapter 6 there is no sharp boundary separating these two types of confined vacua.

dependences range from  $\sim 0.1\%$  effects at  $\beta = 0.5$  to  $\sim 1\%$  effects at  $\beta = 2.0$  which renders them nearly invisible at the  $y$ -scaling used in Fig. 7.3 where the  $\beta$  dependence at  $m^2 = 0$  is shown.  $\langle S_{\square} \rangle / \beta$  and  $\sigma_S$  depend more strongly on  $m^2$  as  $\beta$  increases.

A striking observation is that  $\langle S_{\square} \rangle / \beta$  and  $\sigma_S$  depend analytically (within errors) on  $m^2$  for  $\beta = 0.5$ , even when crossing the phase boundary at  $m^2 = 2.7(1)$ . Then, at  $\beta = \beta_C$  the phase transition is visible as a non-analytic, but continuous behavior at  $m^2 = 0$  for both cases. For  $\beta = 2.0$ , both  $\langle S_{\square} \rangle / \beta$  and  $\sigma_S$  change discontinuously at  $m_C^2 = -1.1(1)$ . These results suggest that for any  $\beta > \beta_C$  the phase transition in the electric sector produces discontinuous behavior in the magnetic sector. Note, however, that this does not imply that the  $Z(2)$  breaking transition of  $\langle \bar{\ell} \rangle$  is of first order.

Last, we attempt to obtain the magnetic screening mass from the plaquette-plaquette correlation function (7.21). Consistent with section 7.1.3 we find that correlations are strongly screened for  $\beta \leq \beta_C$  over ranges smaller than one lattice site at any value of  $m^2$  so that no signal for  $m_{\xi}^{\text{mag}}$  can be obtained. At  $\beta > \beta_C$ ,  $m_{\xi}^{\text{mag}}$  appears to be independent of  $m^2$  within numerical precision. In Fig. 7.11 we show  $m_{\xi}^{\text{mag}}(m^2)$  for  $\beta = 2.0$  on  $N_S = 12, 24$  lattices. Note that the  $N_S = 12$  lattice is somewhat noisy at this scale but in agreement with  $N_S = 24$  within errors. The value  $m_{\xi}^{\text{mag}}(m^2) \approx 3.0$  is consistent with Fig. 7.4. The phase transition at  $m^2 = -1.1(1)$  is not visible.

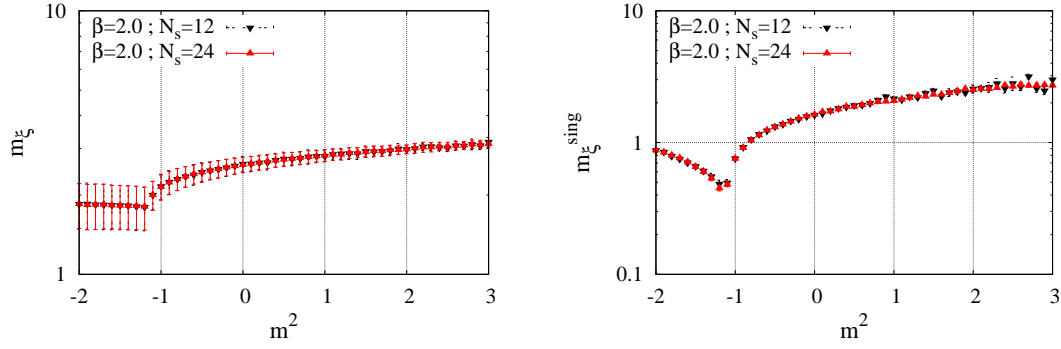


Figure 7.7: Inverse correlation length for matrix-matrix two-point function (left) and singlet channel (right) measured on  $N_s = 12, 24$  at  $\beta = 2.0$ .

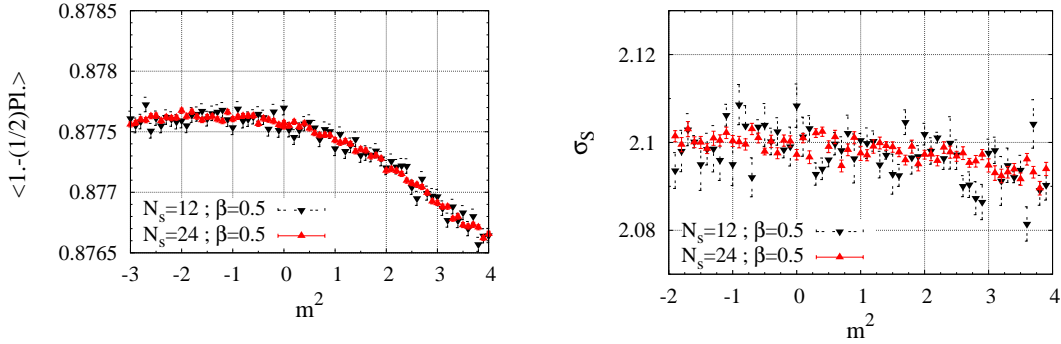


Figure 7.8: WILSON action  $\langle S_{\square} \rangle / \beta$  (left) and spatial string tension  $\sigma_S$  (right), measured on  $N_s = 12, 24$  lattices at  $\beta = 0.5$  (which is  $\leq \beta_C$ ). A weak  $m^2$  dependence is observed. The phase transition is not visible.

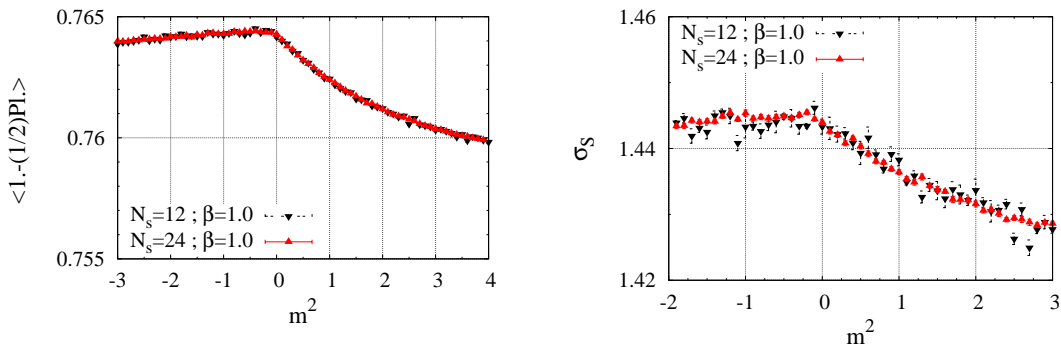


Figure 7.9: WILSON action  $\langle S_{\square} \rangle / \beta$  (left) and spatial string tension  $\sigma_S$  (right), measured on  $N_s = 12, 24$  lattices at  $\beta = 1.0 = \beta_C$ . Both observables show continuous but non-analytic behavior at the phase transition point  $m \approx 0$ .

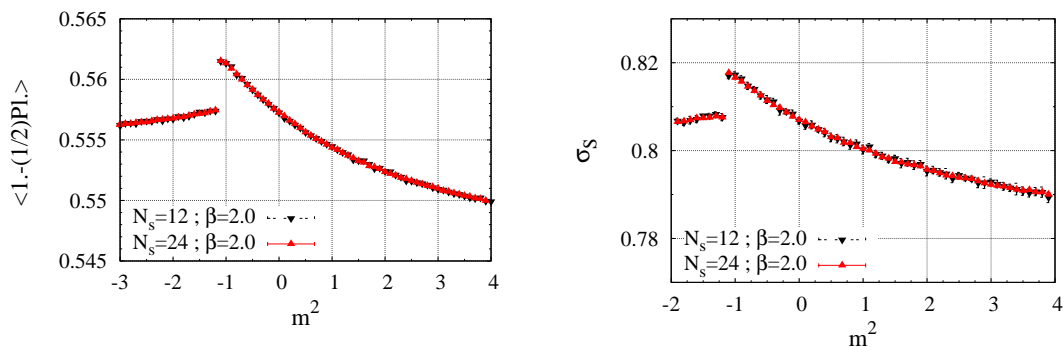


Figure 7.10: WILSON action  $\langle S_{\square} \rangle / \beta$  and spatial string tension  $\sigma_S$ , measured on  $N_S = 12, 24$  lattices at  $\beta = 2.0$ . The  $m^2$  dependence of  $\langle S_{\square} \rangle / \beta$  and  $\sigma_S$  is much stronger than for  $\beta = 0.5$  (Fig. 7.8). Both observables change discontinuously at the phase transition at  $m^2 \approx -1.1$ .

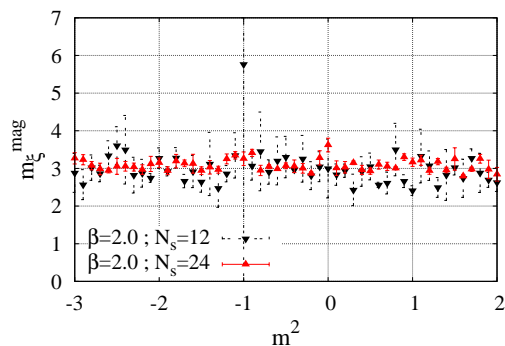


Figure 7.11: Inverse plaquette-plaquette correlation length measured on  $N_S = 12, 24$  for  $\beta = 2.0$ . No  $m^2$  dependence or lattice size scaling is visible. The phase transition at  $m^2 \approx -1.1$  is also not seen.

### 7.2.2 Effective Polyakov loop potential

We are again interested in the distribution of eigenvalues of the WILSON line  $\mathbf{L}$ . However, in contrast to the previous chapter we focus entirely on the distribution of the average of  $\lambda_1$  and  $\lambda_2$ , which we define as

$$\rho(\mathbf{x}) = \frac{1}{2} |\lambda_1(\mathbf{x}) + \lambda_2(\mathbf{x})| = \sqrt{\ell^2}. \quad (7.23)$$

Moreover, we will for the most part directly discuss the potential

$$V_{\text{eff}}(\rho) = -\log P(\rho), \quad (7.24)$$

rather than discussing the probability distribution  $P(\rho)$  at length. Our goal is to find an effective parameterization of  $V_{\text{eff}}(\rho)$  in terms of  $\beta$  and  $m^2$  and to see whether the dynamics generate any additional terms that are not present in the “bare” potential. We will show

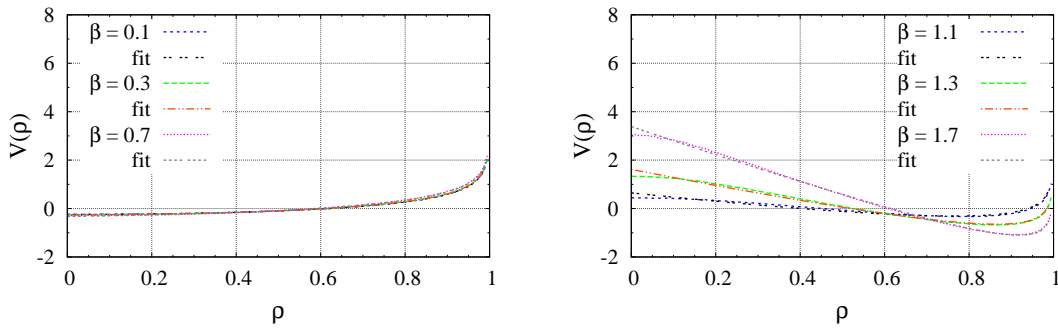


Figure 7.12: Effective potential for  $V_{\text{eff}}(\rho)$  at  $m^2 = 0$ , fitted with (7.26).

Left: For  $\beta < \beta_C$  the potential is well described by  $V_{\text{Vdm}}$ . Right: For  $\beta > \beta_C$  spontaneous breaking of the  $Z(2)$  symmetry is observed. A non-analytic term  $\sim \sqrt{\ell^2}$  contributes to the potential.

that in the deconfined region a non-analytic contribution  $\sim \sqrt{\ell^2}$  arises, which is distinct from the VANDERMONDE potential

$$V_{\text{Vdm}} = -\frac{1}{2} \log(1 - \ell^2) = -\frac{1}{2} \log(1 - \rho^2), \quad (7.25)$$

generated by the  $SU(2)$  integration measure and the mass term  $\sim -m^2 \ell^2$  which is present in the action (7.1).

All measurements presented here were performed on a  $N_s = 24$  cubic lattice. This appears to be close to the infinite volume limit. We have checked that the coefficients of the model functions discussed below do not change much with volume for  $N_s \geq 12$ . For each combination of  $\beta$  and  $m^2$  5000 independent configurations were generated.

We find that for a broad range of  $\beta$  and  $m^2$  the effective potential is well described by the form

$$V_{\text{fit}}(\rho) = -\frac{1}{2} \log(1 - \rho^2) + a - b\rho + c\rho^2. \quad (7.26)$$

Note that the linear term proportional to  $\rho = \sqrt{\ell^2}$  is not to be confused with a  $Z(2)$  background field  $\sim -h\ell$ . It is non-analytic and does not break the  $Z(2)$  symmetry explicitly.

Fig. 7.12 shows results for  $V_{\text{eff}}(\rho)$  for the case  $m^2 = 0$  for various values of  $\beta$  above and below the phase transition which occurs at  $\beta_C = 1.00(1)$ , with the corresponding fit curves. Below  $\beta_C$  we find that  $a = b = c = 0$  in the potential defined by (7.26), hence the effective potential coincides with the VANDERMONDE potential  $V_{\text{Vdm}}$ . This is in agreement with our prior findings for zero gauge fields.

For  $\beta > \beta_C$  both coefficients  $a$  and  $b$  are non-zero. Fig. (7.13) shows the  $\beta$  dependence of  $a$  and  $b$  at  $m^2 = 0.0$ . The figure clearly illustrates how deviations from the VANDERMONDE potential set in at  $\beta_C$  and grow with rising  $\beta$ . The quadratic coefficient  $c$  does not appear. As one would expect, and as we will confirm in the following,  $c$  is roughly proportional to the mass term in the bare potential. We find, that the non-analytic coefficient  $b$  can be parameterized at  $m^2 = 0$  by the *ansatz*

$$b(\beta) = b_0(\beta - \beta_C)^r \theta(\beta - \beta_C), \quad (7.27)$$

which is motivated by the observation of an approximately linear rising of  $b$  above  $\beta_C$  (seen in Fig. 7.13). The solid line in Fig. 7.13 was obtained by fixing  $\beta_C = 0.9$  and performing a  $\chi^2$  fit for  $b_0$  and  $r$ , that yields

$$b_0 = 7.1(1) , \quad r = 0.82(4) . \quad (7.28)$$

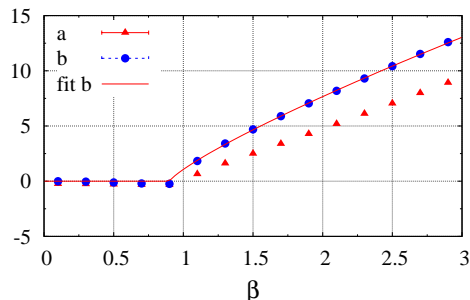


Figure 7.13:  $\beta$  dependence of fit coefficients of the ansatz (7.26) for  $V_{\text{eff}}(\rho)$  at  $m^2 = 0$ . The solid line corresponds to a parameterization of  $b(\beta)$  by eq. (7.27).

The *ansatz* (7.26) also works for non-zero  $m^2$ , when  $\beta$  is smaller than  $\beta \approx 5.0$ . We have confirmed this for a broad range in the  $\beta - m^2$  plane. We show explicit results for fixed  $\beta = 1.0$  in Fig. 7.14 and for  $\beta = 2.0$  in Fig. 7.15. The phase transition is clearly visible, when going from large negative to large positive values of  $m^2$  as a shift of the minimum of  $V_{\text{eff}}$  from  $\rho \approx 0$  to  $\rho \approx 1$ . Moreover, the results confirm that the phase transition is of second order at  $\beta = 2.0, 1.0$ , since for the entire range of  $m^2$  there is a single potential minimum. The  $m^2$  dependence of the coefficients  $a, b, c$  is shown explicitly for  $\beta = 1.0$  and  $\beta = 2.0$  in Fig. 7.16. The quadratic coefficient  $c$  appears to depend linearly on  $m^2$  except for a discontinuous gap at the phase transition. The linear coefficient  $b$  was set to zero by hand in the confined phase. It yields improvements of the  $\chi^2$  per degree of freedom only in the deconfined phase.

At non-zero  $m^2$ , a parameterization of the non-analytic coefficient  $b$  is more complicated than the simple expression (7.27). An *ansatz* that works, as indicated by the solid line in Fig. 7.16 (which shows the  $m^2$  dependence of the coefficients for different values of  $\beta$ ), is

$$b(\beta, m^2) = \tilde{b}(\beta) \theta(m^2 + \tilde{m}^2(\beta)) \times \left\{ 1 - \left[ \sinh \left( 2 \left[ g(\beta) (m^2 + \tilde{m}^2(\beta)) + \tilde{\beta}_C \right] \right) \right]^{-5} \right\} . \quad (7.29)$$

with the constant

$$\tilde{\beta}_C = \log(1 + \sqrt{2}) . \quad (7.30)$$

This is similar to the magnetization in the 2D ISING model [122]

$$M(\beta) = \theta(\beta - \tilde{\beta}_C) \left( 1 - [\sinh(2\beta J)]^{-4} \right)^{\frac{1}{8}} . \quad (7.31)$$

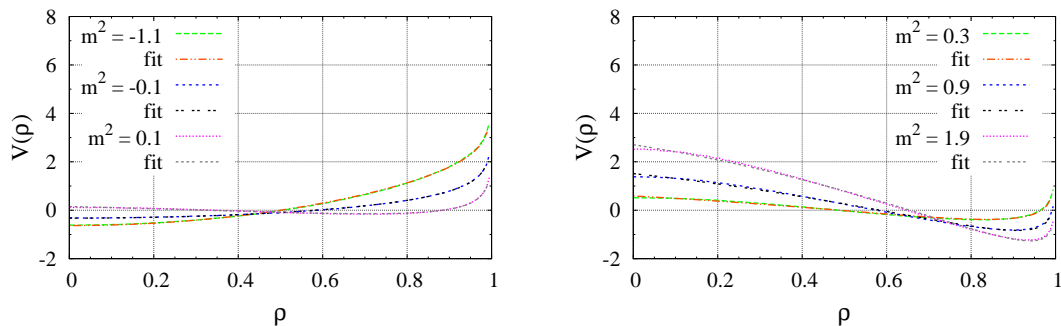


Figure 7.14: Effective potential  $V_{\text{eff}}(\rho)$  for  $\beta = 1.0$  for different  $m^2$  in the confined (left) and deconfined (right) phases, together with the corresponding  $\chi^2$  fit to eq. (7.26).

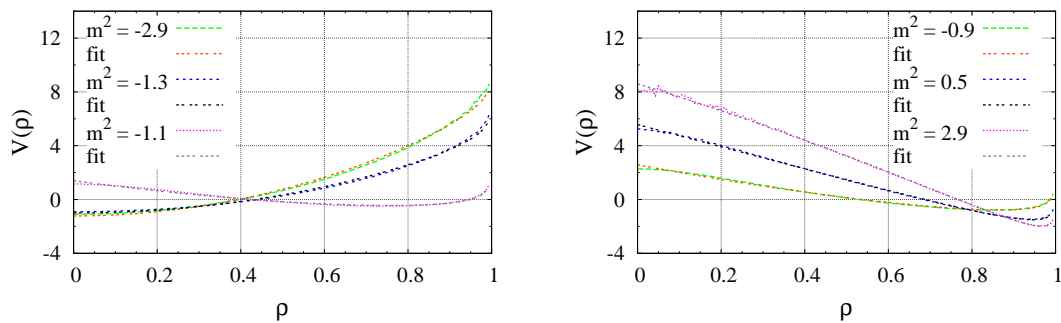


Figure 7.15: Effective potential  $V_{\text{eff}}(\rho)$  for  $\beta = 2.0$  for different  $m^2$  in the confined (left) and deconfined (right) phases, together with the corresponding  $\chi^2$  fit to eq. (7.26).

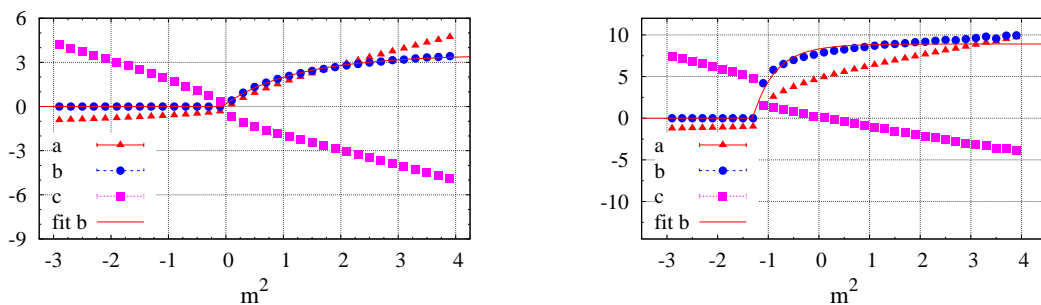


Figure 7.16:  $m^2$  dependence of fit parameters of the ansatz (7.26) for  $V_{\text{eff}}(\rho)$  at  $\beta = 1.0$  (left) and  $\beta = 2.0$  (right). The solid lines represent a modelling of  $b(\beta, m^2)$  with the ansatz (7.29).

Note that this is a purely heuristic analogy, motivated only by the  $m^2$  dependencies shown in fig. 7.16 and does not imply a deeper connection from universality arguments (the exponents in Eqs. (7.29) and (7.31) also differ). Once the  $\beta$  dependencies of the parameters  $\tilde{m}^2$ ,  $g$  and  $\tilde{b}$  in (7.29) have been obtained, it also describes  $b(\beta, m^2 = 0.0)$ , however less accurately than (7.27), since separate data sets (with fixed  $\beta$  and variable  $m^2$ ) consisting mainly of measurements far from  $m^2 = 0$  are used to obtain  $\tilde{m}^2(\beta)$ ,  $g(\beta)$  and  $\tilde{b}(\beta)$ . Fitting (7.29) directly to  $b(\beta, m^2 = 0.0)$  is not feasible, due to the large number of additional parameters that arise with the  $\beta$  dependencies of  $\tilde{m}^2$ ,  $g$  and  $\tilde{b}$ . There is also no straight-forward way to obtain (7.27) analytically from (7.29).

The constant  $\tilde{\beta}_C$ , which is the critical point of the ISING model, has been included into our *ansatz* (7.29) because choosing a form analogous to (7.31) implicitly assigns that particular value of the coupling strength a special meaning, which should be “filtered out” since our model deconfines at a completely different point. We find that isolating  $\tilde{\beta}_C$  in such a way simplifies the  $\beta$  dependence of the other fit-parameters in (7.29) greatly.

The additional  $\beta$  dependent coefficients introduced in (7.29) act as follows:  $g(\beta)$  modifies the coupling strength,  $\tilde{m}^2(\beta)$  generates a shift along the horizontal axis and  $\tilde{b}(\beta)$  changes the scale. They can be parameterized as power laws

$$\begin{aligned} \tilde{m}^2(\beta) &= m_0^2 + m_0'^2 \beta^w, \\ \tilde{b}(\beta) &= b_0' + b_0'' \beta^v, \\ g(\beta) &= g_0 + g_0' \beta^u, \end{aligned} \tag{7.32}$$

with constants which are obtained by  $\chi^2$  fit and are summarized in the following table:

$m_0^2 = 2.2(1)$	$m_0'^2 = -2.1(1)$	$w = -1.2(1)$
$b_0' = -2.5(4)$	$b_0'' = 6.0(4)$	$v = 0.90(4)$
$g_0 = 0.038(1)$	$g_0' = 0.017(1)$	$u = 2.8(1)$

The  $\beta$  dependence of  $\tilde{m}^2(\beta)$ ,  $\tilde{b}(\beta)$  and  $g(\beta)$  is shown in Fig. 7.17, together with their corresponding fit curves.

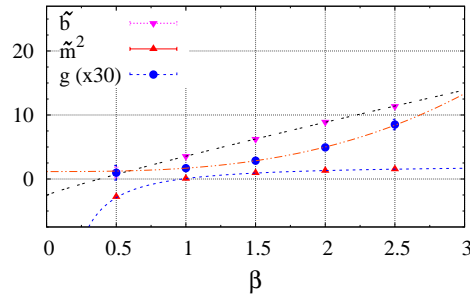


Figure 7.17:  $\beta$  dependence of the coefficients  $\tilde{m}^2$ ,  $\tilde{b}$  and  $g$  defined by eq. (7.29), with respective parameterizations by eq. (7.32).  $g$  is scaled up by a factor of 30.

### 7.2.3 Effective potential for block spins

To obtain a potential for the *long wavelength modes* we average the POLYAKOV loops over small blocks before computing the histogram of the thermal distribution. This averages out the hard spatial field modes and thus corresponds to a “cooling” of the system. We calculate cubic *block spin averages* defined as

$$\bar{\ell}_i^{(k)} = \frac{1}{k^3} \sum_{\mathbf{n}} \frac{1}{2} \text{Tr} \mathbf{L}(\mathbf{i} + \mathbf{n}), \quad \mathbf{n} = (0, 0, 0) \dots (k, k, k),$$

where  $k$  is the side-length in terms of lattice sites. We investigate the cases  $k = 2, 3, 4$ . For each combination of  $\beta, m^2$ , block-spins are measured on 2500 independent lattice configurations.

The effect that an increase of the size  $k$  of the block spin has on the shape of the potential is illustrated in Fig. 7.18 for two exemplary points in the confined ( $\beta = 0.5, m^2 = 0.0$ ) and deconfined phases ( $\beta = 1.5, m^2 = 0.0$ ) for the range  $k = 1 \dots 3$ . One observes, that with rising  $k$  the potential become narrower, more symmetric and more strongly peaked around the expectation value of the POLYAKOV loop  $|\bar{\ell}|$ . This is expected as a consequence of the *central limit theorem*<sup>2</sup>.

We take the potential for  $k = 3$  as a good approximation for the long distance sector. This is motivated as follows: We consider the block spin potential for different values of  $k$  and find the position  $\rho_{\min}$  of the potential minimum. The deviation of  $\rho_{\min}$  from the actual expectation value  $\langle |\bar{\ell}| \rangle$  of the POLYAKOV loop is taken as a measure for the validity of the approximation. For a valid approximation  $\Delta_\rho = \rho_{\min} - \langle |\bar{\ell}| \rangle$  should be small. This can be understood in analogy to a mean field self consistency criterium. Fig. 7.19 shows the  $\beta$  dependence of  $\Delta_\rho$  for  $m^2 = 0.0$  and the  $m^2$  dependence for  $\beta = 2.0$ . At  $k = 3$  the minimum of the effective potential differs at most by  $\simeq 0.03$  from the numerical value of  $\langle |\bar{\ell}| \rangle$ . This maximal deviation occurs precisely at the phase transition. At this point, within our numerical precision,  $k = 4$  does not do significantly better. Away from the phase transition

<sup>2</sup>The theorem states that the distribution  $P'(\bar{x})$  of the average of  $N$  random numbers, which are drawn from a distribution  $P(x)$  for which a reduced second moment exists, approaches a Gaussian distribution for  $N \rightarrow \infty$ . For proof see Ref. [92].



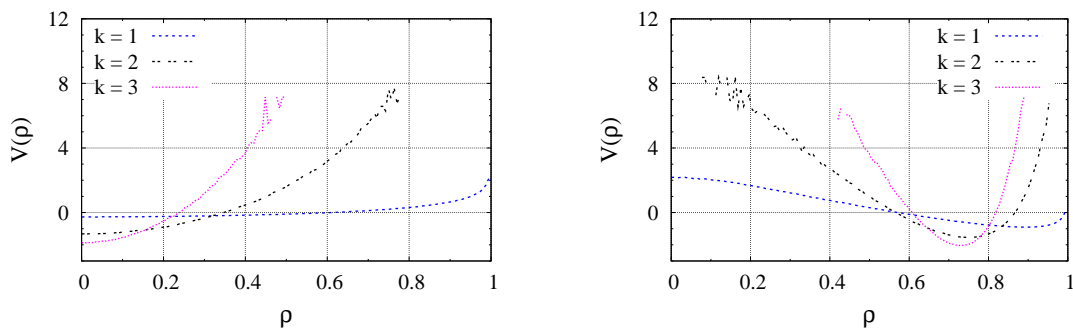


Figure 7.18: Effective potential  $V_{\text{eff}}$  for  $k = 1, 2, 3$  block-spins at  $\beta = 0.5/m^2 = 0.0$  (left) and  $\beta = 1.5/m^2 = 0.0$  (right) measured on  $N_s = 24$ . Averaging  $\ell$  over cubes of side length  $k$  causes the potential to become more strongly peaked.

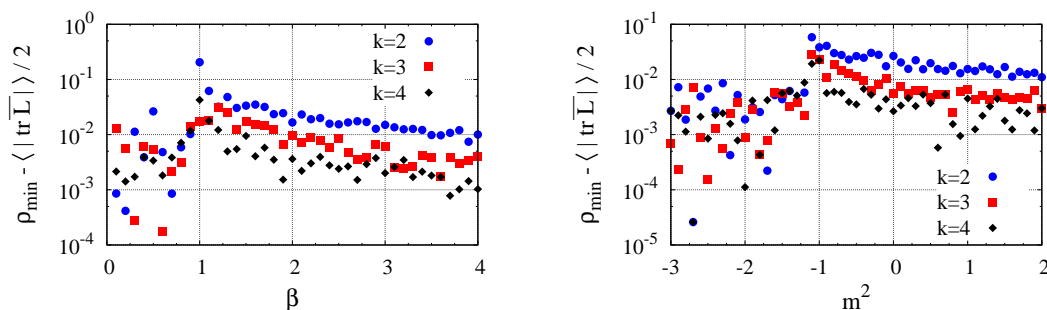


Figure 7.19: Difference between position of minimum of the block-spin potential and measured POLYAKOV loop expectation value for  $k = 2, 3, 4$  blocks, measured at  $m^2 = 0.0$  for a range of  $\beta$  (left) and at  $\beta = 2.0$  for a range of  $m^2$  (right).

$\Delta_\rho$  is less than  $\simeq 0.01$  for  $k = 3$ .  $k = 4$  does slightly better here, but reduces our statistics significantly. We have also checked that the results discussed below are stable when going from  $k = 3$  to  $k = 4$  and will discuss an explicit example. We refrain from discussing the  $k = 2$  case in detail. It appears to lie in an intermediate regime where contributions from the short range modes are not completely suppressed.

The *ansatz* (7.26), which was used for the POLYAKOV loop potential at a single site, is not applicable for the long wavelength modes. The block spin averaging procedure appears to suppress the non-analytic term in most regions of the phase diagram (a possible exception is discussed below). It appears that for large ranges of  $\beta, m^2$  the potential is well described by

$$V(\rho) = -d_0 \frac{1}{2} \log(1 - \rho^2) + d_1 + d_2 \rho^2 + d_4 \rho^4, \quad (7.33)$$

which is similar to a LANDAU-GINZBURG mean field theory for the POLYAKOV loop. The averaging appears to generate a quartic self-interaction term, which was not present in the

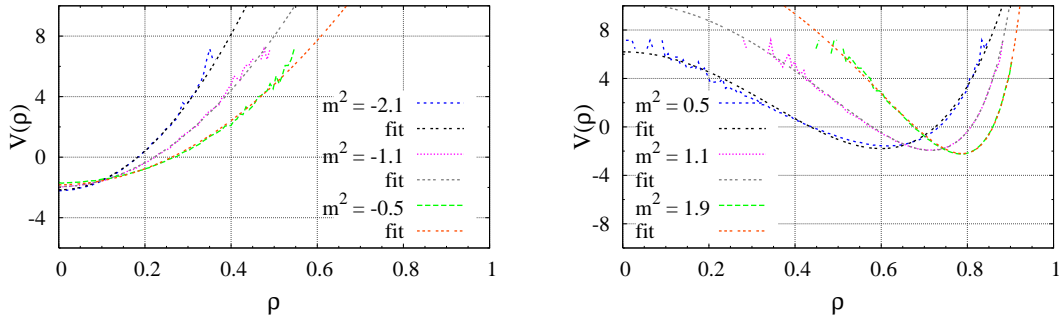


Figure 7.20: Effective potential for  $k = 3$  block-spins at  $\beta = 1.0$  for exemplary values of  $m^2$  in the confined (left) and deconfined (right) phases, with the corresponding  $\chi^2$  fits defined by eq. (7.33).

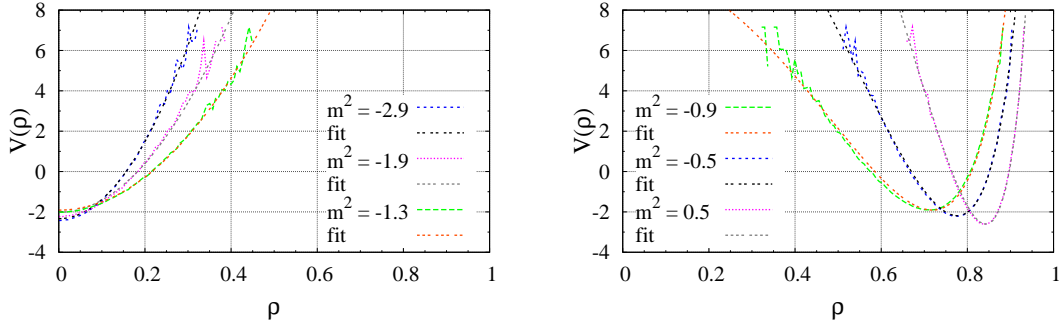


Figure 7.21: Effective potential for  $k = 3$  block-spins at  $\beta = 2.0$  for exemplary values of  $m^2$  in the confined (left) and deconfined (right) phases, with the corresponding  $\chi^2$  fits defined by eq. (7.33).

“bare” action. However, in contrast to a standard mean field model the VANDERMONDE potential must also be multiplied by a coefficient  $d_0$ , which depends on the location in the  $\beta - m^2$  plane.

Explicit results for the numerical potential and the  $\chi^2$  fit defined by Eq. (7.33) are shown for  $\beta = 1.0$  in Fig. 7.20 and for  $\beta = 2.0$  in Fig. 7.21 for different values of  $m^2$  in the confined and deconfined phases. Below the transition the results are consistent with  $d_0 = d_4 = 0$ . This is not surprising, since in the confined phase, the potential is essentially parabolic around  $\ell = 0$  and there is little sensitivity to higher powers of  $\ell$ .

The  $\beta/m^2$  dependence of the fit parameters from Eq. (7.33) is shown for  $m^2 = 0$  as a function of  $\beta$  in Fig. 7.22 and for fixed  $\beta = 1.0/2.0$  as a function of  $m^2$  in Fig. 7.23. For  $m^2 = 0$  there appears to be a region close above the phase transition where the potential is well described by a sum of quadratic and quartic terms, while the VANDERMONDE contribution vanishes. The figure shows  $d_0$  to fluctuate somewhat around zero, however we have confirmed that setting  $d_0 = 0$  by hand yields a decent  $\chi$  fit. A similar region is visible above the phase transition for  $\beta = 1.0$ . A comparison to the  $\beta = 2.0$  case suggests that this region

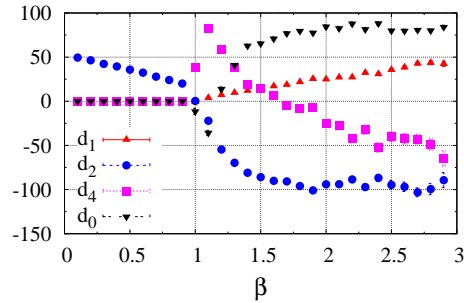


Figure 7.22: Parameters of  $\chi^2$  fit of (7.33) to the effective potential for  $k = 3$  block-spins at  $m^2 = 0.0$  for a range of  $\beta$ . Below  $\beta_C$ ,  $d_4$  and  $d_0$  are set to zero by hand.

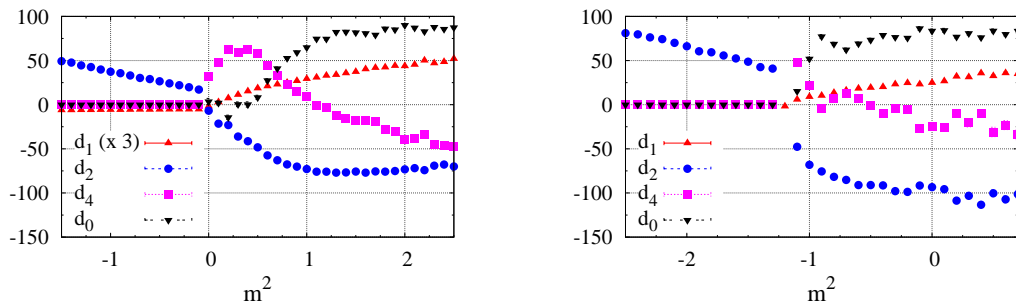


Figure 7.23: Parameters of  $\chi^2$  fit of (7.33) to the effective potential for  $k = 3$  block-spins at  $\beta = 1.0$  (left) and  $\beta = 2.0$  (right) for a range of  $m^2$ . In the confined phase  $d_4$  and  $d_0$  are set to zero by hand.

becomes narrower when going to larger  $\beta$  (which corresponds to weaker coupling in the  $4D$  theory).

The figures indicate that with rising  $\beta$  or  $m^2$  respectively,  $d_0$  rises gradually from zero above the phase transition and saturates at  $d_0 \approx 80$  deep in the deconfined phase, while the quartic coefficient drops from a positive value close above the phase transition to negative values for large  $\beta$  or  $m^2$ .

To confirm that the observed suppression of  $d_0$  above the phase transition at intermediate values of  $\beta$  is a real dynamical effect and not just an artifact generated by the lack of sensitivity to the VANDERMONDE potential for  $\langle |\ell| \rangle \ll 1$  we have checked that fixing  $d_0$  to its asymptotic value ( $d_0 \approx 80$ ) gives a less accurate fit and increases  $\chi^2$  per degree of freedom roughly by a factor of two in the region close above the deconfining phase transition.

To further investigate the origin of the suppression of  $d_0$ , we attempt to model the potential in the region above the phase transition with a different function, assuming a fixed VANDERMONDE potential term equal to the asymptotic value, but also including additional terms. We find that, within our numerical accuracy, it is possible to replace the suppression of the VANDERMONDE by another non-analytic term  $\sim \sqrt{\ell}$  like for the case  $k = 1$ . We find that the *ansatz*

$$V(\rho) = -d_0 \frac{1}{2} \log(1 - \rho^2) + d_1 + d'_0 \rho + d_2 \rho^2 + d_4 \rho^4, \quad \text{with} \quad d_0 \equiv 80, \quad (7.34)$$

fits the effective potential around  $\rho \approx 0$  even slightly better than (7.33), which shows small deviations around this point. The coefficient  $d'_0$  is negative in the region above the phase transition. However, the improvement of the  $\chi^2$  per degree of freedom is below the percent level and the *ansatz* (7.34) fails entirely at large  $\beta$  or large  $m^2$  (away from the phase transition) by generating a potential that is not bounded from below.

The result (7.34) suggests that the suppression of the VANDERMONDE term may be an artifact due to incomplete cooling of short-range fluctuations at  $k = 3$ . We thus investigate the cases [ $\beta = 1.0$ /variable  $m^2$ ] and [ $m^2 = 0$ /variable  $\beta$ ] also for  $k = 4$ . The extracted coefficients for this case are shown in Fig. 7.24. We observe, that sensitivity to the quartic coefficient diminishes at large  $\beta$ , which is expected since the potential becomes narrower and thus closer to parabolic. Nevertheless, the results are consistent with the case  $k = 3$  up to an overall scaling factor and a slight suppression of the quartic term close to the phase transition. The VANDERMONDE term must be modified by a parameter also at  $k = 4$ .

#### 7.2.4 Large $\beta$ limit

At very large  $\beta$  we find evidence that the order of the phase transition changes from second order to first order.

As seen in Fig. 7.25, the POLYAKOV loop expectation value changes very sharply from the confined to the deconfined phase for  $\beta \geq 2.0$ . While the transition is very abrupt already at  $\beta = 2.0$ , we have discussed in section 7.2.2 that for this particular value of  $\beta$  the effective potential for the POLYAKOV loop shows a single minimum for the entire range of  $m^2$  considered (above, below and exactly at the phase transition). This confirms the phase transition to be of second order.

The second plot in Fig. 7.25 shows however, that for  $\beta = 5.0$  there are clearly two distinct minima of the effective potential close to the phase transition. This indicates that

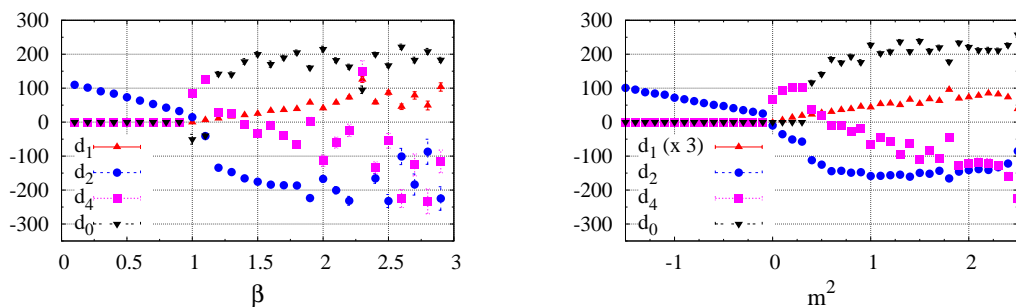


Figure 7.24: Parameters of  $\chi^2$  fit of (7.33) to the effective potential for  $k = 4$  block-spins at  $m^2 = 0.0$  for a range of  $\beta$  (left) and at  $\beta = 1.0$  for a range of  $m^2$  (right). Sensitivity to the quartic term is lost at large  $\beta$ . The results appear consistent with the  $k = 3$  case up to a scaling factor.

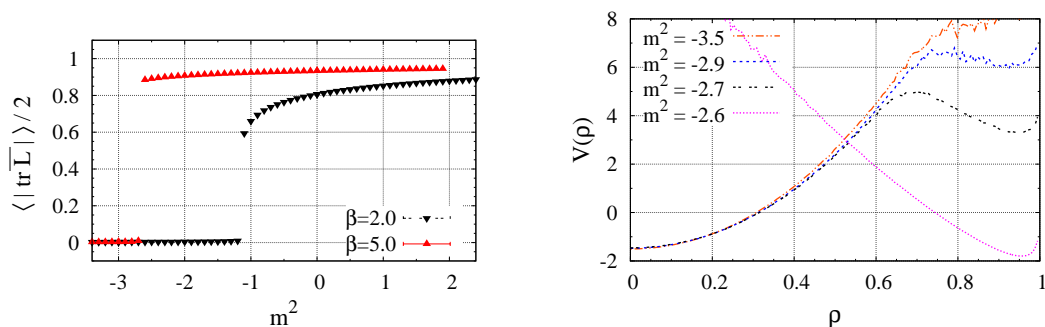


Figure 7.25: Left: POLYAKOV loop expectation value for  $\beta = 2.0$  and  $\beta = 5.0$ . Right: Effective potential for  $\beta = 5.0$  at values of  $m^2$  slightly above and slightly below the phase transition. Two distinct minima are observed.

two meta-stable states coexist close to the transition, which is characteristic for a first order transition.

## 7.3 Autocorrelations

The binning method was used to estimate the integrated autocorrelation time of our updating algorithm, which consists of sweeps with [5 random/2 over-relaxed] METROPOLIS hits for each site and [8 random/3 over-relaxed] hits for each link. We measured  $\tau_{\text{int}}$  for the volume averaged POLYAKOV loop  $\langle |\bar{l}| \rangle$  as well as for the WILSON action  $\langle \mathcal{S}_{\square} \rangle$ , for [ $m^2 = 0.0/\beta$  variable] and [ $\beta = 2.0/m^2$  variable]. For  $N_s = 12, 16$  lattices 400000 sweeps were performed for each combination of  $\beta/m^2$ . For  $N_s = 24$  we performed 100000 sweeps. We find that for the entire parameter range considered, the autocorrelation time for  $\langle \mathcal{S}_{\square} \rangle$  is  $\lesssim 5$  sweeps on  $N_s = 24$  and displays only a mild increase on the order of  $\sim 1$  when approaching the phase

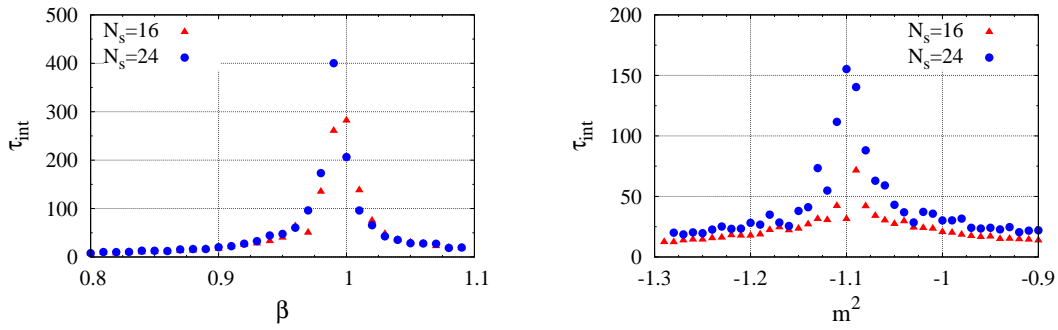


Figure 7.26: Integrated autocorrelation time of  $\langle |\bar{\ell}| \rangle$  for  $[m^2 = 0.0/\beta$  variable] (left) and  $[\beta = 2.0/m^2$  variable] (right) measured in the phase transition region on  $N_s = 16, 24$  lattices.

transition. We refrain from showing the explicit figures. For  $\langle |\bar{\ell}| \rangle$  we display the results of the  $N_s = 16, 24$  lattices in Fig. 7.26. We do not obtain errorbars for  $\tau_{\text{int}}$  and take the measured results as rough estimates. The final bin-size is slightly larger than the  $\tau_{\text{int}}$  estimate for each case. While autocorrelations are modest (on the order of  $\lesssim 25$ ) far from the transition we find massive critical slowing down when approaching the phase transition. We find that several hundreds of configurations need to be discarded between measurements, close to the phase boundary. We choose to discard 500 configurations at the phase boundary for the  $N_s = 24$  lattice and 300 for the  $N_s = 12, 16$  lattices.

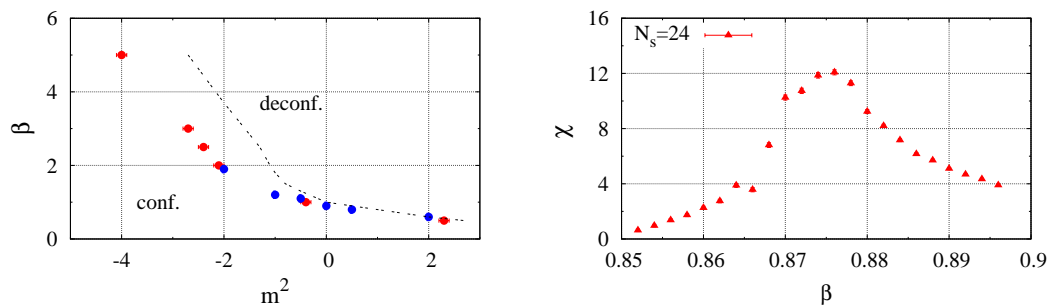


Figure 7.27: Left: Phase diagram within a time-plaquette single counting scheme. The points denote single counting measurements. The dotted line corresponds to the estimated phase boundary in the double counting scheme (for error estimates see Fig. 7.6). Right: Susceptibility at  $m^2 = 0.0$  for a range of  $\beta$ , close to the phase boundary.

## 7.4 Single counting scheme

In the final section of this chapter we now discuss quantitative and qualitative differences that arise when going from a time-plaquette double counting scheme to a single counting scheme. Since in our code the spatial and the time-like contributions to the action (7.1) are well separated this is technically straight-forward. Our main focus here is to show which aspects of the model are qualitatively different, so we will not discuss every observable in detail here and will restrict ourselves to exemplary results. We discuss the effective potential for the POLYAKOV loop at a single site, a full investigation of the block spin averaged field, however, has not been performed. Also, we focus this discussion on the immediate physical results, and refrain from quoting sample sizes and autocorrelation times.

We measure the POLYAKOV loop expectation value  $\langle |\bar{\ell}| \rangle$  in wide ranges of  $\beta$  and  $m^2$  to obtain the phase diagram. The result is shown in Fig. 7.27 (left). The phase boundary at  $m^2 > 0$  is very similar to the double counting scheme (Fig. 7.6). However, at  $m^2 < 0$  the phase boundary runs at a somewhat different angle. In Fig. 7.27 (right) we show the susceptibility  $\frac{\partial \langle |\bar{\ell}| \rangle}{\partial \beta}$  at  $m^2 = 0.0$ . The peak is consistent with

$$\beta_C = 0.8730(2) , \quad (7.35)$$

which was obtained by Ref. [123] for  $N_\tau = 1$   $SU(2)$  gauge theory (although this reference does not discuss explicitly how boundary conditions were treated). It differs only slightly from the double counting scheme for which we found  $\beta_C = 1.00(1)$ . The matrix-matrix correlation length also seems to diverge at  $\beta_C \approx 0.87$  (see Fig. 7.30, left). We find that the general qualitative behavior of the electric screening masses is the same as in the double counting scheme: They vanish only exactly at the phase boundary in infinite volume. No massless excitations exist, deep in the confined or deconfined phase.

The phase boundary has the same qualitative structure as in the previous discussions: The phase transition is of second order for small  $\beta$  and then turns to first order when  $\beta$  becomes large. We illustrate this in Fig. 7.28 where the effective potential of the POLYAKOV loop at a single site is shown, when crossing the phase boundary at  $\beta = 2.0$  (left) and  $\beta = 5.0$

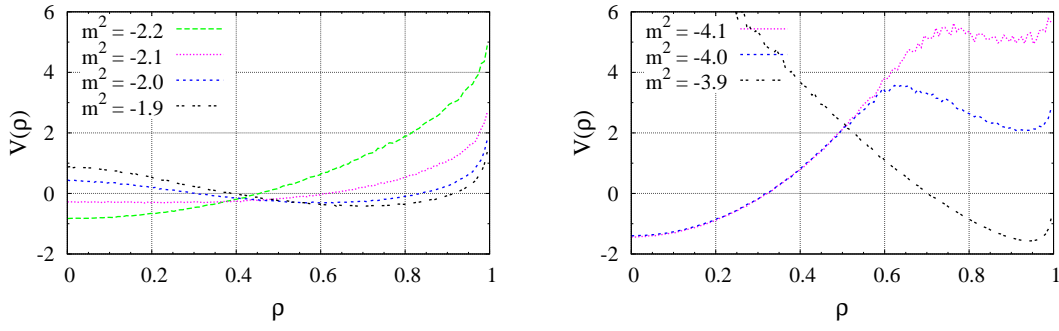


Figure 7.28: Effective potential  $V_{\text{eff}}$  for POLYAKOV loop at a single site, calculated in time-like plaquette single counting scheme at  $\beta = 2.0$  (left) and  $\beta = 5.0$  (right) for exemplary values of  $m^2$  in the confined and deconfined phases.

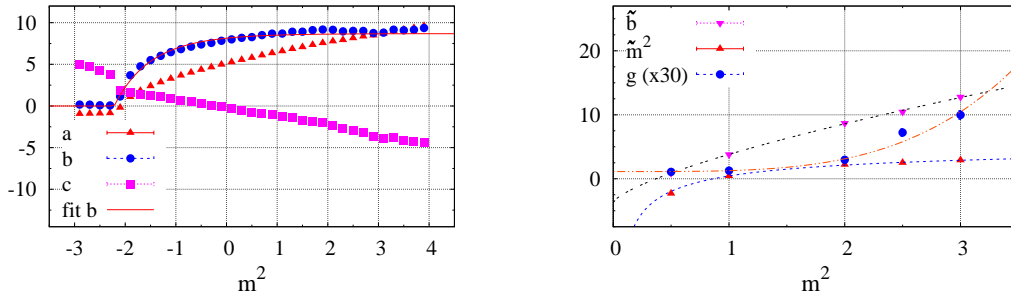


Figure 7.29: Left: The parameters of the effective potential (7.26) at  $\beta = 2.0$ . The solid line represents a  $\chi^2$  fit using eq. (7.29) to the non-analytic coefficient  $b(\beta, m^2)$ . Right: The  $\beta$  dependence of the parameters of eq. (7.29).

(right). Two distinct minima can be seen at  $\beta = 5.0$  close to the phase transition.  $V_{\text{eff}}(\rho)$  can be parameterized analogous to (7.26) with linear and quadratic terms in  $\rho$ . Eqs. (7.29) and (7.32) can be used to model the non-analytic coefficient  $b$ , the parameters of (7.32) being summarized in the following table:

$m_0^2 = 6.2(9)$	$m_0'^2 = -5.8(9)$	$w = -0.5(2)$
$b_0' = -3.7(9)$	$b_0'' = 7.5(9)$	$v = 0.71(7)$
$g_0 = 0.037(3)$	$g_0' = 0.004(2)$	$u = 3.8(6)$

Fig. 7.29 shows the resulting parameterization of  $g(\beta)$ ,  $\tilde{m}^2(\beta)$  and  $\tilde{b}(\beta)$ , as well as an explicit example ( $\beta = 2.0$ ) of the  $m^2$  dependence of the parameters  $a, b, c$  of eq. (7.26).

The magnetic sector shows a qualitatively somewhat different behavior than in the double counting scheme. Although the magnetic screening mass (Fig. 7.30 right) behaves similar to our previous discussions (vanishing signal for the two-point function below  $\beta_C$ , a constant



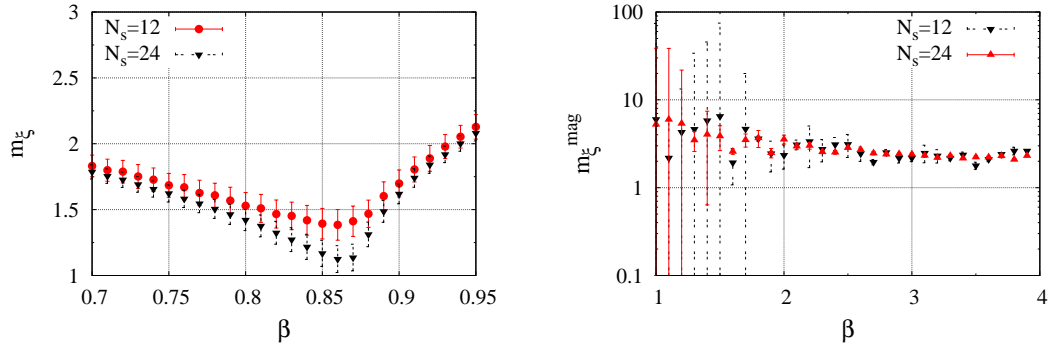


Figure 7.30: Left: The electric screening mass from the matrix-matrix correlation function  $m^2 = 0.0$ . Right: The inverse plaquette-plaquette correlation length.

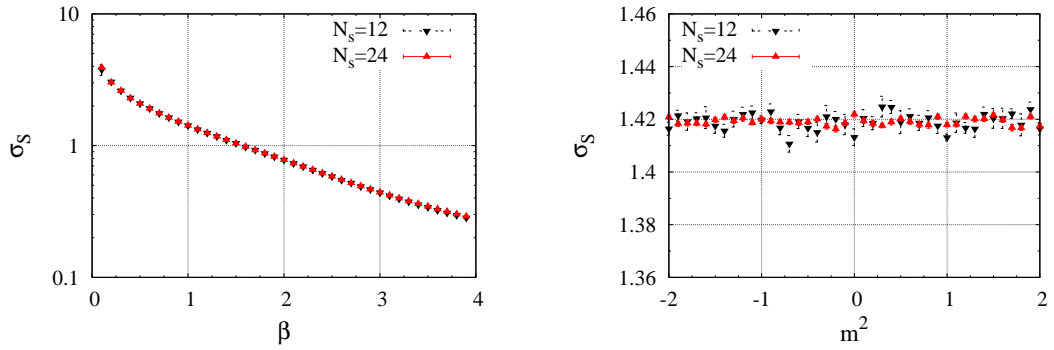


Figure 7.31: The spatial string tension  $\sigma_S$  in the time plaquette single counting scheme as function of  $\beta$  at  $m^2 = 0.0$  (left) and as a function of  $m^2$  at  $\beta = 1.0$  (right).

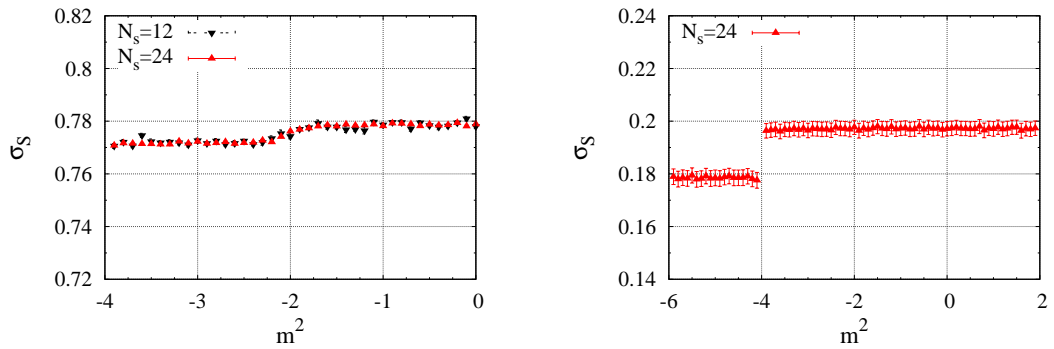


Figure 7.32: The spatial string tension  $\sigma_S$  in the time plaquette single counting scheme at  $\beta = 2.0$  (left) and at  $\beta = 5.0$  (right).

mass above  $\beta_C$  and no dependence on  $m^2$ ) there are differences in the behavior of the spatial string tension and the WILSON action. In Figs. 7.31 and 7.32 we show  $\sigma_S$  obtained on  $N_S = 12, 24$  lattices in various regions of the phase diagram. Fig. 7.31 (left) shows the case [ $m^2 = 0.0$  / variable  $\beta$ ]. Here we find consistency with our prior results: The string tension shrinks continuously with rising  $\beta$  and does not display any special behavior at  $\beta_C$ . However, when measuring at fixed  $\beta$  and variable  $m^2$ , we find that there is no dependency of  $\sigma_S$  on  $m^2$  at all at  $\beta < \beta_C$ . For  $\beta > \beta_C$  we find that at exactly the phase transition there is (consistent with the double counting results) a sharp increase of  $\sigma_S$  on the order of  $\sim 1\%$ , which becomes stronger with rising  $\beta$ . However, away from the transition, even at  $\beta > \beta_C$ ,  $\sigma_S$  appears to be completely independent of  $m^2$ . The behavior of the WILSON action  $\langle S_{\square} \rangle / \beta$  is analogous (we refrain from showing explicit figures). This differs from the double counting scheme, in which a weak  $m^2$  dependence of both  $\sigma_S$  and  $\langle S_{\square} \rangle / \beta$  is seen, even for values of  $m^2$  far from the transition.

## 8 Results in four dimensions

In this chapter we summarize our efforts towards the goal of matching the three dimensional effective theory of WILSON lines to the full gauge theory in four dimensions. The ultimate aim of such an effort is to obtain the temperature dependencies of the coupling constants  $\beta$  and  $m^2$  defined in the previous chapters. We state clearly however, that this aim is far beyond the scope of this work. The results presented in this chapter represent only a first attempt of obtaining a qualitative comparison of the phase structures of both theories. We approach the problem by simulating a  $4D$  pure gauge theory with a fixed time-like extent  $N_\tau$  and measuring bare values for similar observables as in the  $3D$  case. We obtain the WILSON line  $\mathbf{L}(\mathbf{x})$  as an effective three dimensional field by multiplying the link variables along a straight closed path in the time direction.

This chapter is structured as follows: We begin by reproducing well-known results for observables in  $4D$  YANG-MILLS theory, to establish numerical consistency. The first result is the critical value of the coupling constant  $\beta$ . A second order phase transition is known to occur, where the POLYAKOV loop becomes non-zero for large  $\beta$ . Next we calculate the WILSON action and CREUTZ ratios and compare them to literature.

We then proceed to calculate two point function of the WILSON line. We show that the behavior of the inverse correlation length is in agreement with the  $3D$  theory. Next, we compute the effective potential for the POLYAKOV loop, for single sites as well as for block spins, and show that a parameterization similar to the  $3D$  case is possible. The central result of this chapter is the observation that the effective potential for block spins has a similar qualitative structure as in the  $3D$  effective theory, with a VANDERMONDE contribution which vanishes in a small region close above the phase transition.

All results presented in this chapter were obtained with a modified version of the MILC collaboration's public lattice gauge theory code<sup>1</sup>, which uses the KENNEDY-PENDLETON heat bath algorithm to update the link variables.

### 8.1 Phase transition

Ref. [124] calculated the expectation value of  $SU(2)$  POLYAKOV loops for different time-like lattice sizes  $N_\tau$  and extracted the critical point  $\beta_c$ . The following table contains shows the findings of this reference for  $N_\tau = 2, 4, 6$  :

$N_\tau$	$\beta_C$
2	1.8800(30)
4	2.2986(6)
6	2.4265(30)

<sup>1</sup>See <http://physics.indiana.edu/~sg/milc.html>

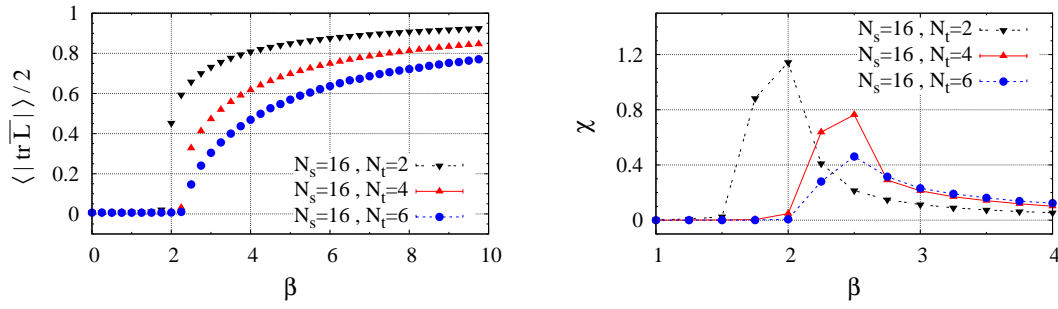


Figure 8.1: Expectation value of volume averaged POLYAKOV loop  $\langle |\bar{L}| \rangle$  (left) and susceptibility  $\chi = \frac{\partial \langle |\bar{L}| \rangle}{\partial \beta}$  (right), measured on  $N_s = 16$ .

We measure the volume averaged POLYAKOV loop on a  $N_s = 16$  and  $N_t = 2, 4, 6$  lattices for a large range of  $\beta$ . Fig. 8.1 shows our findings, together with the respective susceptibilities  $\chi = \frac{\partial \langle |\bar{L}| \rangle}{\partial \beta}$ . The peaks of the susceptibilities for the different  $N_t$  are in agreement with the table shown above, within numerical precision.

## 8.2 Wilson action

The expectation value of the 4D WILSON action over  $\beta$

$$\frac{1}{\beta} \langle S_{\square} \rangle = \frac{1}{V} \left\langle \sum_{\square} \left( 1 - \frac{1}{2} \text{Re Tr } \mathbf{U}_{\square} \right) \right\rangle. \quad (8.1)$$

was calculated by CREUTZ. In Ref. [2] the results for  $N_s = N_t = 10$  are presented for a large range of  $\beta$ . We reproduce these results, and present them in Fig. 8.2.

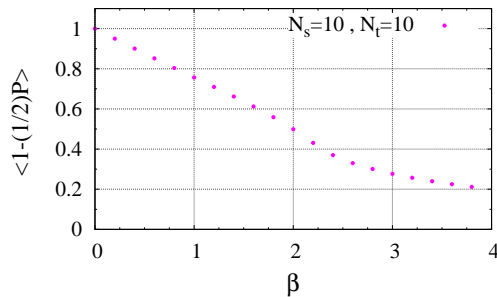


Figure 8.2: The WILSON action over  $\beta$ , measured on  $N_s = N_t = 10$ . Reproduces Ref. [2].

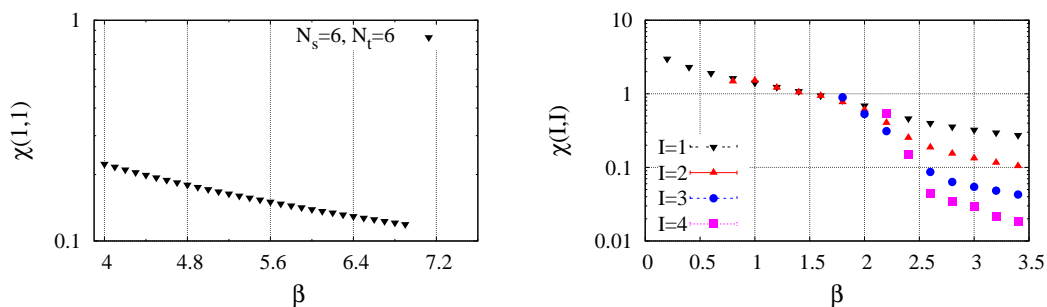


Figure 8.3: Left: The first order string tension  $\chi(1,1)$ . This figure agrees precisely with Ref. [125]. Right:  $\chi(I,I)$  for  $I = 1 \dots 4$  measured on  $N_s = N_t = 10$ . This figure agrees with Ref. [126].

### 8.3 Creutz ratios

Refs. [125] and [126] calculated CREUTZ ratios

$$\chi(I, J) = -\ln \left( \frac{W(I, J) W(I-1, J-1)}{W(I, J-1) W(I-1, J)} \right), \quad (8.2)$$

for the special case  $I \equiv J$  in the 4D gauge theory. Ref. [125] calculated  $\chi(1,1)$  on  $N_s = N_t = 6$ , while Ref. [126] calculated the cases  $I = 1 \dots 4$  on  $N_s = N_t = 10$  for a range of  $\beta$ . We recalculate both cases and find that our results are in agreement with both references. Our measurements are presented in Fig. 8.3.

### 8.4 Two-point functions

We measure the two point matrix-matrix correlation function of the WILSON line defined by

$$\mathcal{C}_{\mathbf{L}}(r) = \frac{1}{3} \frac{1}{N_s^3} \sum_{\hat{\mathbf{r}}, \mathbf{r}_0} \frac{1}{2} \left\langle \text{tr} \mathbf{L}^\dagger(\mathbf{r}_0) \mathbf{U}_{\mathbf{r}_0, \mathbf{r}_0+\mathbf{r}} \mathbf{L}(\mathbf{r}_0 + \mathbf{r}) \mathbf{U}_{\mathbf{r}_0, \mathbf{r}_0+\mathbf{r}}^\dagger \right\rangle, \quad (8.3)$$

on  $N_s = 16, 32 / N_t = 4$  lattices, where the parallel transporter  $\mathbf{U}_{\mathbf{r}_0, \mathbf{r}_0+\mathbf{r}}$  is included to ensure gauge invariance. We extract the inverse correlation length  $m$ . Our results for a range of  $\beta$  are shown in Fig. 8.4 (left), together with POLYAKOV measurements on the same lattices (right). We find that the mass is non-zero both above and below the phase transition point, but drops at  $\beta_c$ . The absence of GOLDSTONE modes is evident, and agrees with the 3D effective theory.

### 8.5 Single site loop potential

We determine the effective potential of the POLYAKOV loop at a single site

$$V_{\text{eff}}(|\ell|) = -\log P(|\ell|), \quad (8.4)$$

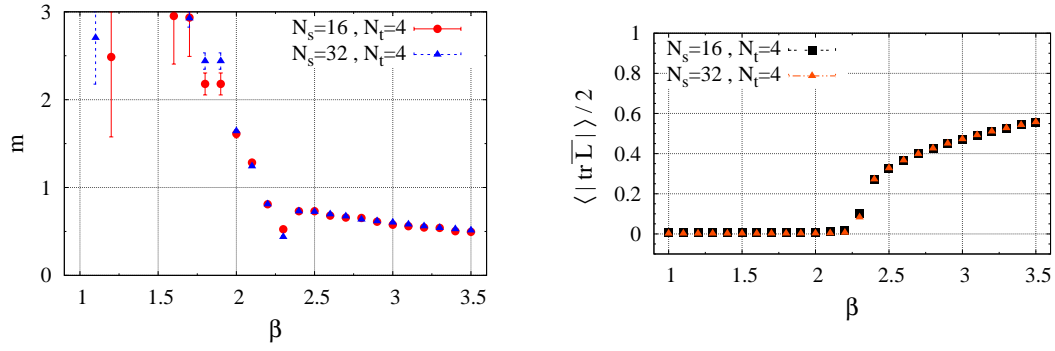


Figure 8.4: Inverse correlation length (mass) measured on  $N_s = 16, 32 / N_t = 4$  close to phase transition point (left) with respective POLYAKOV loop measurement (right).

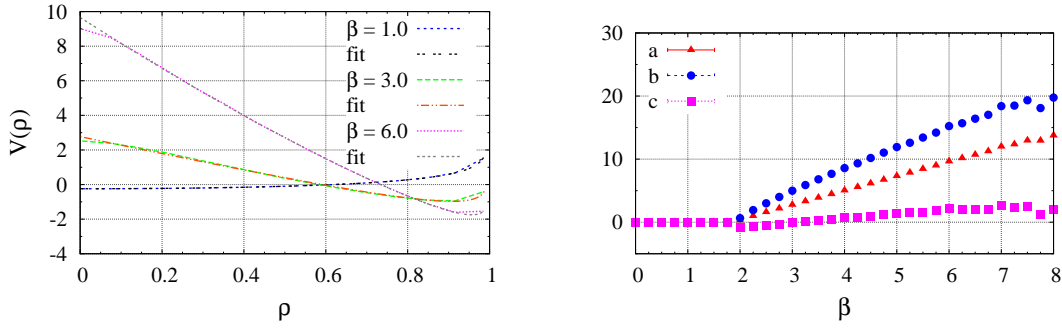


Figure 8.5: Single site POLYAKOV loop potential measured on  $N_s = 16/N_\tau = 2$  with fit curves defined by (8.5) for various values of  $\beta$  above and below  $\beta_c$  (left) with corresponding  $\beta$  dependence of fit-parameters (right).

for  $N_s = 16$  from the probability distribution  $P(|\ell|)$ , which is obtained via histogramming. We find that similar to the 3D effective theory, a parameterization of the potential according to

$$V_{\text{fit}}(|\ell|) = -\frac{1}{2} \log(1 - |\ell|^2) + a - b|\ell| + c|\ell|^2 \quad (8.5)$$

is possible. Figs. 8.5 and 8.6 show the resulting  $\beta$  dependence of the parameters  $a, b, c$  for  $N_\tau = 2$  and  $N_\tau = 4$  respectively.

We confirm that a non-analytic contribution  $\sim \sqrt{\ell^2}$  exists also in the 4D theory. However, the quadratic coefficient which was proportional to the mass term in the effective theory appears to be very small compared to the other contributions.

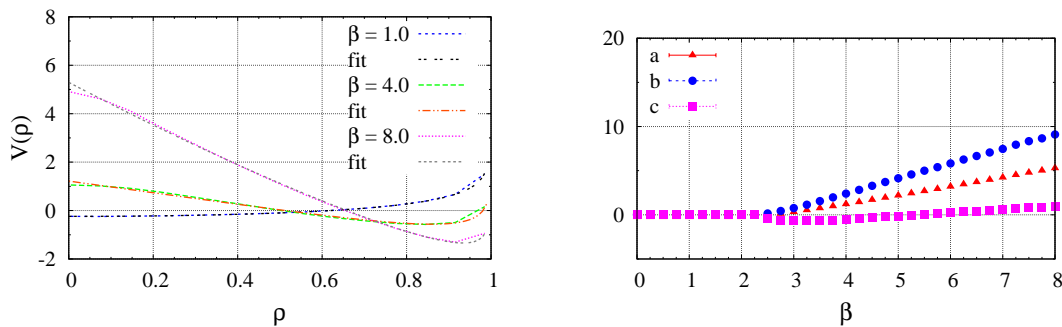


Figure 8.6: Single site POLYAKOV loop potential measured on  $N_s = 16/N_\tau = 4$  with fit curves defined by (8.5) for various values of  $\beta$  above and below  $\beta_c$  (left) with corresponding  $\beta$  dependence of fit-parameters (right).

## 8.6 Block spin potential

We compute the effective potential for POLYAKOV loop block spins

$$\bar{\ell}_i^{(k)} = \frac{1}{k^3} \sum_{\mathbf{n}} \frac{1}{2} \text{Tr} \mathbf{L}(\mathbf{i} + \mathbf{n}), \quad \mathbf{n} = (0, 0, 0) \dots (k, k, k),$$

with  $k = 3$  on a  $N_s = 16/N_\tau = 4$  lattice for several values of  $\beta$ . We find that analogous to the 3D theory, a modelling with the *ansatz*

$$V(\rho) = -d_0 \frac{1}{2} \log(1 - \rho^2) + d_1 + d_2 \rho^2 + d_4 \rho^4, \quad (8.6)$$

is possible. Moreover, we find that the qualitative behavior of the fit-parameters  $d_{0\dots 4}$  is in agreement with the findings discussed in section 7.2.3. Above  $\beta_c$  there is a region where the parameter  $d_0$  can be set to zero. At large  $\beta$  it saturates at an asymptotic value. We show the potentials, together with the fit curves and the  $\beta$  dependence of the parameters in Fig. 8.7. We show the potential explicitly only in the deconfined phase, since below  $\beta_c$  it is simply parabolic around  $\ell = 0$ . Note the similarity to Fig. 7.23.

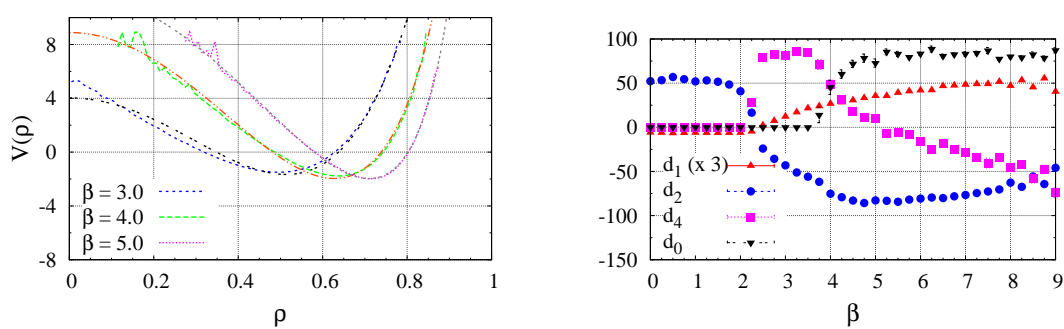


Figure 8.7: Block spin potential measured on  $N_s = 16/N_\tau = 4$  with fit curves defined by (8.6) for various values of  $\beta$  above  $\beta_c$  (left) with corresponding  $\beta$  dependence of fit-parameters (right).



## 9 Summary and conclusions

We have performed Monte-Carlo simulations of an effective theory of  $SU(2)$  WILSON lines in three dimensions. First results were obtained without gauge fields,  $A_i^a = 0$ . The main purpose of the investigation of this limiting case was a study of eigenvalue repulsion in the deconfined phase of a  $SU(2)$  matrix model. The kinetic term exhibits a global  $SU_L(2) \times SU_R(2)$  symmetry which is broken explicitly to  $SU(2)$  by the loop potential<sup>1</sup>.

The phase diagram is sketched in Fig. 6.6. In the absence of a potential, at  $m^2 = 0$ , the theory is essentially a standard spin-model. At small  $\beta$  the effective mass of the WILSON lines is large and they fluctuate independently from site to site. Confinement is realized in a trivial way since  $\bar{\mathbf{L}} \rightarrow \mathbf{0}$  for each configuration. This remains true for small  $|m^2|$ . To deconfine, a large upside-down potential ( $m^2 > 0$ ) is required to align the WILSON lines to the unit matrix. Hence, for small  $\beta$  the phase transition arises due to the effective *loop potential*, in a regime where  $SU_L(2) \times SU_R(2)$  is broken strongly.

There is a second-order phase transition at  $\beta_c \simeq 0.942$  (and  $m^2 = 0$ ) where the masses (inverse correlation lengths) of the POLYAKOV loop  $\ell = \text{Tr } \mathbf{L}/2$  and of the adjoint fields  $\tilde{\ell}^a = -i \text{Tr } \mathbf{L} \boldsymbol{\tau}^a/2$  vanish. This is associated with spontaneous breaking of  $SU_L(2) \times SU_R(2)$  to  $SU(2)$ , where three GOLDSTONE modes appear. We have confirmed that the “length”  $u^2 = \text{Tr } \bar{\mathbf{L}}^\dagger \bar{\mathbf{L}}/2$  of  $\bar{\mathbf{L}}$  acquires a non-zero expectation value for  $\beta > \beta_c$ . Hence, we expect that a weak background field  $-h \text{tr } \mathbf{L}$ ,  $h \rightarrow 0$ , shifts the phase boundary to  $m^2 < 0$ .

Very large lattice coupling  $\beta \gg 1$  corresponds to the extreme weak-coupling limit of the original four-dimensional theory; the effective theory can nevertheless confine because it incorporates the global  $Z(N)$  symmetry for the POLYAKOV loop. At large  $\beta$  fluctuations are suppressed and the WILSON lines are again forced to align, this time by the nearest-neighbor interaction (kinetic term). The direction of alignment is determined by the loop potential. A standard potential with positive curvature ( $m^2 < 0$ ) is minimized by WILSON lines with no singlet component, hence eigenvalues repel and the theory confines. On the other hand, an upside-down potential ( $m^2 > 0$ ) leads to  $\mathbf{L}(\mathbf{x}) \sim \mathbf{1}$  and so to eigenvalue attraction and deconfinement. For  $\beta \gg 1$  even a weak potential suffices to trigger the locking into (or out of) the center of the group. This leads to a sharp transition directly to a perturbative deconfined phase without eigenvalue repulsion.

We have measured the distributions of the eigenvalues of the WILSON line in the non-perturbative deconfined phase above, but close to,  $\beta_c$ . They show clearly the emergence of eigenvalue repulsion even for “temperatures” (i.e.  $m^2$ ) not extremely close to the phase boundary. It is only relatively deep in the deconfined phase ( $m^2 \gtrsim 1$ ) that the distribution of eigenvalues peaks near 1, which corresponds to the perturbative vacuum. These results confirm the suggestion of ref. [51] that eigenvalue repulsion in the deconfined phase does arise at intermediate values of the nearest-neighbor coupling  $\beta$ , due to fluctuations of the Wilson lines, provided that the non-perturbative “fuzzy-bag” term approximately cancels

---

<sup>1</sup>Note that a  $\mathbf{L} \rightarrow \Omega_L \mathbf{L} \Omega_R$  transformation changes the eigenvalues of  $\mathbf{L}$ , while  $\mathbf{L} \rightarrow \Omega^\dagger \mathbf{L} \Omega$  does not.

the perturbative loop potential. Such a “fuzzy bag” contribution in the effective theory makes it possible to reach the region of small  $m^2$  in the phase diagram.

In the confined phase at  $\beta > \beta_c$  the volume-averaged WILSON line  $\bar{\mathbf{L}}$  approaches the center-symmetric vacuum [51, 81, 127, 128]

$$\mathbf{L}_c = \text{diag} (1, z, z^2, \dots, z^{N-1}) \quad , \quad (z \equiv e^{2\pi i/N}) \quad , \quad (9.1)$$

which for two colors corresponds to  $\mathbf{L}_c = i\sigma_3$  (up to an overall  $SU(2)$  rotation). This is due to the fact that the Wilson lines align at large  $\beta$ , and  $m^2 < 0$  favors a direction orthogonal to unity. We repeat that this is not the case when  $\beta$  is small, where instead  $\bar{\mathbf{L}} \rightarrow 0$  for  $m^2 \simeq 0$ .

We proceeded to perform simulations of the effective theory of WILSON lines coupled to gauge fields. After mapping the phase diagram (Fig. 7.6), we have investigated the effective potential for the average of the eigenvalues of the  $SU(2)$  WILSON line, which is equal to the absolute value of the POLYAKOV loop. We found that a form containing non-analytic contributions can describe the extracted potential. This non-analytic term was not present in the action, and therefore must arise from the dynamics.

We extracted a similar effective potential also for the long wavelength modes of the POLYAKOV loop and found that this can be described by a mean-field type potential with quadratic and quartic terms plus an effective VANDERMONDE potential which depends on the couplings. Just above the phase boundary, in the deconfined phase, the effective VANDERMONDE potential contributes little. Deeper into the deconfined phase its coefficient increases and eventually appears to approach a constant.

A non-trivial vacuum where confinement is driven by repulsion of eigenvalues of the WILSON line exists also when gauge fields are included. However, unlike for the case  $A_i^a = 0$  there is no exact phase boundary to a phase where the WILSON line averages over the entire group manifold with elements of the group center included. Moreover there exists no global alignment in the confined phase. Measurements of two-point functions confirm the expectation that no GOLDSTONE modes exist in any region of the phase diagram. We found also that the effect of a deconfining phase transition of the WILSON line on the gauge sector is extremely weak.

Our simulations may provide useful insight into the structure of mean-field type models for the deconfining phase transition. For example, so-called “POLYAKOV-NJL” models have recently been studied extensively. Such models attempt to describe QCD thermodynamics over a range of quark masses, from the pure-gauge limit to physical QCD; they require an *ansatz* for the effective potential for the POLYAKOV loop. For example, in early works on this subject [129] a quadratic potential for  $\ell$  has been used, plus a VANDERMONDE contribution (per lattice site) which is constant and temperature independent. Our results appear to indicate, however, that if a standard potential with terms  $\sim \ell^2$  and  $\sim \ell^4$  (plus cubic  $Z(3)$  invariants for the case of three colors) is used, that a temperature dependent VANDERMONDE contribution should also be allowed for.

## Outlook

There is much potential for future work in this field. Specifically, a precise non-perturbative matching of the coupling constants of the effective theory to the underlying four-dimensional

---

theory remains an open project. It would be interesting to see whether the structure of  $Z(2)$  domain walls of the  $3D$  theory can be matched to  $4D$   $SU(2)$  YANG-MILLS theory.

One should investigate how the results change when including higher order terms of the perturbative potential of the WILSON line. One could also extend the simulations to  $SU(3)$  gauge group where a first-order phase transition occurs. The *ansatz*  $V_{\text{eff}}$  for the effective potential of the POLYAKOV loop is not directly generalizable to other  $SU(N)$  groups. It would be interesting to see whether a generalizable definition of  $V_{\text{eff}}$  in terms of the group characters of  $\mathbf{L}$  can be obtained.

A detailed study of the critical behavior of the theory via BINDER cumulants would be interesting. One could extract critical exponents and compare them to the three dimensional ISING universality class along the critical line.

Also, one could investigate to what extent quantitative comparisons to complimentary  $3D$  effective theories are possible, for instance by performing analytic weak and strong coupling expansions.



# Appendices



# A Group theory

In this appendix we summarize the group theoretical concepts which are of immediate relevance to our work. For a general introductory text about this broad subject and its applications to particle physics, see Ref. [130].

## Definition of a group

A group  $G$  is a set with a binary operation, which assigns every ordered pair of elements a third element and which fulfills the conditions:

- Closure property:

$$\text{If } f, g \in G \text{ then } h = fg \in G . \quad (\text{A.1})$$

- Associativity:

$$\text{For } f, g, h \in G , f(gh) = (fg)h \in G . \quad (\text{A.2})$$

- Identity element:

$$\text{There exists an element } e \text{ so that } ef = fe = f, \text{ for all } f \in G . \quad (\text{A.3})$$

- Inverse element:

$$\text{For all } f \in G , \text{ there exists an } f^{-1} \in G , \text{ so that } f^{-1}f = ff^{-1} = e . \quad (\text{A.4})$$

A group is called **Abelian** if it is *commutative*, i.e.

$$fg = gf \text{ for all } f, g \in G . \quad (\text{A.5})$$

A group is called **finite** if it has a finite number of elements. If a subset  $H$  of elements of  $G$  also fulfills the above axioms it is called a **subgroup** of  $G$ .

## Representations

A representation of a group  $G$  is a mapping of the elements onto a set of linear operators  $D$  (or  $n \times n$  matrices correspondingly) with the properties

- $D(e) = \mathbf{1}$ , i.e. the identity element is mapped onto the identity operator (or the unit matrix).
- $D(f)D(g) = D(fg)$ , i.e. the multiplication law is preserved.

The dimension of the linear space on which a representation acts is called the **dimension of the representation**. A given group can have many representations of different dimensionality.

## Cyclic groups

A cyclic group is a group which has an element  $g$  such that every element of the group (including  $g$ ) can be obtained as a multiplicative power of  $g$ , i.e.

$$\text{For all } f \in G \text{ there exists an integer } n \text{ so that } f = g^n . \quad (\text{A.6})$$

The cyclic group with  $N$  elements is called  $Z(N)$ . The group  $Z(N)$  can be represented by the  $N$ -th complex *roots of unity* :

$$D(g_j) = e^{2\pi i \frac{j}{N}} , \quad j = 1 \dots N . \quad (\text{A.7})$$

Here  $D(e) = D(g_N) \equiv D(g_0)$ . The dimension of this representation is one.  $Z(N)$  is ABELIAN for all  $N$ . The most important cyclic group for this work is  $Z(2)$ , which has two elements that can be represented by  $D(e) = 1$ ,  $D(g) = -1$ .

## Lie groups

A group, of which the elements  $g \in G$  depend smoothly on a set of continuous parameters, i.e.

$$g \equiv g(\alpha) , \quad (\text{A.8})$$

is called a **Lie group**. Here we understand smoothness as the notion that neighboring points in the parameter space map to neighboring points in group space. LIE groups are smooth manifolds and therefore can be studied by differential calculus.

There is a certain freedom in parameterizing the linear operators of a given representation of a LIE group. One can choose a parameterization such that in some neighborhood of the identity the group elements can be described by a function of  $N$  real parameters  $\alpha_a$  with  $a = 1 \dots N$ , and such that  $\{\alpha_a = 0 \forall a\}$  corresponds to the identity operator

$$D(\alpha)|_{\alpha=0} = 1 . \quad (\text{A.9})$$

$D(\alpha)$  can then be TAYLOR expanded around  $\alpha = 0$

$$D(d\alpha) = 1 + id\alpha_a X_a + \dots . \quad (\text{A.10})$$

The operators

$$X_a = -i \frac{\partial}{\partial \alpha_a} D(\alpha)|_{\alpha=0} , \quad (\text{A.11})$$

are called **generators** of the group representation and form a vector space. They are of major importance, because the entire multiplication law of the group is contained in their commutation relation

$$[X_a, X_b] = if_{abc} X_c . \quad (\text{A.12})$$

The commutator (A.12) is called **Lie algebra** and  $f_{abc}$  are the **structure constants**. They are totally anti-symmetric, i.e.

$$f_{abc} = -f_{bac} = f_{bca} , \quad (\text{A.13})$$

and are the same for all representations of a group. Moreover, generators that fulfill the same LIE algebra, generate representations of the same group.



For the group representation defined by (A.9) and (A.10) and (A.12), the **exponential parameterization** is a straight forward generalization to non-infinitesimal  $\alpha$ . It is obtained by raising  $D(d\alpha)$  to infinite power:

$$D(\alpha) = \lim_{k \rightarrow \infty} (1 + id\alpha_a X_a/k)^k = e^{i\alpha_a X_a} . \quad (\text{A.14})$$

### Group center

The center of a group  $G$ , denoted here as  $Z(G)$ , is the set of all group elements that commute with all elements of  $G$ , i.e.

$$Z(G) = \{z \in G \mid zg = gz \text{ for all } g \in G\} . \quad (\text{A.15})$$

$Z(G)$  is an ABELian subgroup of  $G$ . Every group has a center, but the center can be trivial, consisting only of the identity element. The statement that a group  $G$  is ABELian is equal to the statement  $Z(G) = G$ .

### Special unitary groups

An important class of LIE groups are the special unitary groups  $SU(N)$ . They are the groups which are defined by  $N \times N$  matrices  $U$  which satisfy

$$U^{-1} = U^\dagger \quad ; \quad \det U = 1 , \quad (\text{A.16})$$

when the binary group operation is the matrix product. The special unitary group  $SU(N)$  is a subgroup of the unitary group  $U(N)$ , which is the larger group in which the condition  $\det U = 1$  does not hold.

Special unitary groups are non-ABELian groups which are **compact**. Intuitively speaking, compactness means that an infinite number of random steps on the group manifold will bring one arbitrarily close to any group element. They are also **simply connected**, which means that there exists a path between any two points on the group manifold, and this path can be continuously deformed without leaving the manifold, into any other path connecting these endpoints. Each group of  $SU(N)$  possesses a non-trivial center, which can be mapped one to one onto the cyclic group  $Z(N)$ .

The generators  $X_a$  of  $SU(N)$  are traceless, hermitian matrices<sup>1</sup>. In the defining or **fundamental** representation they are  $N \times N$  matrices. One can immediately see from the exponential parameterization that the conditions  $X_a = X_a^\dagger$  and  $\text{Tr } X_a = 0$  guarantee (A.16):

- Consider the matrix product  $UU^\dagger = e^{i\alpha_a X_a} e^{-i\alpha_b X_b^\dagger}$ . With  $X_a = X_a^\dagger$  we find that  $[i\alpha_a X_a, -i\alpha_b X_b^\dagger] = [i\alpha_a X_a, -i\alpha_b X_b] = -i\alpha_a i\alpha_b i f_{abc} X_c = 0$  due to anti-symmetry of the  $f_{abc}$ . Thus one can simply add the exponents and finds  $UU^\dagger = \mathbf{1}$ .
- We have shown above that for  $A = i\alpha_a X_a$  it holds that  $AA^\dagger = A^\dagger A$ , thus  $A$  is diagonalizable:  $A = Y^{-1} D Y$ . Using the properties of matrix exponentials it follows that  $U = e^A = e^{Y^{-1} D Y} = Y^{-1} e^D Y$ . Now note that from  $\det(VW) = \det V \det W$

<sup>1</sup>This is a matter of convention. An equivalent definition of  $SU(N)$  can be obtained using anti-hermitian generators

and  $\det(V^{-1}) = (\det V)^{-1}$  it follows that  $\det(X^{-1}AX) = \det A$ . Thus  $\det U = \det(e^A) = \det(e^D)$ . The exponential of a diagonal matrix is simply the matrix where the diagonal elements are exponentiated. Thus  $\det U$  is simply the product of diagonal elements:  $\det U = \det(e^{d_0} \cdots e^{d_N}) = e^{\text{Tr} D}$ . Since  $\text{Tr} D = \text{Tr}(YAY^{-1}) = \text{Tr} A = 0$ , we find  $\det U = 1$ .

### States and operators of $SU(N)$

For a given representation of a LIE group, a group element  $g$  can be thought of as a transformation of the basis of the linear space upon which the representation acts. Thus, any column vector  $\mathbf{x}$  of this space is transformed as

$$\mathbf{x} \mapsto \mathbf{x}' = D(g) \mathbf{x} . \quad (\text{A.17})$$

The transformation law for the corresponding row vector is obtained by taking the adjoint

$$\mathbf{x}^\dagger \mapsto \mathbf{x}'^\dagger = \mathbf{x}^\dagger D(g)^\dagger , \quad (\text{A.18})$$

where for  $SU(N)$  we have  $D(g)^\dagger = D(g)^{-1}$ . Since  $D(g)$  is a linear transformation, the transformed vector  $D(g) \mathbf{x}$  must transform the same as (A.17) under action of another group element  $f$ :

$$D(g) \mathbf{x} \mapsto D(f)D(g) \mathbf{x} = D(f)D(g)D(f)^\dagger D(f) \mathbf{x} . \quad (\text{A.19})$$

Here we have inserted the unit operator  $\mathbf{1} = D(f)^\dagger D(f)$ . This implies that operators  $D(g)$  transform as

$$D(g) = D(f)D(g)D(f)^\dagger , \quad (\text{A.20})$$

and expressions of the form  $\mathbf{x}^\dagger D(g) \mathbf{x}$  are invariant.

### Quaternionic parameterization

All dynamical variables of the theories studied in this work are operators in the fundamental representation of  $SU(2)$ , which is generated by the PAULI matrices

$$\sigma_1 = \begin{pmatrix} 0 & 1 \\ 1 & 0 \end{pmatrix} , \quad \sigma_2 = \begin{pmatrix} 0 & -i \\ i & 0 \end{pmatrix} , \quad \sigma_3 = \begin{pmatrix} 1 & 0 \\ 0 & -1 \end{pmatrix} . \quad (\text{A.21})$$

A specific way to parameterize complex  $2 \times 2$  matrices in general and  $SU(2)$  matrices in particular exists, which is sometimes called the *quaternionic parameterization*. This parameterization is particularly convenient for numerical simulations because it allows one to express arithmetic operations involving  $SU(2)$  matrices in terms of a small set of real numbers. We use this parameterization exclusively throughout this work. It is constructed by exploiting the fact that the PAULI matrices, together with the unit matrix, form a complete basis of the vector space of complex  $2 \times 2$  matrices. Consider  $A$  to be such a general matrix. It can be written as the linear combination

$$A = a_0 \mathbf{1} + ia_j \sigma_j = \begin{pmatrix} a_0 + i a_3 & a_2 + i a_1 \\ -a_2 + i a_1 & a_0 - i a_3 \end{pmatrix} , \quad (\text{A.22})$$

where the  $a_i$  are complex numbers which completely characterize the matrix  $A$ . The trace and the determinant of  $A$  are then simply

$$\text{Tr } A = 2a_0 , \quad (\text{A.23})$$

$$\det A = a_0^2 + a_1^2 + a_2^2 + a_3^2 . \quad (\text{A.24})$$

If the numbers  $a_i$  are real and define a point on the *four dimensional unit sphere*, i.e.

$$a^2 = 1 , \quad (\text{A.25})$$

(here we introduce the notation  $a^2 = a_0^2 + \mathbf{a} \cdot \mathbf{a} = a_0^2 + a_1^2 + a_2^2 + a_3^2$ ) then the matrix  $A$  is an element of  $SU(2)$ . To see this, consider a second matrix  $B = b_0 \mathbf{1} + ib_j \sigma_j$  with complex coefficients  $b_i$ . The product  $AB^\dagger$  can be written as

$$\begin{aligned} (AB^\dagger)_{11} &= (a_0 b_0^* + a_1 b_1^* + a_2 b_2^* + a_3 b_3^*) + i (a_3 b_0^* - a_0 b_3^* + a_1 b_2^* - a_2 b_1^*) \\ (AB^\dagger)_{12} &= (a_2 b_0^* - a_0 b_2^* + a_3 b_1^* - a_1 b_3^*) + i (a_1 b_0^* - a_0 b_1^* + a_2 b_3^* - a_3 b_2^*) \\ (AB^\dagger)_{21} &= -(a_2 b_0^* - a_0 b_2^* + a_3 b_1^* - a_1 b_3^*) + i (a_1 b_0^* - a_0 b_1^* + a_2 b_3^* - a_3 b_2^*) \\ (AB^\dagger)_{22} &= (a_0 b_0^* + a_1 b_1^* + a_2 b_2^* + a_3 b_3^*) - i (a_3 b_0^* - a_0 b_3^* + a_1 b_2^* - a_2 b_1^*) . \end{aligned}$$

If  $B \equiv A$  and  $a_i = b_i \in \mathbb{R}$  then the off-diagonal elements, as well as the imaginary parts of the diagonal elements are zero and

$$\text{Tr } (AA^\dagger) = 2 \det A = 2a^2 . \quad (\text{A.26})$$

If  $a^2 = 1$  then  $AA^\dagger = \mathbf{1}$  and thus  $A \in SU(2)$ . Note that this is a complete parameterization: All elements of  $SU(2)$  can be written in terms of  $a_i \in \mathbb{R}$ . One also sees immediately that

$$\text{Tr } A = \text{Tr } A^\dagger \in \mathbb{R} \text{ for } A \in SU(2) . \quad (\text{A.27})$$

With this parameterization it can be shown that the sum of two  $SU(2)$  matrices is proportional to another  $SU(2)$  matrix. Note that from (A.22) and (A.24) it follows that

$$A + B = (a_0 + b_0) \mathbf{1} + i(a_j + b_j) \sigma_j , \quad (\text{A.28})$$

and

$$\det(A + B) = (a_0 + b_0)^2 + (a_1 + b_1)^2 + (a_2 + b_2)^2 + (a_3 + b_3)^2 . \quad (\text{A.29})$$

Thus, if  $a_i, b_i \in \mathbb{R}$  then  $\det(A + B) \in \mathbb{R}$  and  $\det(A + B) \geq 0$ . The case  $A + B = 0$  is trivially proportional to a  $SU(2)$  matrix. For  $A + B \neq 0$ , if one defines a matrix  $X$  such that

$$X \cdot \sqrt{\det(A + B)} = A + B , \quad (\text{A.30})$$

one finds that

$$\det X = \det \left[ \frac{A + B}{\sqrt{\det(A + B)}} \right] = \frac{\det(A + B)}{\det(A + B)} = 1 , \quad (\text{A.31})$$

and therefore  $X \in SU(2)$  by the above argument. The statement generalizes immediately to sums of an arbitrary number of  $SU(2)$  matrices. If  $M$  is a sum over any number of  $SU(2)$  matrices, then one finds

$$M = c U \text{ with } c \in \mathbb{R}, U \in SU(2) \text{ and } c = |\det M|^{1/2} = \sqrt{\frac{\text{Tr } M M^\dagger}{2}}. \quad (\text{A.32})$$

Another straight forward observation is that for any matrices  $A, B$  with real coefficients  $a_i, b_i$  one finds

$$\text{Tr}(AB^\dagger) = \text{Tr}(A^\dagger B) = 2(a_0 b_0 + a_1 b_1 + a_2 b_2 + a_3 b_3), \quad (\text{A.33})$$

$$\text{Tr}(AB) = \text{Tr}(A^\dagger B^\dagger) = 2(a_0 b_0 - a_1 b_1 - a_2 b_2 - a_3 b_3). \quad (\text{A.34})$$

These formulae are useful, since expressions containing such traces of products occur frequently.

Note that in the quaternionic representation, the  $Z(2)$  center of  $SU(2)$  is given by the unit matrix together with its negative counterpart. It is trivial to show that  $\pm \mathbf{1}$  form a representation of  $Z(2)$  and commute with all  $A = a_0 \mathbf{1} + i a_j \sigma_j$ .

Last we obtain the eigenvalues of a matrix  $A$  in terms of  $a_i$ . The characteristic polynomial is

$$\det(A - \lambda \mathbf{1}) = a_0^2 + a_1^2 + a_2^2 + a_3^2 - 2\lambda a_0 + \lambda^2 = \det A - 2\lambda a_0 + \lambda^2 \equiv 0. \quad (\text{A.35})$$

Thus, for  $A \in SU(2)$  one finds

$$\lambda_{1,2} = a_0 \pm \sqrt{a_0^2 - 1}. \quad (\text{A.36})$$

## Group integration

Assume one wishes to express an integral over a compact LIE group  $G$  of a function  $f(g)$  of group elements as an ordinary integral over a set of parameters  $\alpha_i$ . Thus, one wishes to find a weight function  $J(\alpha)$  so that

$$\int dg f(g) = \int d\alpha_1 \dots d\alpha_n J(\alpha) f(g(\alpha)). \quad (\text{A.37})$$

A group integral is well-defined, if under arbitrary changes of the parameterization, the weight function transforms like

$$\int d\beta J(\beta) f(g(\beta)) = \int d\alpha \left\| \frac{\partial \alpha}{\partial \beta} \right\|^{-1} J(\beta) f(g(\alpha)), \quad (\text{A.38})$$

where  $\left\| \frac{\partial \alpha}{\partial \beta} \right\|$  is the Jacobian determinant for the change of variables<sup>2</sup>. A unique expression for a function  $J(\alpha)$  that satisfies (A.38) can be found, if one assumes that the *group measure*  $dg$  (also known as HAAR *measure*) is invariant under shift of the integration variable, i.e.

$$\int dg f(g) = \int dg f(g' g) = \int dg f(g g') \quad \text{for any } g' \in G. \quad (\text{A.39})$$

<sup>2</sup>For a general treatment of the topic with detailed proofs, see Ref. [2].

For the quaternionic parameterization of  $SU(2)$  discussed above, the group integral assumes the particularly simple form

$$\int dg f(g) = \pi^{-2} \int d^4a \delta(a^2 - 1) f(g) . \quad (\text{A.40})$$

We make use of this expression at various points throughout this work.



## B Summary of consistency checks

In this appendix we summarize the cross-checks in which our numerics have shown to reproduce existing literature.

### KSS model

For the chiral model defined by

$$S = -\frac{1}{2}\beta \sum_{\langle ij \rangle} \text{tr}(\mathbf{L}_i \mathbf{L}_j^\dagger + \text{h.c.}) , \quad (\text{B.1})$$

we reproduce the results of Refs. [106, 108] for the internal energy per link

$$E = \frac{1}{3N_s^3} \sum_{\langle ij \rangle} \text{tr}(\mathbf{L}_i \mathbf{L}_j^\dagger) . \quad (\text{B.2})$$

See section 6.1.3.

### Three dimensional pure gauge theory

We simulate pure  $SU(2)$  Yang-Mills theory

$$S = \beta \sum_{\square} \left(1 - \frac{1}{2} \text{Re Tr } \mathbf{U}_{\square}\right) , \quad (\text{B.3})$$

on a  $N_s = 48^3$  lattice and measure

$$\frac{1}{\beta} \langle S_{\square} \rangle = \left\langle \left(1 - \frac{1}{2} \text{Re Tr } \mathbf{U}_{\square}\right) \right\rangle \quad (\text{B.4})$$

for  $\beta = 6, 7, 9$  on 700 independent configurations. The following table shows our results together with the values obtained by Ref. [118]:

$\beta$	$\langle S_{\square} \rangle / \beta$	Ref. [118]
6	0.17527(9)	0.1752161(16)
7	0.14899(8)	0.1488698(13)
9	0.11475(7)	0.1145493(10)

We find consistency within statistical errors.

### 3D effective theory with magnetic fields in limit $m^2 = 0$

For the theory

$$S = \beta \sum_{\square} \left(1 - \frac{1}{2} \text{Re Tr } \mathbf{U}_{\square}\right) - \frac{1}{2} \beta \sum_{\langle ij \rangle} \text{tr} (\mathbf{L}_i \mathbf{U}_{ij} \mathbf{L}_j^{\dagger} \mathbf{U}_{ij}^{\dagger} + \text{h.c.}) . \quad (\text{B.5})$$

with a time-plaquette single counting scheme, we find that the peak of the susceptibility

$$\chi = \frac{\partial \langle |\bar{\ell}| \rangle}{\partial \beta} \quad (\text{B.6})$$

is consistent within errors with the value  $\beta_C = 0.8730(2)$ , which was obtained by Ref. [123] for  $N_{\tau} = 1$   $SU(2)$  gauge theory. See section 7.4.

### 4D gauge theory

For the pure  $SU(2)$  gauge theory in four dimension we reproduce the following:

- In section 8.1 we reproduce the results of Ref. [124] for the critical coupling strength  $\beta_c$ , where the POLYAKOV loop becomes non-zero, on  $N_s = 16$  and  $N_{\tau} = 2, 4, 6$  lattices.
- In section 8.2 we reproduce the WILSON action measurements of Ref. [2] on  $N_s = N_t = 10$  lattices for a range of  $\beta$ .
- In section 8.3 we reproduce the CREUTZ ratios  $\chi(1, 1)$  on  $N_s = N_t = 6$  of Ref. [125] and  $\chi(I, I)$   $I = 1 \dots 4$  on  $N_s = N_t = 10$  of Ref. [126].



## Bibliography

- [1] M. E. Peskin and D. V. Schroeder, *An introduction to quantum field theory*. Harper-Collins Publishers, New York, 1995.
- [2] M. J. Creutz, *Quarks, Gluons and Lattices*. Cambridge University Press, Cambridge, 1983.
- [3] H. Fritzsche, M. Gell-Mann, and H. Leutwyler, *Advantages of the Color Octet Gluon Picture*, *Phys. Lett.* **B47** (1973) 365–368.
- [4] D. J. Gross and F. Wilczek, *Ultraviolet behavior of non-abelian gauge theories*, *Phys. Rev. Lett.* **30** (1973) 1343–1346.
- [5] H. D. Politzer, *Reliable perturbative results for strong interactions*, *Phys. Rev. Lett.* **30** (1973) 1346–1349.
- [6] M. Gyulassy and L. McLerran, *New forms of QCD matter discovered at RHIC*, *Nucl. Phys.* **A750** (2005) 30–63, [[nucl-th/0405013](#)].
- [7] M. A. Stephanov, *QCD phase diagram: An overview*, *PoS LAT2006* (2006) 024, [[hep-lat/0701002](#)].
- [8] F. Karsch, *Lattice QCD at high temperature and density*, *Lect. Notes Phys.* **583** (2002) 209–249, [[hep-lat/0106019](#)].
- [9] C. E. Detar, *Quark - gluon plasma in numerical simulations of lattice QCD*, [hep-ph/9504325](#).
- [10] K. G. Wilson, *Confinement of Quarks*, *Phys. Rev.* **D10** (1974) 2445–2459.
- [11] R. V. Gavai and S. Gupta, *Quark number susceptibilities, strangeness and dynamical confinement*, *Phys. Rev.* **D64** (2001) 074506, [[hep-lat/0103013](#)].
- [12] F. Karsch, E. Laermann, and A. Peikert, *The pressure in 2, 2+1 and 3 flavour QCD*, *Phys. Lett.* **B478** (2000) 447–455, [[hep-lat/0002003](#)].
- [13] F. Karsch, E. Laermann, and A. Peikert, *Quark mass and flavor dependence of the QCD phase transition*, *Nucl. Phys.* **B605** (2001) 579–599, [[hep-lat/0012023](#)].
- [14] G. 't Hooft, *On the Phase Transition Towards Permanent Quark Confinement*, *Nucl. Phys.* **B138** (1978) 1.
- [15] B. Svetitsky and L. G. Yaffe, *Critical Behavior at Finite Temperature Confinement Transitions*, *Nucl. Phys.* **B210** (1982) 423.

- [16] A. M. Polyakov, *Thermal Properties of Gauge Fields and Quark Liberation*, *Phys. Lett.* **B72** (1978) 477–480.
- [17] O. Philipsen, *Lattice QCD at finite temperature and density*, *Eur. Phys. J. ST* **152** (2007) 29–60, [0708.1293].
- [18] L. D. McLerran and B. Svetitsky, *Quark Liberation at High Temperature: A Monte Carlo Study of  $SU(2)$  Gauge Theory*, *Phys. Rev.* **D24** (1981) 450.
- [19] J. Christensen and P. H. Damgaard, *Critical behavior at the deconfinement phase transition of  $SU(2)$  lattice gauge theory in  $(2+1)$ -dimensions*, *Nucl. Phys.* **B348** (1991) 226–256.
- [20] L. D. McLerran and B. Svetitsky, *A Monte Carlo Study of  $SU(2)$  Yang-Mills Theory at Finite Temperature*, *Phys. Lett.* **B98** (1981) 195.
- [21] J. Engels, J. Fingberg, K. Redlich, H. Satz, and M. Weber, *The onset of deconfinement in  $SU(2)$  lattice gauge theory*, *Z. Phys.* **C42** (1989) 341.
- [22] J. Engels, F. Karsch, and K. Redlich, *Scaling properties of the energy density in  $SU(2)$  lattice gauge theory*, *Nucl. Phys.* **B435** (1995) 295–310, [hep-lat/9408009].
- [23] J. Engels, S. Mashkevich, T. Scheideler, and G. Zinovev, *Critical behaviour of  $SU(2)$  lattice gauge theory A complete analysis with the  $\chi^2$ -method*, *Phys. Lett.* **B365** (1996) 219–224, [hep-lat/9509091].
- [24] G. Boyd *et al.*, *Thermodynamics of  $SU(3)$  Lattice Gauge Theory*, *Nucl. Phys.* **B469** (1996) 419–444, [hep-lat/9602007].
- [25] O. Kaczmarek, F. Karsch, E. Laermann, and M. Lutgemeier, *Heavy quark potentials in quenched QCD at high temperature*, *Phys. Rev.* **D62** (2000) 034021, [hep-lat/9908010].
- [26] A. Dumitru, Y. Hatta, J. Lenaghan, K. Orginos, and R. D. Pisarski, *Deconfining phase transition as a matrix model of renormalized Polyakov loops*, *Phys. Rev.* **D70** (2004) 034511, [hep-th/0311223].
- [27] O. Kaczmarek, F. Karsch, P. Petreczky, and F. Zantow, *Heavy Quark Anti-Quark Free Energy and the Renormalized Polyakov Loop*, *Phys. Lett.* **B543** (2002) 41–47, [hep-lat/0207002].
- [28] S. Gupta, K. Huebner, and O. Kaczmarek, *Polyakov loop in different representations of  $SU(3)$  at finite temperature*, *Nucl. Phys.* **A785** (2007) 278–281, [hep-lat/0608014].
- [29] O. Kaczmarek, S. Gupta, and K. Huebner, *Renormalization of Polyakov loops in fundamental and higher representations*, *PoS LAT2007* (2007) 195, [0710.2277].
- [30] Y. Hidaka and R. D. Pisarski, *Zero Point Energy of Renormalized Wilson Loops*, *Phys. Rev.* **D80** (2009) 074504, [0907.4609].

- 
- [31] S. Gupta, K. Huebner, and O. Kaczmarek, *Renormalized Polyakov loops in many representations*, *Phys. Rev.* **D77** (2008) 034503, [0711.2251].
- [32] **STAR** Collaboration, J. Adams *et al.*, *Experimental and theoretical challenges in the search for the quark gluon plasma: The STAR collaboration's critical assessment of the evidence from RHIC collisions*, *Nucl. Phys.* **A757** (2005) 102–183, [nucl-ex/0501009].
- [33] J.-P. Blaizot, *High temperature phase of QCD*, *Nucl. Phys.* **A785** (2007) 1–9, [nucl-th/0611104].
- [34] O. Kaczmarek, F. Karsch, F. Zantow, and P. Petreczky, *Static quark anti-quark free energy and the running coupling at finite temperature*, *Phys. Rev.* **D70** (2004) 074505, [hep-lat/0406036].
- [35] J. O. Andersen and M. Strickland, *Resummation in Hot Field Theories*, *Ann. Phys.* **317** (2005) 281–353, [hep-ph/0404164].
- [36] Y. Schroder, *Weak-coupling expansion of the hot QCD pressure*, *PoS JHW2005* (2006) 029, [hep-ph/0605057].
- [37] J. O. Andersen, M. Strickland, and N. Su, *Gluon Thermodynamics at Intermediate Coupling*, 0911.0676.
- [38] J. O. Andersen, E. Braaten, and M. Strickland, *Hard-thermal-loop resummation of the free energy of a hot gluon plasma*, *Phys. Rev. Lett.* **83** (1999) 2139–2142, [hep-ph/9902327].
- [39] J. O. Andersen, E. Braaten, E. Petitgirard, and M. Strickland, *HTL perturbation theory to two loops*, *Phys. Rev.* **D66** (2002) 085016, [hep-ph/0205085].
- [40] J. O. Andersen, E. Petitgirard, and M. Strickland, *Two-loop HTL thermodynamics with quarks*, *Phys. Rev.* **D70** (2004) 045001, [hep-ph/0302069].
- [41] J.-P. Blaizot and E. Iancu, *The quark-gluon plasma: Collective dynamics and hard thermal loops*, *Phys. Rept.* **359** (2002) 355–528, [hep-ph/0101103].
- [42] A. Dumitru and R. D. Pisarski, *Two-point functions for SU(3) Polyakov loops near  $T(c)$* , *Phys. Rev.* **D66** (2002) 096003, [hep-ph/0204223].
- [43] R. Falcone, R. Fiore, M. Gravina, and A. Papa, *Screening masses in the SU(3) pure gauge theory and universality*, *Nucl. Phys.* **B785** (2007) 19–33, [0704.3882].
- [44] A. Dumitru, J. Lenaghan, and R. D. Pisarski, *Deconfinement in matrix models about the Gross-Witten point*, *Phys. Rev.* **D71** (2005) 074004, [hep-ph/0410294].
- [45] J. Christensen and P. H. Damgaard, *Conformal invariance at a deconfinement phase transition in (2+1)-dimensions*, *Phys. Rev. Lett.* **65** (1990) 2495–2498.
- [46] J. Christensen and P. H. Damgaard, *Finite size scaling and conformal symmetry around the (2+1)-dimensional SU(2) deconfinement phase transition*, *Nucl. Phys.* **B354** (1991) 339–368.

- [47] P. H. Damgaard, *The free energy of higher representation sources in lattice gauge theories*, *Phys. Lett.* **B194** (1987) 107.
- [48] A. Velytsky, *Equilibrium criterion and effective spin models for finite temperature gauge theories*, *Phys. Rev.* **D78** (2008) 034505, [0805.4450].
- [49] C. Wozar, T. Kaestner, A. Wipf, T. Heinzl, and B. Pozsgay, *Phase Structure of  $Z(3)$ -Polyakov-Loop Models*, *Phys. Rev.* **D74** (2006) 114501, [hep-lat/0605012].
- [50] R. D. Pisarski, *Quark-gluon plasma as a condensate of  $SU(3)$  Wilson lines*, *Phys. Rev.* **D62** (2000) 111501, [hep-ph/0006205].
- [51] R. D. Pisarski, *Effective theory of Wilson lines and deconfinement*, *Phys. Rev.* **D74** (2006) 121703, [hep-ph/0608242].
- [52] R. D. Pisarski, *Notes on the deconfining phase transition*, hep-ph/0203271.
- [53] M. J. Teper,  *$SU(N)$  gauge theories in 2+1 dimensions*, *Phys. Rev.* **D59** (1999) 014512, [hep-lat/9804008].
- [54] A. Dumitru and D. Smith, *Eigenvalue repulsion in an effective theory of  $SU(2)$  Wilson lines in three dimensions*, *Phys. Rev.* **D77** (2008) 094022, [0711.0868].
- [55] D. Smith, *Lattice simulation of a center symmetric three-dimensional effective theory for  $SU(2)$  Yang-Mills*, *Nucl. Phys.* **A820** (2009) 227–230, [0810.1129].
- [56] D. Smith, *Effective potential for Polyakov loops from a center symmetric effective theory in three dimensions*, 0911.4037.
- [57] E. Braaten and A. Nieto, *Effective field theory approach to high temperature thermodynamics*, *Phys. Rev.* **D51** (1995) 6990–7006, [hep-ph/9501375].
- [58] E. Braaten and A. Nieto, *Free Energy of QCD at High Temperature*, *Phys. Rev.* **D53** (1996) 3421–3437, [hep-ph/9510408].
- [59] E. Braaten and A. Nieto, *On the convergence of perturbative QCD at high temperature*, *Phys. Rev. Lett.* **76** (1996) 1417–1420, [hep-ph/9508406].
- [60] K. Farakos, K. Kajantie, K. Rummukainen, and M. E. Shaposhnikov, *The Electroweak phase transition at  $m(H)$  approximately =  $m(W)$* , *Phys. Lett.* **B336** (1994) 494–501, [hep-ph/9405234].
- [61] K. Farakos, K. Kajantie, K. Rummukainen, and M. E. Shaposhnikov, *3-D physics and the electroweak phase transition: Perturbation theory*, *Nucl. Phys.* **B425** (1994) 67–109, [hep-ph/9404201].
- [62] K. Farakos, K. Kajantie, K. Rummukainen, and M. E. Shaposhnikov, *3-d physics and the electroweak phase transition: A Framework for lattice Monte Carlo analysis*, *Nucl. Phys.* **B442** (1995) 317–363, [hep-lat/9412091].
- [63] J. Kapusta, *Finite-temperature field theory*. Cambridge University Press, Cambridge, 1989.

- 
- [64] M. L. Bellac, *Thermal field theory*. Cambridge University Press, Cambridge, 1996.
- [65] T. Appelquist and J. Carazzone, *Infrared Singularities and Massive Fields*, *Phys. Rev.* **D11** (1975) 2856.
- [66] P. H. Ginsparg, *First Order and Second Order Phase Transitions in Gauge Theories at Finite Temperature*, *Nucl. Phys.* **B170** (1980) 388.
- [67] T. Appelquist and R. D. Pisarski, *High-Temperature Yang-Mills Theories and Three-Dimensional Quantum Chromodynamics*, *Phys. Rev.* **D23** (1981) 2305.
- [68] S. Nadkarni, *Dimensional Reduction in Hot QCD*, *Phys. Rev.* **D27** (1983) 917.
- [69] S. Nadkarni, *Dimensional Reduction in Finite Temperature Quantum Chromodynamics. 2*, *Phys. Rev.* **D38** (1988) 3287.
- [70] N. P. Landsman, *Limitations to Dimensional Reduction at High Temperature*, *Nucl. Phys.* **B322** (1989) 498.
- [71] P. de Forcrand, A. Kurkela, and A. Vuorinen, *Center-Symmetric Effective Theory for High-Temperature  $SU(2)$  Yang-Mills Theory*, *Phys. Rev.* **D77** (2008) 125014, [0801.1566].
- [72] T. Heinzl, T. Kaestner, and A. Wipf, *Effective actions for the  $SU(2)$  confinement-deconfinement phase transition*, *Phys. Rev.* **D72** (2005) 065005, [hep-lat/0502013].
- [73] L. Dittmann, T. Heinzl, and A. Wipf, *An effective lattice theory for Polyakov loops*, *JHEP* **06** (2004) 005, [hep-lat/0306032].
- [74] C. P. K. Altes, *ZQCD and universal matching to domain walls*, *Nucl. Phys.* **A820** (2009) 219c–222c, [0810.3325].
- [75] A. Dumitru, R. D. Pisarski, and D. Zschiesche, *Dense quarks, and the fermion sign problem, in a  $SU(N)$  matrix model*, *Phys. Rev.* **D72** (2005) 065008, [hep-ph/0505256].
- [76] D. Diakonov and M. Oswald, *Covariant derivative expansion of Yang-Mills effective action at high temperatures*, *Phys. Rev.* **D68** (2003) 025012, [hep-ph/0303129].
- [77] D. Diakonov and M. Oswald, *Covariant derivative expansion of fermionic effective action at high temperatures*, *Phys. Rev.* **D70** (2004) 016006, [hep-ph/0312126].
- [78] D. Diakonov and M. Oswald, *Gauge invariant effective action for the Polyakov line in the  $SU(N)$  Yang-Mills theory at high temperatures*, *Phys. Rev.* **D70** (2004) 105016, [hep-ph/0403108].
- [79] D. J. Gross, R. D. Pisarski, and L. G. Yaffe, *QCD and Instantons at Finite Temperature*, *Rev. Mod. Phys.* **53** (1981) 43.
- [80] R. D. Pisarski, *Fuzzy bags and Wilson lines*, *Prog. Theor. Phys. Suppl.* **168** (2007) 276–284, [hep-ph/0612191].

- 
- [81] P. N. Meisinger, T. R. Miller, and M. C. Ogilvie, *Phenomenological equations of state for the quark-gluon plasma*, *Phys. Rev.* **D65** (2002) 034009, [hep-ph/0108009].
- [82] E. Megias, E. Ruiz Arriola, and L. L. Salcedo, *Dimension two condensates and the Polyakov loop above the deconfinement phase transition*, *JHEP* **01** (2006) 073, [hep-ph/0505215].
- [83] E. Megias, E. Ruiz Arriola, and L. L. Salcedo, *Chiral Lagrangian at finite temperature from the Polyakov- Chiral Quark Model*, *Phys. Rev.* **D74** (2006) 114014, [hep-ph/0607338].
- [84] E. Megias, E. Ruiz Arriola, and L. L. Salcedo, *The quark-antiquark potential at finite temperature and the dimension two gluon condensate*, *Phys. Rev.* **D75** (2007) 105019, [hep-ph/0702055].
- [85] E. Megias, E. Ruiz Arriola, and L. L. Salcedo, *Trace Anomaly, Thermal Power Corrections and Dimension Two condensates in the deconfined phase*, *Phys. Rev.* **D80** (2009) 056005, [0903.1060].
- [86] Y. Hidaka and R. D. Pisarski, *Suppression of the Shear Viscosity in a "semi" Quark Gluon Plasma*, *Phys. Rev.* **D78** (2008) 071501, [0803.0453].
- [87] Y. Hidaka and R. D. Pisarski, *Hard thermal loops, to quadratic order, in the background of a spatial 't Hooft loop*, *Phys. Rev.* **D80** (2009) 036004, [0906.1751].
- [88] A. Vuorinen and L. G. Yaffe, *Z(3)-symmetric effective theory for SU(3) Yang-Mills theory at high temperature*, *Phys. Rev.* **D74** (2006) 025011, [hep-ph/0604100].
- [89] A. Kurkela, *Framework for non-perturbative analysis of a Z(3)- symmetric effective theory of finite temperature QCD*, *Phys. Rev.* **D76** (2007) 094507, [0704.1416].
- [90] I. Montvay and G. Münster, *Quantum fields on a lattice*. Cambridge University Press, Cambridge, 1994.
- [91] T. DeGrand and C. DeTar, *Lattice Methods for Quantum Chromodynamics*. World Scientific Publishing, Singapore, 2006.
- [92] B. A. Berg, *Markov Chain Monte Carlo Simulations and Their Statistical Analysis*. World Scientific Publishing, Singapore, 2004.
- [93] N. Metropolis, A. Rosenbluth, M. Rosenbluth, A. Teller, and E. Teller *Chem. Phys.* **21** (1953) 1087.
- [94] P. de Forcrand and O. Jahn, *Monte Carlo overrelaxation for SU(N) gauge theories*, hep-lat/0503041.
- [95] M. Creutz, *Overrelaxation and Monte Carlo Simulation*, *Phys. Rev.* **D36** (1987) 515.
- [96] F. R. Brown and T. J. Woch, *Overrelaxed Heat Bath and Metropolis Algorithms for Accelerating Pure Gauge Monte Carlo Calculations*, *Phys. Rev. Lett.* **58** (1987) 2394.

- 
- [97] M. Creutz, *Monte Carlo Study of Quantized  $SU(2)$  Gauge Theory*, *Phys. Rev.* **D21** (1980) 2308–2315.
- [98] A. D. Kennedy and B. J. Pendleton, *Improved Heat Bath Method for Monte Carlo Calculations in Lattice Gauge Theories*, *Phys. Lett.* **B156** (1985) 393–399.
- [99] N. Cabibbo and E. Marinari, *A New Method for Updating  $SU(N)$  Matrices in Computer Simulations of Gauge Theories*, *Phys. Lett.* **B119** (1982) 387–390.
- [100] C. P. Korthals Altes, J. Jurkiewicz, and J. Groeneveld, *Order Parameters in Spin Spin and Plaquette Lattice Theories*, *Acta Phys. Polon.* **B12** (1981) 615–636.
- [101] K. Huang, *Quarks, Leptons and Gauge Fields*. World Scientific Publishing, Singapore, 1992.
- [102] A. Velytsky, *Finite temperature  $SU(2)$  gauge theory: critical coupling and universality class*, *Int. J. Mod. Phys.* **C19** (2008) 1079–1093, [0711.0748].
- [103] T. G. Kovacs and E. T. Tomboulis, *The  $SU(2) \times SU(2)$  chiral spin model in terms of  $SO(3)$  and  $Z(2)$  variables: Vortices and disorder*, *Phys. Lett.* **B321** (1994) 75–79, [hep-lat/9311005].
- [104] T. G. Kovacs and E. T. Tomboulis,  *$SO(3)$  vortices and disorder in the 2-d  $SU(2)$  chiral model*, *Phys. Lett.* **B367** (1996) 254–258, [hep-lat/9508010].
- [105] J. B. Kogut, M. Snow, and M. Stone, *Mean Field and Monte Carlo Studies of  $SU(N)$  Chiral Models in Three-Dimensions*, *Nucl. Phys.* **B200** (1982) 211.
- [106] P. Dreher, *A Finite sized scaling study in three-dimensional  $SU(N) \times SU(N)$  and  $U(N)$  Heisenberg models and finite temperature QCD*, *Nucl. Phys.* **B389** (1993) 265–284.
- [107] P. Dreher, *On the order of the phase transition in three-dimensional  $SU(N) \times SU(N)$  and  $U(N) \times U(N)$  Heisenberg models and finite temperature QCD*, *Phys. Lett.* **B281** (1992) 127–132.
- [108] A. Guha and S. C. Lee, *Improved mean field studies of  $SU(N)$  chiral models and comparison with numerical simulations*, *Nucl. Phys.* **B240** (1984) 141.
- [109] B. Svetitsky, *Symmetry Aspects of Finite Temperature Confinement Transitions*, *Phys. Rept.* **132** (1986) 1–53.
- [110] C. X. Chen and C. E. Detar, *A phenomenological lattice model of the high temperature phase transition in Quantum Chromodynamics*, *Phys. Rev.* **D35** (1987) 3963.
- [111] V. Koch, *Introduction to Chiral Symmetry*, nucl-th/9512029.
- [112] H. Leutwyler, *On the foundations of chiral perturbation theory*, *Ann. Phys.* **235** (1994) 165–203, [hep-ph/9311274].

- 
- [113] S. Elitzur, *Impossibility of Spontaneously Breaking Local Symmetries*, *Phys. Rev.* **D12** (1975) 3978–3982.
- [114] L. H. Ryder, *Quantum field theory*. Cambridge University Press, Cambridge, 1996 (second edition).
- [115] W. H. Press, B. P. Flannery, S. A. Teukolsky, and W. T. Vetterling, *Numerical Recipes in C: The Art of Scientific Computing*. Cambridge University Press, Cambridge, 1992.
- [116] J. C. Myers and M. C. Ogilvie, *Exotic phases of finite temperature  $SU(N)$  gauge theories with massive fermions:  $F$ ,  $Adj$ ,  $A/S$* , *PoS LATTICE2008* (2008) 201, [0809.3964].
- [117] J. C. Myers and M. C. Ogilvie, *Exotic phases of finite temperature  $SU(N)$  gauge theories*, *Nucl. Phys.* **A820** (2009) 187c–190c, [0810.2266].
- [118] A. Hietanen and A. Kurkela, *Plaquette expectation value and lattice free energy of three-dimensional  $SU(N)$  gauge theory*, *JHEP* **11** (2006) 060, [hep-lat/0609015].
- [119] G. S. Bali, K. Schilling, J. Fingberg, U. M. Heller, and F. Karsch, *Computation of the spatial string tension in high temperature  $SU(2)$  gauge theory*, *Int. J. Mod. Phys.* **C4** (1993) 1179–1193, [hep-lat/9308003].
- [120] P. N. Meisinger and M. C. Ogilvie, *String Tension Scaling in High-Temperature Confined  $SU(N)$  Gauge Theories*, 0905.3577.
- [121] Y. Schroeder and M. Laine, *Spatial string tension revisited*, *PoS LAT2005* (2006) 180, [hep-lat/0509104].
- [122] R. Fiore, F. Gliozzi, and P. Provero, *Critical behavior of 3D  $SU(2)$  gauge theory at finite temperature: Exact results from universality*, *Phys. Rev.* **D58** (1998) 114502, [hep-lat/9806017].
- [123] R. Ben-Av, H. G. Evertz, M. Marcu, and S. Solomon, *Critical acceleration of finite temperature  $SU(2)$  gauge simulations*, *Phys. Rev.* **D44** (1991) 2953–2956.
- [124] J. Fingberg, U. M. Heller, and F. Karsch, *Scaling and asymptotic scaling in the  $SU(2)$  gauge theory*, *Nucl. Phys.* **B392** (1993) 493–517, [hep-lat/9208012].
- [125] M. Creutz and K. J. M. Moriarty,  *$U(N)$  and  $SU(N)$  lattice gauge theories, in the weak coupling region, in four-dimensions*, *J. Phys.* **G9** (1983) L207–L210.
- [126] M. Creutz, *Asymptotic Freedom Scales*, *Phys. Rev. Lett.* **45** (1980) 313.
- [127] P. N. Meisinger, M. C. Ogilvie, and T. R. Miller, *Gluon quasiparticles and the Polyakov loop*, *Phys. Lett.* **B585** (2004) 149–154, [hep-ph/0312272].
- [128] M. Schaden, *A center-symmetric  $1/N$  expansion*, *Phys. Rev.* **D71** (2005) 105012, [hep-th/0410254].



- 
- [129] K. Fukushima, *Chiral effective model with the Polyakov loop*, *Phys. Lett.* **B591** (2004) 277–284, [[hep-ph/0310121](#)].
- [130] H. Georgi, *Lie Algebras in Particle Physics*. Westview Press, Colorado, 1999.



## Acknowledgments

Firstly, I thank my parents for their support and encouragement.

I am indebted to Adrian Dumitru and Stefan Schramm for offering me the opportunity to work on this project and supervising my work. Their support and guidance has been exceptional.

I thank Rob Pisarski, Michael Strickland and Zsolt Schram for the many discussions, encouragement and useful comments. I also thank Christoph Blume for providing insight from an experimentalists point of view and acting as an external advisor.

Thanks Aleksi Kurkela, Jorge Noronha, Philippe De Forcrand, Andras Patkos and Miklos Gyulassy for the hospitality and helpful discussions.

Thanks to Horst Stoecker, Henner Buesching, the Frankfurt Institute for Advanced Studies (FIAS) and the Helmholtz Research School for Quark Matter Studies (HQM) for their support.

I thank Joseph Riedl, Werner Kexel and Hans-Peter May for laying the groundwork for my subsequent studies of theoretical physics.

For the company and the many useful discussions I would like to thank my friends and colleagues, Yun Guo, Mauricio Martinez, Sascha Vogel, Andrej El, Torsten Schuerhoff, Frank Michler, Nan Su, Fritz Kretzschmar, Daniel Yueker and Veronica Dexheimer.

In addition, I thank Marcy Chaloupka for much helpful assistance. Lastly, I also thank Kirsten Schneider for the support and encouragement. I apologize deeply for any negligent omissions.

The numerical simulations presented here were performed at the Center for Scientific Computing (CSC) at Frankfurt University. The code is based in part on the MILC collaboration's public lattice gauge theory code, see <http://physics.utah.edu/~detar/milc.html>.



# Curriculum vitae

## Personal particulars:

Name: Dominik Smith  
Gender: Male  
Date of Birth: 17. Nov. 1981  
Place of Birth: Chattanooga, Tennessee, USA  
Nationalities: German, (US)American  
Languages: Native in German and English  
Address: Adalbertstr. 28, 60486, Frankfurt am Main, Germany  
Email: smith@th.physik.uni-frankfurt.de

## Academic tutors:

- Prof. Adrian Dumitru
- Prof. Stefan Schramm
- Prof. Christoph Blume

## Educational background:

- Since Sep. 2006, Postgraduate theoretical physics, Frankfurt International Graduate School for Science (FIGGS) and Goethe University Frankfurt am Main. Topic: *Effective theories of  $SU(N)$  Wilson lines.*
- 2003-2006, Theoretical physics, Institute of Theoretical Physics, Goethe University Frankfurt am Main, diploma (MS), grade average: (1.2), thesis: *Lattice simulation of the Ising model in two dimensions.*
- 2001-2003, Physics, Goethe University Frankfurt am Main, pre-diploma, grade average: (1.3).
- 1992-2001, Gymnasium, Carl Schurz Schule, Frankfurt am Main, Abitur, grade average: (1.4).
- 1988-1992, Elementary school, Engelbert Humperdinck Schule, Frankfurt am Main.

**Other training, workshops and activities:**

- Workshop *Lattice Practices 2008*, DESY in Zeuthen, Germany, 8.-10.10.2008.
- Since Sep. 2006, participant in the *Helmholtz Research School for Quark Matter Studies (H-QM)* structured PhD education program:
  1. Course on *Career and Leadership*, Park Hotel, Oberursel, Germany, 2.-4.10.2009.
  2. Course on *Advanced Presentation Skills*, Haus Sonnenberg, St.Andreasberg, Germany, 15.-17.7.2008.
  3. Course on *Research Skills Development*, Easthampsted Park, London, England, 26.-29.6.2007.
  4. Lecture week on *Non-heavy-ion LHC physics (Higgs, SUSY and Co.)*, Manigod, French Alps, 8.-13.2.2009, contributed a presentation on *Measurements of the Top Quark Properties*
  5. Lecture week on *High pT Physics*, Castle Blankenheim, Eifel, Germany, 16.-20.3.2008, contributed a presentation on *Jet Finding Algorithms*
  6. Lecture week on *Heavy Ion Physics*, Haus Humboldtstein, Remagen, Germany, 1.-5.4.2007, contributed a presentation on *Charmonium Physics*

**Teaching experience:**

- Coordination and administration of exercise groups
  1. *Theoretical Physics I/II: Classical Mechanics*, Prof. Joachim Maruhn, summer term 2009.
  2. *Theoretical Physics: Nuclei and Elementary Particles*, Prof. Adrian Dumitru, summer term 2008.
- Teaching of exercise groups
  1. *Theoretical Physics III: Electrodynamics*, Prof. Walter Hofstetter, winter term 2008/09.
  2. *Theoretical Physics I: Classical Mechanics*, Prof. Joachim Maruhn, winter term 2007/08.
  3. *Theoretical Physics VI: Quantum Mechanics II*, Prof. Claudius Gros, summer term 2007.
  4. *Theoretical Physics IV: Quantum Mechanics I*, Prof. Claudius Gros, summer term 2006.
  5. *Theoretical Physics V: Thermodynamics and Statistical Mechanics*, Prof. Horst Stöcker, winter term 2005/06.
  6. *Theoretical Physics IV: Quantum Mechanics I*, Prof. Horst Stöcker, summer term 2005.
  7. *Theoretical Physics III: Electrodynamics*, Prof. Horst Stöcker, winter term 2004/05.

# Publications

## Reviewed publications:

- Adrian Dumitru and Dominik Smith, *Eigenvalue repulsion in an effective theory of  $SU(2)$  Wilson lines in three dimensions*, Phys. Rev. D 77, 094022 (2008) [arXiv:0711.0868].

## Conference proceedings:

- Dominik Smith, *Lattice simulation of a center symmetric three-dimensional effective theory for  $SU(2)$  Yang-Mills*, contributed to Strong and ElectroWeak Matter (SEWM) 2008, Nucl. Phys. A 820, 227-230 (2009) [arXiv:0810.1129].

## Preprints:

- Dominik Smith, *Effective potential for Polyakov loops from a center symmetric effective theory in three dimensions*, [arXiv:0911.4037]

## Presentations:

- Talks at conferences
  1. *Conference of the German Physics Society (DPG) 2010*, session T 25.3, Bonn, Germany, Effective potential for Polyakov loops from a center symmetric effective theory in three dimensions, 15.-19.3.2010
  2. *Norwegian Winter Workshop on QCD in Extreme Conditions*, Trondheim, Norway, Effective potential for Polyakov loops from a center symmetric effective theory in three dimensions, 24.-26.2.2010
  3. *Conference of the German Physics Society (DPG) 2009*, session HK 68.7, Bochum, Germany, Lattice simulation of a center symmetric three dimensional effective theory for  $SU(2)$  Yang-Mills, 16.-20.3.2009
  4. *Conference of the German Physics Society (DPG) 2009*, session T 24.2, Munich, Germany, Lattice simulation of a center symmetric three dimensional effective theory for  $SU(2)$  Yang-Mills, 9.-13.3.2009

5. *Conference of the German Physics Society (DPG) 2008*, session HK 28.4, Darmstadt, Germany, Eigenvalue repulsion in an effective theory of  $SU(2)$  Wilson lines in three dimensions, 10.-14.3.2008
  6. *Conference of the German Physics Society (DPG) 2007*, session HK 14.8, Gießen, Germany, Lattice simulations of a  $SU(N)$  matrix model, 12.-16.3.2007.
- Poster presentations
    1. *International Conference on Particles And Nuclei 2008 (PANIC 2008)*, Eilat, Israel, 9.-14.11.2008.
    2. *Strong and ElectroWeak Matter 2008 (SEWM 08)* Amsterdam, the Netherlands, 26.-29.8.2008.
  - Other talks
    1. *ETH Hönggerberg*, Zürich, Switzerland, Effective potential for Polyakov loops from a center symmetric effective theory in three dimensions, host: Phillippe de Forcrand, 8.12.2009
    2. *Brookhaven National Lab*, Upton, New York, USA, Effective potential from a  $Z(2)$  symmetric dimensional reduced theory of Wilson lines, host: Robert Pisarski, 5.11.2009
    3. *Columbia University*, New York, USA, Effective potential from a  $Z(2)$  symmetric dimensional reduced theory of Wilson lines, host: Miklos Gyulassy, 4.11.2009
    4. *Stony Brook University*, Stony Brook, New York, USA, Effective potential from a  $Z(2)$  symmetric dimensional reduced theory of Wilson lines, host: Jacobus Verbaarschot, 28.10.2009
    5. *Lorand Eotvos University, Department of Theoretical Physics*, Budapest, Hungary, host: Andras Patkos, 29.10.2008.
    6. *Atomki (Institute for Nuclear Research)*, Debrecen, Hungary, host: Zsolt Schram, 30.10.2008.



# Index

- abelian group, 95
- acceptance rate, 22
- additive color model, 3
- algorithms
  - heat bath, 24
    - Creutz, 25
    - Kennedy-Pendleton, 27
    - Metropolis, 22
    - overrelaxation, 23
- associativity, 95
- asymptotic freedom, 4
- autocorrelation, 19, 54
  
- balance, 19
- binning, 21
- block spin, 72
- Boltzmann weight, 18
  
- center, 97
- central limit theorem, 72
- chiral model, 40
  - Kogut, Stone and Snow, 40
- closure property, 95
- color, 3
- compactness, 97
- consistency checks, 103
- Creutz heat bath, 25
- critical slowing down, 20
- cyclic group, 96
  
- Debye mass, 44
- detailed balance, 19
- Dyson formula, 35
  
- electrostatic QCD, 12
- equilibrium ensemble, 19
- ergodicity, 19
- exponential autocorrelation time, 20
- exponential parameterization, 97
  
- finite group, 95
  - generator, 96
  - gluon, 3
  - group measure, 100
  - group theory, 95
  
- Haar measure, 100
- hadron, 3
- hard-thermal-loop formalism, 6
- heat bath, 24
  
- identity element, 95
- importance sampling, 18
- integrated autocorrelation time, 21
- interaction measure, 6
- inverse element, 95
- Ising model, 18, 69
  
- Kennedy-Pendleton heat bath, 27
- KSS model, 40
  
- lattice simulation, 17
- Lie algebra, 96
- Lie group, 96
  
- Markov chain, 18
- Matsubara frequency, 11
- mean field, 46
  - free energy, 47
- Metropolis algorithm, 22
- Metropolis criterium, 22
- Monte Carlo simulation, 18
  
- N-hit-Metropolis, 23
- nonlinear sigma model, 40
  
- overrelaxation, 23
  
- partition function, 18

plaquette, 36  
Polyakov loop, 6

QCD, 3  
quantum chromodynamics, 3  
quark, 3  
quasi-heat-bath, 25  
quaternionic parameterization, 98

representation, 95  
roots of unity, 96

sequential updating, 22  
simply connected, 97  
spatial string tension, 62  
special unitary group, 97  
string tension, 62  
structure constants, 96  
SU(2)  
    axial transformations, 40  
    vector transformations, 40  
subgroup, 95  
susceptibility, 43

thermal ensemble, 17  
trace anomaly, 6  
transition matrix, 19

Vandermonde potential, 53

Wilson action, 32, 60  
Wilson loop, 61

Z(N), 96